LOCKHEED MARTIN ENERGY RESEARCH LIBRARIES
3 4456 0449171 6

ORNL/TM-7305

ornl

OAK
RIDGE
NATIONAL
LABORATORY

UNION
CARBIDE

The Development, Implementation, and Verification of Multicycle Depletion Perturbation Theory for Reactor Burnup Analysis

J. R. White
Computer Sciences Divison

OAK RIDGE NATIONAL LABORATORY
CENTRAL RESEARCH LIBRARY
CIRCULATION SECTION
4500N ROOM 175
LIBRARY LOAN COPY
DO NOT TRANSFER TO ANOTHER PERSON
If you wish someone else to see this report, send in name with report and the library will arrange a loan.
UCN-7969 (3 9-77)

OPERATED BY
UNION CARBIDE CORPORATION
FOR THE UNITED STATES
DEPARTMENT OF ENERGY

Printed in the United States of America. Available from
National Technical Information Service
U.S. Department of Commerce
5285 Port Royal Road, Springfield, Virginia 22161
NTIS price codes—Printed Copy: A09 Microfiche A01

This report was prepared as an account of work sponsored by an agency of the United States Government. Neither the United States Government nor any agency thereof, nor any of their employees, makes any warranty, express or implied, or assumes any legal liability or responsibility for the accuracy, completeness, or usefulness of any information, apparatus, product, or process disclosed, or represents that its use would not infringe privately owned rights. Reference herein to any specific commercial product, process, or service by trade name, trademark, manufacturer, or otherwise, does not necessarily constitute or imply its endorsement, recommendation, or favoring by the United States Government or any agency thereof. The views and opinions of authors expressed herein do not necessarily state or reflect those of the United States Government or any agency thereof.

ORNL/TM-7305
Distribution Category UC-77

Contract No. W-7405-eng-26

ENGINEERING PHYSICS DIVISION

THE DEVELOPMENT, IMPLEMENTATION, AND VERIFICATION OF MULTICYCLE DEPLETION PERTURBATION THEORY FOR REACTOR BURNUP ANALYSIS*

J. R. White
Computer Sciences Division

(Sponsor: D. E. Bartine)

Date Published: August 1980

*Submitted to the University of Tennessee as a Masters Thesis in the Department of Nuclear Engineering

OAK RIDGE NATIONAL LABORATORY
Oak Ridge, Tennessee 37830
operated by
UNION CARBIDE CORPORATION
for the
DEPARTMENT OF ENERGY

LOCKHEED MARTIN ENERGY RESEARCH LIBRARIES

3 4456 0449171 6

TABLE OF CONTENTS

	PAGE
LIST OF TABLES	v
LIST OF FIGURES	ix
ACKNOWLEDGMENTS	xi
ABSTRACT	xiii
I. INTRODUCTION	1
General Comments	1
Scope and Organization	4
II. THE MULTICYCLE DEPLETION PERTURBATION THEORY FOMULATION	6
The Quasi-Static Burnup Equations	6
The Adjoint Equations of Depletion Perturbation Theory	14
III. SOLUTION OF THE BURNUP EQUATIONS	21
Solution of the Reference Burnup Equations	21
Solution of the Adjoint Depletion Equations	25
IV. NUMERICAL EXAMPLES	38
Interpretation of the Adjoint Functions	38
One-Dimensional Calculations	42
Nuclide Inventory Responses (one time step)	48
A Detailed Example	58
Nuclide Inventory Responses (multiple time steps)	74
K_{eff} Response	78
Reaction Rate Ratio Response	95
Two-Dimensional Calculations	105
Multicycle Calculations	126

PAGE

V. SUMMARY. 141

Conclusions. 141

Recommendations. 144

LIST OF REFERENCES. 149

APPENDIX A. 153

APPENDIX B. 163

LIST OF TABLES

TABLE		PAGE
2.1.	Forward and Adjoint Quasi-Static Burnup Equations	11
2.2.	One-to-One Correspondence Between Forward and Adjoint Depletion Operations.	19
3.1.	Major Modules of the VENTURE/BURNER Computational System. .	23
3.2.	Commonly Used Interface Data Files.	24
4.1.	Reference BOC Nuclide Density Vectors for 1-D Model	44
4.2.	Data Specified for Transmutation Process.	45
4.3.	Selected Data From Reference 1-D Depletion Calculations . .	46
4.4.	Material Perturbations Made to Reference System	47
4.5.	Comparison of DPT Results With Direct Computations for the 1-D, 1-Group Calculations	49
4.6.	Comparison of DPT Results With Direct Computations for the 1-D, 9-Group Calculations	50
4.7.	Final-Time Adjoint Nuclide Density Vectors for ^{232}U Inventory Response.	61
4.8.	$\underline{N}_z^*(t_0^+)$ for ^{232}U Inventory Response.	62
4.9.	P^* Effect for ^{232}U Inventory Response	63
4.10.	Adjoint Source Vectors for ^{232}U Inventory Response.	65
4.11.	Γ^* Effect in Core Zone #1 for ^{232}U Inventory Response . . .	69
4.12.	$\underline{N}_z^*(t_0^-)$ for ^{232}U Inventory Response.	71
4.13.	$\underline{N}_z^*(t_0^-)*V_z$ for ^{232}U Inventory Response	73
4.14.	Comparison of Depletion Perturbation Theory Methods With Direct Methods for Multiple Time Steps.	75
4.15.	Relative N^*, P^*, and Γ^* Effects in Multistep Calculations .	77

TABLE PAGE

4.16. Comparison of Static and Time-Dependent Sensitivity Coefficients for a One Time-Step Problem 79

4.17. Comparison of Static and Time-Dependent Sensitivity Coefficients for a Multiple Time-Step Problem. 81

4.18. Comparison of DPT Results With Direct Calculation for a K_{eff} Response. 83

4.19. Comparison of Zone-Wise Contributions to the Total $\Delta K/K$ for the Single and Multiple Time-Step Calculations . . . 87

4.20. Relative Contribution of the N^*, P^*, and Γ^* Effects to the Total ΔK_{eff} Response 88

4.21. Relative Contribution of the Γ^* Effect to the Total $\Delta K/K$ Response in the Multiple Time-Step Calculation 89

4.22. Adjoint Source Vectors for C8/F9 Response in CZ 1 98

4.23. $N_z^*(t_0^-)*V_z$ for C8/F9 Response in CZ #1. 100

4.24. ^{238}U Capture to ^{239}Pu Fission Cross-Section Ratio. 101

4.25. Description of Perturbation/Response Pairs Utilized in the 2-D Analyses 109

4.26. DPT Versus Direct Calculation for the Total ^{239}Pu Inventory at 91 Days in the 2-D GCFR Model 110

4.27. Spatial Distribution of the Relative Contribution of the ^{238}U Γ^* Effect to the Total ^{239}Pu Inventory. 113

4.28. Weighting Functions for Adjoint Flux Averaging 116

4.29. DPT Versus Direct Calculation for the ^{239}Pu Inventory at 91 Days in the Fourth Axial Blanket Zone of the 2-D GCFR Model 119

TABLE PAGE

4.30. DPT Versus Direct Calculation for the EOC Total ^{239}Pu Inventory Response in the 2-D GCFR Model 123

4.31. Comparison of Relative Computing Requirements for the Forward and Adjoint Depletion Calculations 124

4.32. Qualitative Values of the Importance Function in the Three-Region Example 131

4.33. DPT Versus Direct Calculation for EOC4 ^{239}Pu Inventory Response for Fission Product and Plutonium Perturbations in Core Zone #1. 135

4.34. DPT Versus Direct Calculation for EOC4 ^{239}Pu Inventory Response for the 10% $^{238}U/^{232}Th$ Perturbation to the Radial Blanket Zones 136

4.35. DPT Versus Direct Calculation for EOC4 ^{241}Pu Inventory Response for the 10% $^{238}U/^{232}Th$ Perturbation to the Radial Blanket Zones 137

LIST OF FIGURES

FIGURE		PAGE
2.1.	Schematic Representation of Quasi-Static Burnup Approximation	10
3.1.	Computational Path for Reference Depletion Calculation	26
3.2.	Computational Path for Adjoint Depletion Calculation	28
3.3.	Simplified Flow Chart of Calculational Path Within Modular System	29
3.4.	Detailed Flow Chart of Calculational Path Within the DEPTH Module	30
3.5.	Details of the $\underline{N}^*$, P^*, and $\underline{S}^*$ Calculations	31
4.1.	1-Dimensional Spherical Reactor Calculational Model	43
4.2.	Nonlinear Behavior in the 1-D, 1-Group Calculation Due to Large P^* Effects	52
4.3.	Comparison of Nonlinear Behavior Due to Large N^* and P^* Effects in the 1-D, 9-Group Calculation	53
4.4.	Nonlinear Behavior in the 1-D, 9-Group Calculation Due to Large Γ^* Effects	54
4.5.	Comparison of Flux Spectra at Core Center for a 50% Increase in Stainless Steel Relative to the Reference Case	57
4.6.	Comparison of Γ^* Effects for the 1-Group and 9-Group ^{232}U Inventory Responses	59
4.7.	^{232}U "Uncontaminated" Generalized Adjoint Flux	66
4.8.	Nonlinear Behavior of Uniform Stainless Steel Perturbation on the K_{eff} Response	84

FIGURE PAGE

4.9. Linear Relationship of K_{eff} Response for Separate Stainless Steel Perturbations in Each Core Zone 85

4.10. EOC K_{eff} Generalized Adjoint Flux at 182.6 Days 91

4.11. EOC K_{eff} Generalized Adjoint Flux at 91.3 Days. 92

4.12. EOC K_{eff} Generalized Adjoint Flux at 0.0 Days 93

4.13. 1-D, 9-Group Regular Adjoint Flux 96

4.14. Nonlinear Behavior of Microscopic C8/F9 Response in Core Zone 1. 103

4.15. Comparison of Flux Spectra in CZ 1 for a 100% Decrease in the O-16 Concentration Relative to the Reference Case . . 104

4.16. Two-Dimensional Model of 1500 MWe GCFR. 106

4.17. Total ^{239}Pu Generalized Adjoint Flux Averaged Over all Energy Groups. 115

4.18. Total ^{239}Pu Generalized Adjoint Flux Averaged Over Groups 6-9. 117

4.19. Axial Blanket #4 ^{239}Pu Generalized Adjoint Flux Averaged Over All Energy Groups. 120

4.20. Axial Blanket #4 ^{239}Pu Generalized Adjoint Flux Averaged Over Groups 6-9 121

ACKNOWLEDGMENTS

The author wishes to express his appreciation for the support and encouragement of H. L. Dodds, his major professor, and the University of Tennessee staff members who served on his Graduate Committee.

The author would also like to thank T. J. Burns and M. L. Williams of the Engineering Physics Division at the Oak Ridge National Laboratory for their guidance in the early phase of this work and for the many interesting and helpful discussions contributed throughout the entire study. Thanks are also due G. W. Cunningham and T. B. Fowler for their help in understanding the logic of the VENTURE/BURNER modular code system. In addition, this work would not have been completed were it not for the encouragement and financial support provided by D. E. Bartine of the Engineering Physics Division at the Oak Ridge National Laboratory. Finally, the author is indebted to Fern Stooksbury for typing the many drafts of this report.

The author wishes to express his appreciation for the support and use of the facilities of the Computer Sciences Division, U.S. Department of Energy under contract W-7405-eng-26 with the Union Carbide Corporation Nuclear Division.

ABSTRACT

A generalized depletion perturbation formulation based on the "quasi-static" method for solving realistic multicycle reactor depletion problems is developed and implemented within the VENTURE/BURNER modular code system. The present development extends the original formulation derived by M. L. Williams to include nuclide discontinuities such as fuel shuffling and discharge. This theory is first described in detail with particular emphasis given to the similarity of the forward and adjoint quasi-static burnup equations. The specific algorithm and computational methods utilized to solve the adjoint problem within the newly developed DEPTH (Depletion Perturbation Theory) module are then briefly discussed. Finally, the main features and computational accuracy of this new method are illustrated through its application to several representative reactor depletion problems.

The examples utilized in the study cover the range from one-group one-dimensional reactor models to more complex multigroup two-dimensional calculational representations. A set of multicycle calculations are also presented as a test of the adjoint formulation for problems involving discontinuous nuclide fields. Final-time nuclide inventories, K_{eff}, and the microscopic ^{238}U capture to ^{239}Pu fission ratio were utilized as representative responses of interest. Perturbations to the reference system included variations in the fissile, fertile, structural and coolant material concentrations within the fast reactor models utilized. Material concentrations were perturbed locally and globally so as to change the distribution as well as magnitudes of the nuclide

and neutron fields within the system. The question of nonlinear behavior for certain perturbation/response pairs was also investigated by varying the magnitude of the material perturbations.

The comparison of predicted responses with direct computation for this large calculational data base clearly demonstrates the remarkable predictive capability of the adjoint depletion formulation implemented within the DEPTH module. This new method can accurately account for variations in the time-dependent neutron and nuclide fields arising from variations in the time-step initial conditions. Thus, multicycle depletion perturbation theory represents an attractive alternate computational method for certain types of burnup analyses, with the greatest cost benefits being associated with repetitive-type scoping calculations.

I. INTRODUCTION

General Comments

Recent changes in the U. S. nuclear energy policy have led to a greatly expanded study of proliferation-resistant nuclear fuel cycles. Several preliminary investigations[1-3] have been performed to assess the feasibility of these alternate fuel cycle concepts. The increased interest in fuel burnup analysis, from this viewpoint and others such as fuel reprocessing and waste management, provides justification for further investigation of the present calculational methods for predicting the time-dependent isotopic content of a nuclear reactor.

Over the past several years static perturbation theory methods have been increasingly used for reactor analyses in lieu of more detailed and costly direct computations. Perturbation methods incorporating time dependence have also received some attention[4-6] and recently several authors have demonstrated their applicability to fuel burnup analysis.[7-9] In addition to time and cost advantages, these perturbation methods permit a detailed understanding of the physical mechanisms responsible for the observed behavior of a given response. These benfits could be especially useful for the repetitive-type scoping calculations being performed in current alternate fuel cycle studies as well as in the design analysis of more conventional reactor concepts.

Gandini[4] first proposed the use of time-dependent perturbation theory for the neutron field in connection with the analysis of reactor kinetic experiments. Starting from these generalized perturbation formulations in the neutron field which were obtained from the importance conservation

principle, he later[5] showed that perturbation expressions for the nuclide field could be derived by analogy. For this analysis he simply replaced the neutron and precursor densities with the nuclide density and utilized the buildup and decay matrix in place of the Boltzmann operator. Komata[6] also showed that a time-dependent perturbation theory formulation similar to Gandini's could be derived using both a formal mathematical procedure as used in standard perturbation theory and a variational principle technique as suggested by Pomraning.[10]

Gandini[7] and Tondinelli[8] have applied these new perturbation theory techniques for the nuclide field to burnup and buildup problems during the reactor operating history and to sensitivity analyses of actinide production estimates. Williams[9] has also recently implemented a similar capability into the ORIGEN[11] isotope generation and depletion code and has applied the theory to compute the plutonium production in a thermal reactor with an emphasis on sensitivity and uncertainty analyses.

The above studies, however, did not consider the nonlinear interaction between the neutron and nuclide fields. The neutron flux field was assumed unchanged when a nuclide or data perturbation was made. Kallfelz[12] addressed this problem by linking time-dependent perturbation theory for the nuclide field with static generalized perturbation theory for the flux field. Using this method he was able to calculate the "indirect effect" of a nuclide perturbation.[†] However, the theory was still somewhat limited in scope and could not be applied to typical reactor depletion problems.

[†]It should be noted that this "indirect effect" is very similar to the "Γ^* effect" defined later in this study.

Williams[13-15] has recently developed a coupled neutron/nuclide depletion perturbation theory that is sufficiently general to be applicable to problems of arbitrary complexity. This theoretical framework, derived using a variational principle, is compatible with the conventional "quasi-static" method for solving realistic reactor depletion problems.[†] It has been shown that three adjoint equations (for the flux shape, flux normalization, and nuclide density) are required to fully account for variations in both the neutron and nuclide fields arising from variations in initial conditions and nuclear data. The nuclide density adjoint equation in this coupled formulation is identical to that obtained in the previously mentioned uncoupled formulations. Thus, the present time-dependent perturbation theory is the most general in that it takes into account all first-order effects. Additionally, it should be noted that the coupled formulation reduces to the uncoupled case when zero flux normalization and shape variations are assumed.

The final value problem comprising this coupled set of adjoint equations defines a sensitivity function which relates changes in some specified integral response function to variations in the material concentrations initially loaded in the reactor. Once this importance function has been calculated, the effect of an initial condition perturbation can be estimated by the evaluation of a simple integral expression. Since the importance function is independent of the specific perturbation, a single adjoint calculation allows one to investigate the effects of any number of initial condition variations.

[†] Beware of difference in terminology from kinetics studies.

Williams has applied this coupled neutron/nuclide depletion perturbation theory to the analysis of two simplistic infinite homogeneous reactor models.[13] In both cases, analytic results obtained using time-dependent perturbation theory agreed well with direct calculation of the perturbed responses. However, prior to the present work, the theory has not been applied to any realistic depletion analysis problems.

In addition, in the derivation of the nuclide adjoint equation, Willaims assumed that the forward nuclide densities were continuous across the time boundaries of the quasi-static approximation. In general, this assumption is not valid. Typical depletion calculations include simulated control rod movement or nuclide (fuel or poison) concentration searches at each time step during the depletion cycle. At cycle boundaries, fuel assembly shuffling and discharge or the addition of makeup feed also result in large nuclide discontinuities. Thus the present theory of Williams, although very general in most aspects, is somewhat restricted by the continuous nuclide field assumption.

Scope and Organization

The objectives of the present work are 1) to extend the capability of depletion perturbation theory as developed by Williams to include nuclide field discontinuities, 2) to implement a procedure for the solution of the resultant adjoint equations, and 3) to evaluate the overall coupled neutron/nuclide time-dependent perturbation theory for a variety of realistic depletion problems by comparison with results obtained using conventional methods.

The achievement of these goals are documented in the remainder of this report. Section II first presents a review of the conventional

depletion equations and then introduces the system of equations adjoint to the forward quasi-static multicycle burnup equations. Section III briefly describes the specific algorithms and computational methods utilized to solve both the forward and adjoint problems. A rather lengthly Section IV presents the numerical results from a variety of test problems utilized to verify the adequacy and generality of multicycle depletion perturbation theory. The major conclusions of the study and some recommendations for future research are presented in Section V. Lastly, Appendices A and B provide a complete derivation of the multicycle adjoint equations and a detailed description of the nuclide adjoint jump condition term involving the generalized adjoint shape function.

II. THE MULTICYCLE DEPLETION PERTURBATION THEORY FORMULATION

The purpose of this section is to present a review of the conventional depletion equations and to introduce the system of equations adjoint to the forward quasi-static burnup equations. It will be shown how a depletion perturbation theory formulism can be developed using these adjoint functions and how it may be used as a computational tool in multicycle reactor depletion analysis.

The Quasi-Static Burnup Equations

In burnup analyses, one is interested in the interaction between the nuclide density field and the neutron flux field within the reactor over relatively long periods of time. The nuclide field obeys the nuclide transmutation equation, while the flux field is assumed to obey the diffusion theory approximation to the neutron transport equation. In general, these coupled equations can be written as,

1. Nuclide Transmutation Equation:

$$\frac{\partial}{\partial t} \underline{N}(\vec{r},t) = \underline{\underline{M}}(\vec{r},t)\, \underline{N}(\vec{r},t) \tag{2.1}$$

where $\underline{N}(\vec{r},t)$ = space and time-dependent nuclide density vector describing the material configuration of the reactor and,

$\underline{\underline{M}}(\vec{r},t)$ = space and time-dependent transmutation operator which can be written as

$$\underline{\underline{M}}(\vec{r},t) = \underline{\underline{T}}(\vec{r},t) + \underline{\underline{D}} \tag{2.2}$$

with $\underline{\underline{T}}(\vec{r},t) = \underline{\underline{T}}\,[\sigma(\vec{r},E,t),\ \phi(\vec{r},E,t)]$

$\underline{\underline{T}}(\vec{r},t)$ = microscopic reaction rate matrix whose off-diagonal elements represent the production rate of nuclide i by nuclide j and whose diagonal terms are the loss rate of nuclide i (ex. $a_{ii} = \int - \sigma_a(\vec{r},E,t)\ \phi(\vec{r},E,t)dE$).

$\underline{\underline{D}}$ = decay matrix whose off-diagonal elements represent the decay rate of nuclide j to nuclide i and whose diagonal elements are the total decay constant for nuclide i.

2. Diffusion Equation (operator notation):

$$B\phi(\vec{r},E,t) = \frac{1}{v}\ \frac{\partial}{\partial t}\ \phi(\vec{r},E,t) \tag{2.3}$$

where

$B = B[\underline{N}(\vec{r},t),\ \sigma(\vec{r},E,t)]$

= diffusion operator (fission operator and a leakage, removal, and inscatter operator).

For depletion analyses, however, $\phi(\vec{r},E,t)$ is usually a slowly varying function of time. Therefore, the term on the right-hand side of equation (2.3) can be neglected giving

$$B(\underline{N},\sigma)\ \phi(\vec{r},E,t) = 0 \quad . \tag{2.4}$$

In writing the above equations, care has been taken to point out that the flux field is dependent on the nuclide field through the diffusion operator and that the nuclide field is a function of the neutron flux through its coupling in the transmutation operator. In addition to this interaction, the flux and nuclide fields are also coupled through the reactor power constraint, given by

3. Reactor Power Constraint:

$$P(t) = \int\int \underline{N}^T(\vec{r},t)\ \underline{\underline{E}}_p\ \underline{\sigma}_f(\vec{r},E,t)\ \phi(\vec{r},E,t)d\vec{r}\ dE \tag{2.5}$$

where

$\underline{\underline{E}}_p$ = diagonal matrix of nuclide-dependent energy per fission conversion factors.

In this study, the system of three coupled nonlinear equations given by equations (2.1), (2.4) and (2.5) is referred to as the general nonlinear burnup equations. In practice, these equations cannot be solved exactly, and therefore some suitable approximation needs to be made.

One practical method for solving the nonlinear burnup equations essentially decouples the flux and nuclide fields by assuming that the flux defined in equation (2.4) is separable in time. Under this assumption, the neutron flux can be written as

$$\phi(\vec{r},E,t) = \alpha(t)\ \psi(\vec{r},E) \quad \text{for } t_1 < t < t_2 \tag{2.6}$$

where $\alpha(t)$ is the time-dependent normalization and $\psi(\vec{r},E)$ is the space- and energy-dependent neutron flux that satisfies the homogeneous time-independent diffusion equation. In this "quasi-static" approximation, t_1 and t_2 define the time interval over which $\psi(\vec{r},E)$ and the cross-section data are assumed constant.

Even with these approximations, the transmutation matrix in equation (2.1) is still a continuous function of time due to the time-dependent flux normalization factor. However, in practice, the flux normalization as specified by the reactor power is also approximated as a piecewise

constant function of time, essentially breaking the interval $t_1 < t < t_2$ into several subintervals. Within each substep, the transmutation matrix is constant in time, making the solution of equation (2.1) quite straightforward. At t_2 a new flux-eigenvalue calculation is performed and the transmutation equation solved once more using the new $\psi(\vec{r},E)$. Utilizing a procedure like this, one can predict the time-dependent performance characteristics of a nuclear reactor.

A schematic representation of this quasi-static burnup approximation is given in Figure 2.1. It should be noted that this approximation introduces discontinuities into the burnup equations. That is, the nuclide density is discontinuous at cycle and time-step boundaries, the flux shape becomes discontinuous at time-step boundaries, and the flux or power normalization is characterized by discrete step changes at sub-step interfaces. As will be shown later, the quasi-static adjoint burnup equations exhibit a similar behavior at the time boundaries.

The detailed forward quasi-static depletion equations, employing the notation described in Appendix A, are summarized in the first half of Table 2.1. Under the quasi-static approximation, equations (2.7) through (2.12) completely define the state of the reactor at any point in time. The first of these equations describes the zone-averaged depletion process for each ijk time interval within each reactor region. The sz subscripts represent subzone s in zone z. The terms in the brackets of equation (2.7) are just a more detailed representation of the transmutation matrix given in equation (2.1), showing its dependence on both the shape and magnitude of the flux. The initial condition at the cycle boundary represents the refueling process, while this condition

OPERATION	TIME BOUNDARY WHERE OPERATION IS ALLOWED		
	CYCLE k	TIME STEP i	SUBSTEP j
REFUELING/SHUFFLING/DISCHARGE	X		
CONTROL MOVEMENT/NUCLIDE SEARCHES	X	X	
FLUX-EIGENVALUE CALC	X	X	
CROSS SECTION ASSIGNMENT	X	X	
POWER NORMALIZATION	X	X	X

NOTATION

x^{ijk} INDICATES THAT x IS CONSTANT OVER THE ijk INTERVAL

$y^{ijk}(t)$ INDICATES THAT y IS A CONTINUOUS FUNCTION OF TIME WITHIN THE ijk INTERVAL

z INDICATES THAT z IS INDEPENDENT OF TIME

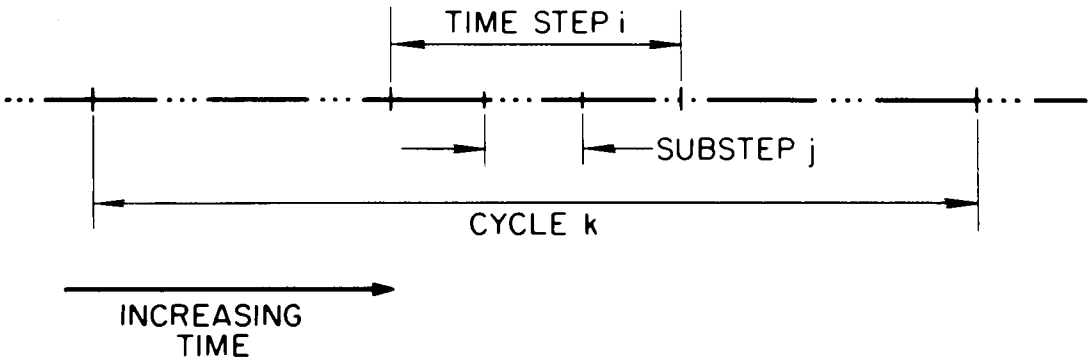

Figure 2.1. Schematic Representation of Quasi-Static Burnup Approximation.

TABLE 2.1

FORWARD AND ADJOINT QUASI-STATIC BURNUP EQUATIONS

FORWARD	ADJOINT
1. Nuclide Density:	1. Adjoint Nuclide Density:
$\frac{d}{dt}\underline{N}_{sz}^{ijk}(t) = \left[\alpha^{ijk}\,\underline{\underline{X}}_{sz}^{ik}\,\underline{\psi}_z^{ik} + \underline{\underline{D}}\right]\underline{N}_{sz}^{ijk}(t)$ (2.7)	$\frac{d}{dt}\underline{N}^{*ijk}_{sz}(t) = -\left[\alpha^{ijk}\,\underline{\underline{X}}_{sz}^{ik}\,\underline{\psi}_z^{ik} + \underline{\underline{D}}\right]^T\underline{N}_{sz}^{*ijk}(t)$ (2.24)
with initial condition	with final condition
$\underline{N}_{sz}^{ik}(t_{ik}) = \underline{C}_{sz}^{ik}(t_{ik})$ (2.8)	$\underline{N}_{sz}^{*}(t_f) = \frac{\partial R}{\partial \underline{N}_{sz}}(t_f)$ (2.25)
where	and jump condition
$\underline{C}^{ik} = \begin{bmatrix}\underline{N}_1\\ \cdot\\ \cdot\\ \cdot\\ \underline{N}_{NREG}\end{bmatrix}^{ik} = \underline{\underline{P}}_{SD}^{ik}\,\underline{Z}^{ik-} + \underline{M}^{ik}$ (2.9)	$\underline{N}_{sz}^{*ijk} = \underline{N}_{sz}^{*ijk+} + \underline{P}_{sz}^{*ijk+}\text{effect} + \underline{\Gamma}_{sz}^{*ijk+}\text{effect}$ (2.26)
$\underline{Z}^{ik-} = \begin{bmatrix}\underline{N}_1\\ \cdot\\ \cdot\\ \cdot\\ \underline{N}_{NREG}\end{bmatrix}^{ik-}$ $\quad \underline{M}^{ik} = \begin{bmatrix}\underline{M}_1\\ \cdot\\ \cdot\\ \cdot\\ \underline{M}_{NREG}\end{bmatrix}^{ik}$	where
	$P_{sz}^{*ijk+}\text{effect} = -P^{*ijk}\,\alpha^{ijk}\,\underline{\underline{E}}_p\,\underline{\underline{\sigma}}_{f_{sz}}^{ik}\,\underline{\psi}_z^{ik}$ (2.27)
	$\underline{\Gamma}_{sz}^{*ijk+}\text{effect} = -\frac{1}{v_z}\int_{v_z}\underline{\Gamma}^{*T}{}^{ik}(\vec{r})\,\frac{\partial}{\partial \underline{N}_{sz}^{ik}}\left\{(\underline{\underline{L}}-\lambda\underline{\underline{F}})\,\underline{\psi}^{ik}(\vec{r})\right\}$ for $j = 1$ (2.28)
	$\underline{\Gamma}_{sz}^{*ijk+}\text{effect} = 0 \quad \text{for } j \neq \underline{1}$
	and adjoint refueling discontinuity
	$\underline{Z}^{*ijk-} = \underline{\underline{P}}_{SD}^{T\,ijk}\,\underline{Z}^{*ijk}$ (2.29)

$\underline{\underline{P}}_{SD}^{ik}$ = shuffling/discharge operator

$\underline{M}^{ik}$ = makeup feed vector

NREG = total number of regions in problem

TABLE 2.1 (continued)

FORWARD	ADJOINT
2. Power Normalization:	2. Power Adjoint:
$P^{ijk} = \alpha^{ijk} \sum_z \sum_s \underline{N}_{sz}^{T^{ijk}} \underline{\underline{E}}_p \underline{\underline{\sigma}}_{f_{sz}}^{ik} \underline{\psi}_z^{ik} v_{sz}$ (2.10)	$P^{*ijk} = \frac{1}{P^{ijk}} \left[\left(\alpha \frac{\partial R}{\partial \alpha} \right)^{ijk} + \alpha^{ijk} \sum_z \sum_s v_{sz} \int_{\text{substep } j} \underline{N}_{sz}^{*T^{ijk}}(t) \underline{\underline{X}}_{sz}^{ik} \underline{\psi}_z^{ik} \underline{N}_{sz}^{ijk}(t)\, dt \right]$ (2.30)
3. Flux Shape:	3. Adjoint Flux Shape:
$(\underline{\underline{L}} - \lambda \underline{\underline{F}})^{ik} \underline{\psi}^{ik}(\vec{r}) = 0$ (2.11)	$(\underline{\underline{L}} - \lambda \underline{\underline{F}})^{T^{ijk}} \underline{\Gamma}^{*ik}(\vec{r}) = \underline{S}_z^{*ik}$ (2.31)
where $\underline{\phi}^{ijk}(\vec{r}) = \alpha^{ijk} \underline{\psi}^{ik}(\vec{r})$	where
$\underline{\underline{L}}$ = leakage, removal and inscatter operator	$\underline{S}_z^{*ik} = \frac{\partial R}{\partial \underline{\psi}_z^{ik}} + (A^{*ik} \cdot \underline{1})$ (2.32)
$\underline{\underline{F}}$ = fission source operator	$+ \sum_j \frac{\alpha^{ijk}}{v_z} \sum_s v_{sz} \int_{\text{substep } j} \underline{N}_{sz}^{*T^{ijk}}(t) \underline{\underline{X}}_{sz}^{ik} \underline{N}_{sz}^{ijk}(t)\, dt$
$\lambda = \frac{1}{K_{eff}}$ = lambda mode eigenvalue	$- \sum_j \frac{1}{v_z} \sum_s v_{sz} P^{*ijk} \alpha^{ijk} \underline{N}_{sz}^{T^{ijk}} \underline{\underline{E}}_p \underline{\underline{\sigma}}_{f_{sz}}^{ik}$

TABLE 2.1 (continued)

FORWARD	ADJOINT
4. Flux Shape Normalization:	4. Additional Relationships:
$\sum_z v_z \sum_g \psi_{gz}^{ik} = 1$ (2.12)	$A^{*ijk} = -\sum_j \left(\alpha \frac{\partial R}{\partial \alpha}\right)^{ijk} + \int_{\substack{\text{all}\\\text{space}}} \left[\underline{\psi}(\vec{r}) \frac{\partial R}{\partial \underline{\psi}(\vec{r})}\right]^{ik} d\vec{r}$ (2.33)
	$\int_{\substack{\text{all}\\\text{space}}} \left[\underline{\Gamma}^{*T}(\vec{r}) \underline{\underline{F}}\, \underline{\psi}(\vec{r})\right]^{ik} d\vec{r} = 0$ (2.34)
	$\sum_z v_z \left(\underline{\psi}_z^T \underline{S}_z^*\right)^{ik} = 0$ (2.35)

at the time-step interface is to account for control rod movement or any other discontinuity in the nuclide field.

The reactor power constraint (equation 2.10) along with equation (2.12) are the defining equations for the normalization constant, α^{ijk}. Similarly, the time-independent diffusion equation written in operator notation (equation (2.11)) defines the spectral and spatial flux distribution. When taken together, the normalization and distribution functions describe the total group flux vector, $\underline{\phi}(\vec{r})$, in the reactor system.

The solution of the above equations is straightforward and several computer codes have been written specifically for this purpose. The specific calculational scheme utilized for this work will be briefly outlined in Section III.

The Adjoint Equations of Depletion Perturbation Theory

A detailed derivation of the multicycle quasi-static adjoint burnup equations is given in Appendix A. The results of this derivation are summarized on the right side of Table 2.1. Before an explanation of these adjoint equations is undertaken, however, their role in depletion perturbation theory will be demonstrated.

The goal of any perturbation theory, whether static or time-dependent, is the prediction of a perturbed response without direct recalculation of the forward problem. In generalized depletion perturbation theory, the specified integral response, R, can be a functional of both the nuclide and flux fields. This functional takes the general form of

$$R = \int f[\underline{N}(\vec{r},t),\ \phi(\vec{r},E,t)]\ d\vec{r}\ dE\ dt \quad . \tag{2.13}$$

For the purpose of this study, however, only final-time responses were considered due to the increased complexity when time integrated responses are considered. Thus, the response functional is written as a delta function in time. That is,

$$R = \int f[\underline{N}(\vec{r},t),\ \phi(\vec{r},E,t)]\ \delta(t - t_f)\ d\vec{r}\ dE\ dt \quad . \tag{2.14}$$

For the derivation of the perturbation expressions relating a change in the reference response to a design or data variation, we will use a variational technique similar to that utilized in reference 13. With this method, the space-continuous form of the forward quasi-static burnup equations defined in equations (2.7)-(2.12) are treated as constraints on the response defined in equation (2.14). These constraint equations are appended to the response functional using Lagrange multipliers. Using this technique one can define the following K-functional

$$\begin{aligned}
K(\underline{N},\alpha,\underline{\psi},\lambda,\beta,P,\underline{C}) &= R(\underline{N},\alpha,\underline{\psi}) \\
&- \sum_k \sum_i \int_{\substack{\text{all}\\ \text{space}}} d\vec{r}\ \underline{\Gamma}^{*T}{}^{ik}(\vec{r})\ [(\underline{\underline{L}} - \lambda\underline{\underline{F}})\ \underline{\psi}(\vec{r})]^{ik} \\
&+ \sum_k \sum_i \sum_j P^{*ijk}\ [P^{ijk} - \alpha^{ijk} \int_{\substack{\text{all}\\ \text{space}}} d\vec{r}\ \underline{N}^{T}{}^{ijk}(\vec{r})\ \underline{\underline{E}}_p\ \underline{\underline{\sigma}}_f^{ik}(\vec{r})\ \underline{\psi}^{ik}(\vec{r})] \\
&- \sum_k \sum_i \sum_j \int_{\substack{\text{all}\\ \text{space}}} d\vec{r} \int_{\substack{\text{substep}\\ j}} dt\ \underline{N}^{*T}{}^{ijk}(\vec{r},t) \left[\frac{d}{dt}\underline{N}^{ijk}(\vec{r},t) - (\underline{\underline{T}}^{ijk}(\vec{r}) + \underline{\underline{D}})\ \underline{N}^{ijk}(\vec{r},t)\right] \\
&- \sum_k \sum_i \int_{\substack{\text{all}\\ \text{space}}} d\vec{r} \int_{\substack{\text{timestep}\\ i}} dt\ \underline{N}^{*T}{}^{ik}(\vec{r},t) \left[\underline{N}^{ik}(\vec{r},t) - \underline{C}^{ik}(\vec{r},t)\right]\ \delta(t - t_{ik}) \\
&- \sum_k \sum_i A^{*ik} \left[\int_{\substack{\text{all}\\ \text{space}}} d\vec{r}\ (\underline{\psi}^{ik^T}(\vec{r}) \cdot \underline{1}) - 1\right] ,
\end{aligned} \tag{2.15}$$

where $\underline{\Gamma}^{*ik}(\vec{r})$, P^{*ijk}, $\underline{N}^{*ijk}(\vec{r},t)$, and A^{*ik} are the Lagrange multipliers.

From the above functional one sees that if K is evaluated with the exact solution to the constraint equation, then

$$K = R \quad . \tag{2.16}$$

A perturbation in either a data parameter β^{ik}, the reactor power P^{ijk}, or the initial condition $\underline{C}^{ik}(\vec{r},t_{ik})$ will result in an alteration in K, or

$$K \rightarrow K' \quad . \tag{2.17}$$

Again, if K' is evaluated with the perturbed solutions to the forward burnup equations, then

$$K' = R' \quad . \tag{2.18}$$

Now expanding K' in a functional Taylor series expansion, one has

$$\begin{aligned} K' = K &+ \left[\frac{\partial K}{\partial \underline{N}}\,\delta\underline{N}\right] + \left[\frac{\partial K}{\partial \alpha}\,\delta\alpha\right] + \left[\frac{\partial K}{\partial \underline{\psi}}\,\delta\underline{\psi}\right] \\ &+ \left[\frac{\partial K}{\partial \lambda}\,\delta\lambda\right] + \left[\frac{\partial K}{\partial \beta}\,\delta\beta\right] + \left[\frac{\partial K}{\partial P}\,\delta P\right] \\ &+ \left[\frac{\partial K}{\partial \underline{C}}\,\delta\underline{C}\right] + 2^{nd} \text{ order terms} \end{aligned} \tag{2.19}$$

where the brackets indicate integration over all phase space. If one can force the quantities $\frac{\partial K}{\partial \underline{N}}$, $\frac{\partial K}{\partial \alpha}$, $\frac{\partial K}{\partial \underline{\psi}}$, and $\frac{\partial K}{\partial \lambda}$ to vanish, then using equations (2.16)-(2.19), one has

$$\Delta R = \left[\frac{\partial K}{\partial \beta}\,\delta\beta\right] + \left[\frac{\partial K}{\partial P}\,\delta P\right] + \left[\frac{\partial K}{\partial \underline{C}}\,\delta\underline{C}\right] + \begin{matrix}\text{2nd order}\\ \text{terms}\end{matrix} . \tag{2.20}$$

Neglecting the second-order terms and assuming $\delta\beta$ is zero (nuclear data perturbations were not considered in this study), equation (2.20) reduces to the following perturbation expression

$$\Delta R = \left[\frac{\partial K}{\partial P}\,\delta P\right] + \left[\frac{\partial K}{\partial \underline{C}}\,\delta \underline{C}\right] \quad . \tag{2.21}$$

From the functional definition in equation (2.15), one has

$$\left[\frac{\partial K}{\partial P}\,\delta P\right] = \sum_k \sum_i \sum_j (P^* \Delta P)^{ijk} \tag{2.22}$$

and

$$\begin{aligned}\left[\frac{\partial K}{\partial \underline{C}}\,\delta \underline{C}\right] &= \sum_k \sum_i \int_{\substack{\text{all}\\ \text{space}}} d\vec{r}\,(\underline{N}^{*T}(\vec{r})\,\Delta \underline{C}(\vec{r}))^{ik} \\ &= \sum_k \sum_i \sum_z \sum_s v_{sz}\,(\underline{N}^{*T}\,\Delta \underline{C})^{ik}_{sz} \quad .\end{aligned} \tag{2.23}$$

Equations (2.21)-(2.23) are the desired generalized depletion perturbation theory expressions. These indicate that if the Lagrange multipliers, P^{*ijk} and $\underline{N}^{*ik}_{sz}$, can be determined, one can predict the change in the reference response due to a perturbation in the reactor power or the time-step initial condition with only the evaluation of a simple integral expression. It should also be emphasized that P^{*ijk} and $\underline{N}^{*ik}_{sz}$ are independent of the specific perturbation and, therefore, only need to be calculated once for each response of interest. Thus several different design perturbations can be investigated once the adjoint functions have been determined.

The true power of depletion perturbation theory as an analytical tool can be realized only if one fully understands the relationship of a design change to the initial condition, $\underline{C}^{ik}$. A sensitivity analysis for any design parameter that can be represented as a nuclide density in the calculational model can be performed using depletion perturbation theory. Design variables such as material choices (fissile, fertile,

structural and coolant), material volume fractions, fissile enrichments and assembly locations (i.e., fuel shuffling), etc., are all represented as nuclide field variations from a reference model. Thus, design perturbations such as these can be represented as an initial condition variation $\Delta \underline{C}^{ik}$, and equation (2.23) can be utilized to predict their effect on some specified response.

The advantages of depletion perturbation theory over static generalized perturbation theory should also be noted. Not only can the immediate effect on a design variation be determined, but the effect of that change on future responses can also be investigated. For example, the effect of a design variation in the initial core specification on the reactivity of subsequent cycles can easily be calculated.

The above generic capabilities and benefits of depletion perturbation theory can be obtained only if the importance functions in equations (2.22) and (2.23) (P^{*ijk} and $\underline{N}_{sz}^{*ik}$, respectively) can be calculated in a straightforward and cost-effective manner. As noted previously, the defining equations for these adjoint functions are derived in Appendix A and are summarized in Table 2.1. Equations (2.24) through (2.35) were derived by forcing the functional derivatives of the K-functional with respect to $\underline{N}$, α, ψ and λ to vanish.

Although the adjoint quasi-static burnup equations appear complicated at first glance, they are very similar in construction and meaning to the forward burnup equations. The forward equations represent an initial value problem while the adjoint set define a final value problem. Each operation performed during the forward depletion calculations has a corresponding adjoint expression. Table 2.2 attempts to display this relationship and thus explain the purpose of each adjoint equation.

TABLE 2.2

ONE-TO-ONE CORRESPONDENCE BETWEEN FORWARD AND ADJOINT DEPLETION OPERATIONS

FORWARD	ADJOINT
Initial condition on nuclide field (Equation 2.8)	Final condition on nuclide adjoint field (Equation 2.25)
Forward depletion calculation (Equation 2.7)	Adjoint depletion calculation (Equation 2.24)
Power normalization (Equation 2.10)	Power adjoint calculation (Equation 2.30)
Flux-eigenvalue calculation (Equation 2.11)	Generalized fixed-source adjoint calculation (Equations 2.31 and 2.32)
Normalization discontinuity	P^* jump condition (Equations 2.26 and 2.27)
Flux shape discontinuity	Γ^* jump condition (Equations 2.26 and 2.28)
Refueling/discontinuous nuclide field (Equations 2.8 and 2.9)	Adjoint refueling discontinuity (Equation 2.29)

Because of the similarity in the forward and adjoint problems, the algorithm previously described for solving the quasi-static burnup equations, if reversed in time, can generally be applied to the adjoint problem. Thus the same computational methods used to solve the forward burnup equations can be utilized with only moderate modifications to calculate the adjoint functions from the expressions tabulated in Table 2.1, page 11. Therefore, in principle, solving the adjoint equations should be no more difficult than solving the forward problem. This also suggests that the adjoint functions needed for the perturbation expressions of equations (2.22) and (2.23) can be generated at roughly the same cost as a standard forward depletion calculation. This means that considerable time and cost benefits could be obtained by using depletion perturbation theory as a computational tool when many design variations need to be investigated. Also, since space and time-dependent sensitivity coefficients are a by-product of this approach, a more detailed understanding of various neutronic processes is possible.

The next section will briefly describe the specific algorithms and computational methods utilized to solve both the forward and adjoint problems. It will also address some of the details of the adjoint calculation and point out where possible improvements could be made.

III. SOLUTION OF THE BURNUP EQUATIONS

As stated previously, several computer codes have been written specifically for the accurate and efficient solution of the forward quasi-static burnup equations. Two of these depletion codes readily available to the author were the CITATION[16] nuclear analysis code and the VENTURE/BURNER modular code system.[17-22] Both of these solve the forward equations exactly as formulated in Table 2.1, page 11.

The CITATION code was originally chosen as the basis for a system to solve both the forward and adjoint burnup equations. The two main reasons for this choice was that CITATION is an older and, therefore, more widely used code and also the programming details of the code were much more familiar to the author. It has one major pitfall, however; it cannot solve a generalized fixed-source adjoint problem. After careful study, it became apparent that major code modifications (completely outside the scope of this work) would be necessary to implement this particular capability into the CITATION code. For this reason, the VENTURE/BURNER modular code system was chosen as the basis for the solution of the adjoint system of equations. The purposes of this section are to familiarize the reader with the VENTURE/BURNER computational system and to describe in some detail the solution algorithm for the adjoint equations within this modular system.

Solution of the Reference Burnup Equations

The VENTURE modular computation system for nuclear reactor core analysis has been under continuing development for the last several years. Reactor analysis problems are solved using multigroup finite-difference diffusion theory techniques. Depletion calculations are

possible and one-, two-, and three-dimensional geometries can be employed. Emphasis in the methods development has been placed on satisfying the requirements for analysis of fast breeder reactors. However, thermal reactor calculations using a simplified cross-section treatment can also be performed.

Some of the major code modules in this system and their computational functions are listed in Table 3.1. These modules, along with many others under development, communicate with each other through the use of standardized interface data files.[23-24] These data files, established by the Committee on Computer Code Coordination (CCCC), contain a variety of information ranging from cross-section data to module instructions. Many of the more frequently used interface files are described in Table 3.2.

Of main concern here is the computational path one would follow in performing a typical burnup analysis with this modular system. If an adjoint calculation is to follow, the reference depletion solution is somewhat more complicated due to the amount of information that needs to be saved for the adjoint calculation. Since the adjoint formulation uses the unperturbed flux and nuclide fields from the reference case, the interface files containing this data must be retained. In addition, due to the method of solution of the fixed-source adjoint calculation, one also needs to perform (and store data from) a regular adjoint and perturbation calculation at each time step during the forward depletion calculation. These additional tasks roughly double the cost of a reference depletion calculation relative to one that is not to be followed by an adjoint calculation. However, the data generated from

TABLE 3.1

MAJOR MODULES OF THE VENTURE/BURNER COMPUTATIONAL SYSTEM

MODULE	FUNCTION
VENTURE	Solves usual neutronic eigenvalue, adjoint, fixed source, adjoint fixed-source, and criticality search problems, treating up to three geometric dimensions. Also does first order perturbation analysis.
BURNER	Solves the nuclide chain equations to estimate the nuclide concentrations at the end of an exposure time and also after a shutdown period.
PERTUBAT	Performs detailed first order static perturbation calculations.
RODMOD	Used to position control rods during the calculation of a reactor history.
DENMAN	Manipulates nuclide interface file. Used to simulate fuel management until such a module is available.
DEPTH	New module used to solve adjoint depletion equations.
Depletion Perturbation Theory	

TABLE 3.2

COMMONLY USED INTERFACE DATA FILES

NAME	CONTENT
CONTRL	Module input instructions.
ISOTXS	Nuclide ordered microscopic cross-section data.
GRUPXS	Group ordered microscopic cross-section data
GEODST	Geometry data.
NDXSRF	Nuclide referencing data.
ZNATDN	Nuclide concentrations.
RZFLUX	Zone average fluxes.
RTFLUX	Regular point fluxes
ATFLUX	Adjoint point fluxes. (regular and fixed-source)
EXPOSE	Basic exposure data.
PERTUB	Perburbation integrals.
FIXSRC	Source for either regular or adjoint fixed-source calculation.

NOTE: Several additional "interface files" have been defined for use in DEPTH, the Depletion Perburbation Theory module.

one reference calculation can be utilized in any number of adjoint calculations for various responses of interest.

The basic calculational path for a reference depletion calculation using the VENTURE modular system is shown in Figure 3.1. It is simply the quasi-static algorithm discussed previously. Additional operations such as nuclide searches, control rod positioning, and more detailed perturbation calculations than provided in the VENTURE module could be performed at each time-step interface as desired. The end-of-cycle eigenvalue calculation, listed as optional in Figure 3.1, is usually performed since this point is quite often the final time for the subsequent adjoint calculation. Data generated at this time point may possibly be needed for the final condition on $\underline{N}^*$, as specified by equation (2.25).

Solution of the Adjoint Depletion Equations

Based on the similarity of the forward and adjoint equations, a time-dependent sensitivity module was developed and integrated within the VENTURE/BURNER modular code system. Called DEPTH (for DEpletion Perturbation THeory), the new module solves for the nuclide adjoint vector and normalization or power adjoint ($\underline{N}^*(\vec{r},t)$ and $P^*(t)$, respectively). It then calculates the generalized adjoint source necessary for the flux adjoint calculation. Using this source, the VENTURE module solves for the generalized adjoint shape function, $\Gamma^*(\vec{r},E)$, and evaluates several integrals involving both the forward and adjoint shape function. Calculational control is then returned to DEPTH where the time-step jump conditions are applied using the previously computed adjoint functions. This procedure is repeated for each depletion time step, backwards

PROBLEM SETUP

A. Cross section preparation

B. User input

LOOP OVER NUMBER OF CYCLES

LOOP OVER NUMBER OF TIME STEPS PER CYCLE

1. VENTURE

A. Flux-eigenvalue calculation and power normalization

B. Regular adjoint calculation

C. Perturbation calculation

D. Write regular flux, adjoint flux and perturbation integrals on interface files

2. BURNER

LOOP OVER NUMBER OF SUBSTEPS PER TIME STEP

A. Depletion calculation

B. Power normalization

C. Write time-step nuclide densities on interface files

3. VENTURE (optional)

A. Through D. above

4. FUEL MANAGEMENT MODULE

A. Perform fuel shuffling/discharge/refuel

B. Write nuclide densities on interface file

INTERFACE FILE MANIPULATION

Figure 3.1. Computational Path for Reference Depletion Calculation.

through time, until the initial time (in the forward sense) has been reached.

The above sequence of calculations is outlined in Figure 3.2. Comparison of this solution algorithm for the adjoint equations with that of Figure 3.1 once again emphasizes the parallelism of the two burnup formulisms. In addition to Figure 3.2, a simplified flow chart of the calculational path within the modular system, emphasizing the communication links between modules, is displayed in Figure 3.3.

The detailed calculational logic programmed into the DEPTH module is illustrated in Figures 3.4 and 3.5. A close analysis of this flow chart as well as the programmed equations given in Table 2.1, page 11, should provide sufficient detail even for the most interested reader. As can be seen, much of the coding in DEPTH was devoted to interface file processing and data management. The only numerical computations of interest in the DEPTH module are the solution to the transmutation equation and the evaluation of the time integrals in the P^* and S^* equations. The numerical techniques utilized are quite standard however.

A straightforward matrix exponential solution was applied to the nuclide chain equations.[19] A system of linear first-order equations given by

$$\frac{d}{dt}\,\underline{N}(t) = \underline{\underline{A}}\,\underline{N}(t) \tag{3.1}$$

has the solution

$$\underline{N}(t+\Delta t) = \underline{\underline{B}}\,\underline{N}(t) \tag{3.2}$$

with

PROBLEM SETUP

A. Use cross section and input from reference calc.

B. Interface files produced in reference calc.

C. $\underline{N}^*(t_f) = \frac{\partial R}{\partial \underline{N}}\Big|_{t_f}$ and other user input

LOOP OVER NUMBER OF CYCLES (Plus 1)

LOOP OVER NUMBER OF TIME STEPS PER CYCLE

1. DEPTH (skip to F on first call to DEPTH)

   A. Calc. Γ^* effect using PERTUB interface files

   B. Apply Γ^* jump condition

   C. Write $\underline{N}_{sz}^{*ik}$ on NSTAR "interface file"

   D. Exit if $t = t_0$

   E. Apply adjoint refueling jump condition

   F. Prepare necessary data for present time step from interface files

LOOP OVER NUMBER OF SUBSTEPS PER TIME STEP

   G. Adjoint depletion calc.

   H. Calc. P^* and apply jump condition

   I. Calc. S^* and write FIXSRC interface file

2. VENTURE

   A. Read FIXSRC and other interface file data

   B. Generalized fixed-source adjoint calc.

   C. Perturbation calc.

   D. Write perturbation integrals on PERTUB interface file

Figure 3.2. Computational Path for Adjoint Depletion Calculation.

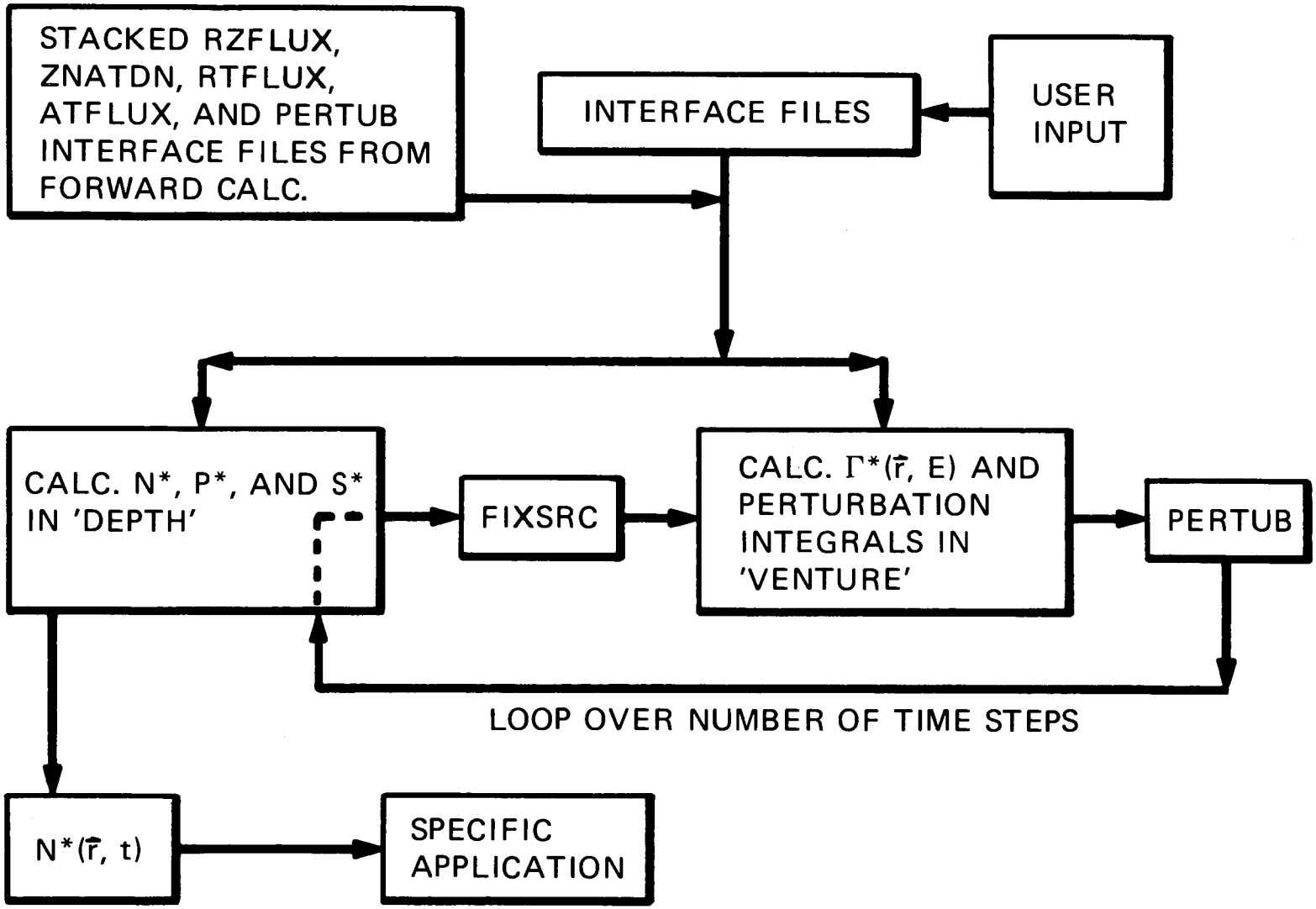

Figure 3.3. Simplified Flow Chart of Calculational Path Within Modular System.

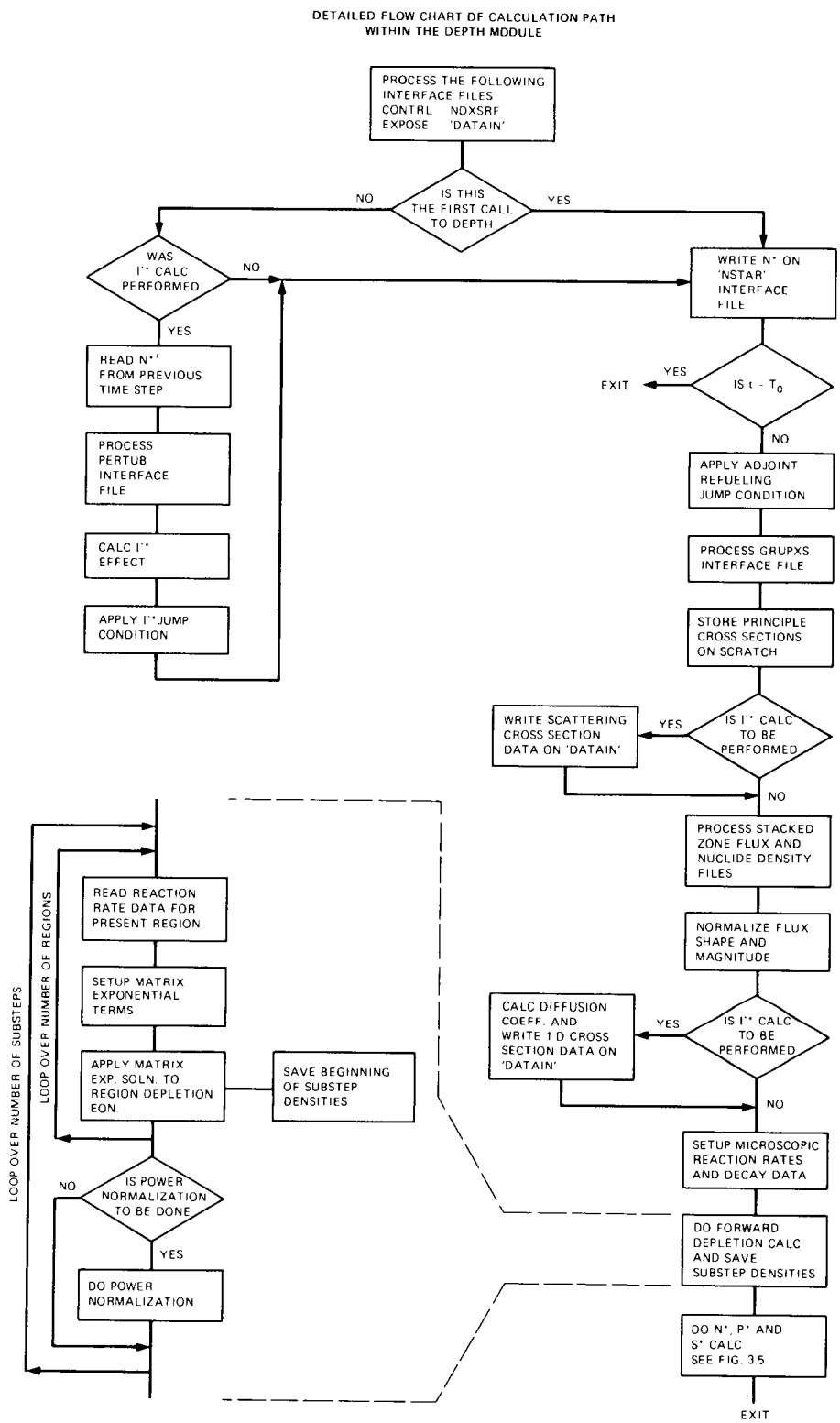

Figure 3.4. Detailed Flow Chart of Calculational Path Within the DEPTH Module.

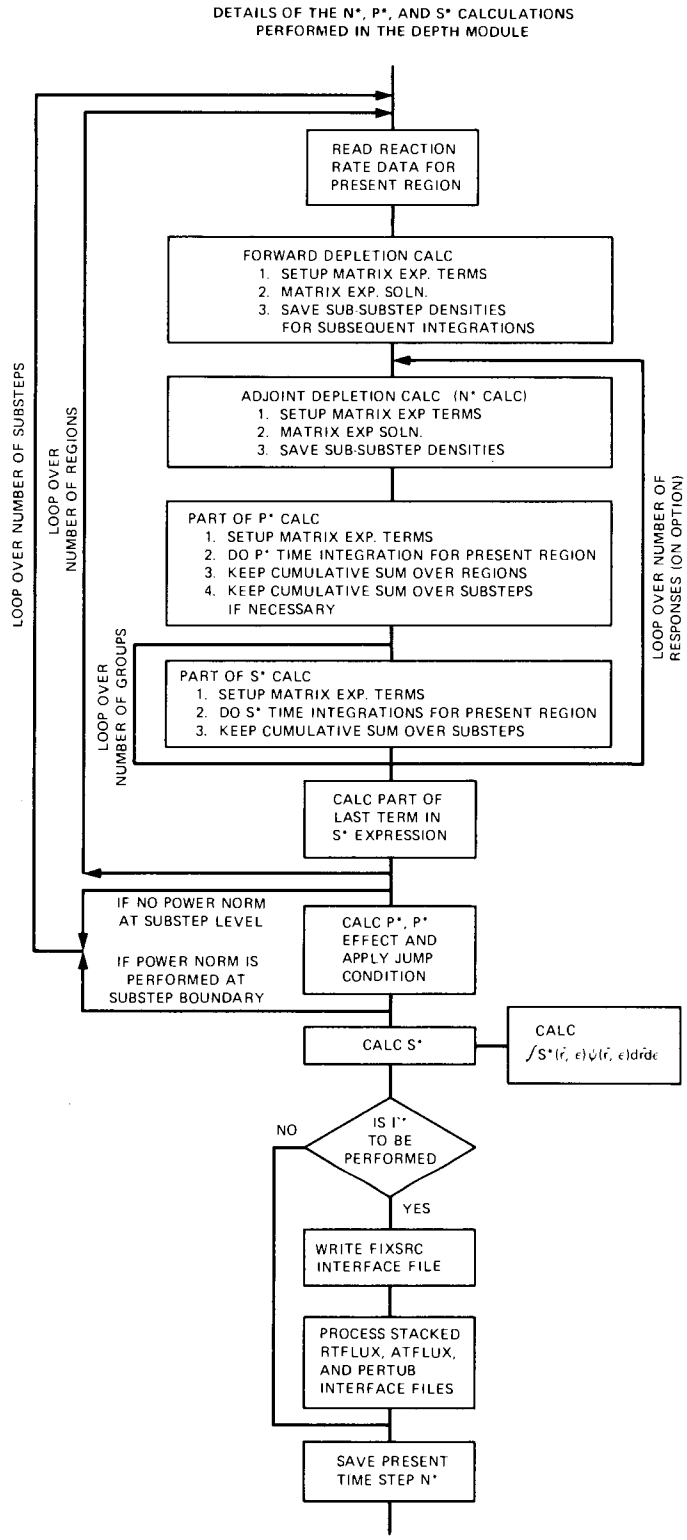

Figure 3.5. Details of the $\underline{N}^*$, P^*, and $\underline{S}^*$ Calculations.

$$\underline{\underline{B}} = \exp\,[\underline{\underline{A}}\Delta t]$$
$$= \underline{\underline{I}} + \underline{\underline{A}}\Delta t + \frac{1}{2!}\,(\underline{\underline{A}}\Delta t)^2 + \ldots \quad . \tag{3.3}$$

Thus, for a given Δt (calculated by DEPTH), the matrix exponential, $\underline{\underline{B}}$, can be easily calculated with convergence limits set by user input. Once $\underline{\underline{B}}$ has been determined, successive matrix multiplications are performed using equation (3.2) to obtain the nuclide density vector at various time points.

In practice only the nonzero elements of $\underline{\underline{A}}$ and $\underline{\underline{B}}$ are stored. In addition to memory requirements, this technique also reduces the computational time required for the evaluation of equation (3.2) since multiplication by zero is eliminated. This simple, efficient, and relatively inexpensive method is utilized to solve both the forward and adjoint burnup equations.

The time integrals are also evaluated using an accurate and efficient numerical scheme.[25] The expression within the integrals is first evaluated using the data generated and stored during a depletion substep. A cubic spline is then fitted to this tabular data. Finally, the fitted spline function is integrated in closed form. The resulting approximation is equivalent to the trapezoid rule plus a correction term involving second derivatives of the spline function. This technique is applied in the evaluation of both P^* and $\underline{S}^*$, equations (2.30) and (2.32), respectively.

Details of the adjoint flux calculation and subsequent evaluation of the perturbation integrals performed within the VENTURE module are documented elsewhere.[18] It should be noted, however, that additional data files from the forward calculation are required for VENTURE to complete its assigned tasks.

The RTFLUX, ATFLUX, and PERTUB data files are necessary for the calculation of the "uncontaminated" generalized adjoint flux. To clarify this statement, recall the generalized adjoint equation (equation (2.31)),

$$(\underline{\underline{L}} - \lambda \underline{\underline{F}})^* \, \underline{\Gamma}^* = \underline{S}^* \tag{3.4}$$

with the associated orthogonality condition (equation (2.34)).

$$\int_{\substack{\text{all}\\ \text{space}}} \underline{\Gamma}^{*T} \underline{\underline{F}} \, \underline{\psi} \, d\vec{r} = 0 \quad . \tag{3.5}$$

Equation (3.4) is an inhomogeneous equation having a general solution made up of homogeneous and particular parts. The regular adjoint flux, $\underline{\phi}^*$, saved in ATFLUX from the forward calculation, is the solution to the homogeneous equation,

$$(\underline{\underline{L}} - \lambda \underline{\underline{F}})^* \, \underline{\phi}^* = 0 \quad . \tag{3.6}$$

Letting $\underline{\Gamma}_p^*$ denote a particular solution, the general solution to equation (3.4) can be written

$$\underline{\Gamma}^* = \underline{\Gamma}_p^* + a \, \underline{\phi}_H^* \quad , \tag{3.7}$$

where "a" is some arbitrary constant. After $\underline{\Gamma}^*_p$ is calculated in the VENTURE module, the unique solution, $\underline{\Gamma}^*$, is determined by "sweeping out" the fundamental mode solution, $\underline{\phi}_H^*$. That is, a unique generalized adjoint function can be defined only if a unique value of "a" exists.

For the problem at hand, the auxiliary condition specified in equation (3.5) can be used to define "a". Substituting equation (3.7) into equation (3.5), one has

$$a = \frac{-\int \underline{\Gamma}_p^* \, \underline{\underline{F}} \, \underline{\psi} \, d\vec{r}}{\int \underline{\phi}_H^{*T} \, \underline{\underline{F}} \, \underline{\psi} \, d\vec{r}} \quad . \tag{3.8}$$

The denominator of equation (3.8) is contained in the PERTUB interface file generated in the forward calculation. The numerator can be evaluated using the contaminated generalized adjoint and the forward point flux file, RTFLUX, also saved from the forward burnup solution. The uniqueness of $\underline{\Gamma}^*$ is then guaranteed by the application of equation (3.7). VENTURE's role is then completed with the evaluation of the following perturbation integrals using the "uncontaminated" generalized adjoint flux,

$$\int \Gamma^*(\vec{r},E) \; \psi \; (\vec{r},E) \; d\vec{r} \quad , \tag{3.9}$$

$$\int \Gamma^*(\vec{r},E) \; \nabla^2 \; \psi \; (\vec{r},E) \; d\vec{r} \quad , \tag{3.10}$$

$$\int \psi \; (\vec{r},E) \left[\int \chi(E) \; \Gamma^*(\vec{r},E) \; dE \right] d\vec{r} \quad . \tag{3.11}$$

These integral evaluations are passed to DEPTH via the PERTUB data file and are then utilized in the evaluation of the Γ^* jump condition.

A key feature built into the DEPTH module is the option to bypass the fixed source adjoint calculation. As apparent from Figure 3.4 and 3.5, the use of this option eliminates a considerable portion of the operations performed in DEPTH. Even more important, however, is the savings associated with bypassing the $\Gamma^*(\vec{r},E)$ calculation within VENTURE, since for many realistic calculational models the forward/adjoint flux

solution completely dominates the overall depletion calculation. Thus, the use of this option allows a fast, inexpensive but less accurate determination of the adjoint importance functions needed for the depletion perturbation expression of equation (2.21).

There are, however, limitations associated with this approximation. When using this option, one implicitly assumes that the perturbation to be investigated will not have a large effect on the spectral or spatial distribution of the flux or that the response of interest is insensitive to such changes. As will be shown in the next section, it is not always obvious which design variations fall into this category. At this point, it will suffice to say that care should be exercised when using this option.

A second feature that may be useful in some instances is available if no $\Gamma^*(\vec{r},E)$ calculation is to be performed. The $\underline{N}^*(\vec{r},t)$ and $P^*(t)$ adjoint importance functions may be determined for any number of responses in one calculation. This option cannot be exercised if the full set of adjoint equations are to be solved because a fixed-source calculation would be necessary for each response. This would be prohibitively expensive in a single calculation. When using the no-Γ^* switch, however, approximate sensitivity coefficients for several responses may be calculated in a single computer run.

Calculational redundancy is also apparent in Figures 3.4 and 3.5, especially in the calculation of the forward nuclide field, $\underline{N}(\vec{r},t)$. The time-dependent nuclide densities were first calculated in the reference depletion calculation. However, only the beginning of time-step concentrations can be saved with the present interface file structure. These concentrations are then passed to DEPTH via a stacked "interface

file." The proper nuclide densities are chosen for the present time interval and another forward depletion calculation is performed so that the beginning of substep densities can be stored. This computation of the nuclide field is necessary because the adjoint solution is performed in reverse time order, thus requiring that the last substep (in the forward sense) be used first in the adjoint calculation. A third forward burnup solution is then performed (see Figure 3.5) so that the nuclide field will be defined at intermediate substep time points for the subsequent P^* and $\underline{S}^*$ time integrations.

An alternate procedure would be to modify the BURNER module to store the forward nuclide concentrations at the desired times and then have DEPTH use these directly. Although this method may be more efficient in terms of computer time, it could create large data-handling problems. In any case, the method programmed seemed to be easier to implement at the time, and, considering the speed of a typical depletion calculation relative to that of an eigenvalue or fixed source problem,it does not compromise a considerable amount of efficiency.

It should be noted that DEPTH was developed as an aid in the evaluation of a time-dependent perturbation method applicable to burnup analysis. As such, it was not intended to be widely distributed as a production module of the VENTURE system. On the other hand, care was taken during the programming phase of this work to insure that the conversion to a fully acceptable and operational module would be a rather straightforward task. The majority of the work would involve the data transfer and storage portions of the code. However, only minor modifications would be required for DEPTH to meet the CCCC's interface file specifications.

Several sample problems have been utilized to examine the adequacy of the DEPTH module as well as the coupled neutron/nuclide perturbation theory concept in general. The following section will describe the details of these test problems and, hopefully, give the reader a better understanding of depletion perturbation theory.

IV. NUMERICAL EXAMPLES

The simplest way to check the validity of a new calculational method is through comparison of results with other well-established numerical techniques. This was the approach taken in this study. Several representative test problems were run using both the DEPTH module and the direct recalculation method to determine various perturbed responses. These sample problems progressed in complexity from simple one-dimensional, one-group cases to more realistic multidimensional, multigroup depletion problems. Multicycle perturbation calculations, utilizing the adjoint refueling discontinuity as discussed previously, were also performed and compared with direct multicycle burnup calculations.

Responses of interest included K_{eff}, reaction rate ratios and nuclide inventories. Due to the simplicity of the adjoint sources involved, the nuclide inventory response was utilized most often. However, the more detailed sources required for the other responses were determined for several cases of interest.

Perturbations to the reference system included variations in the fissile, fertile, structural and coolant material concentrations within the fast reactor models utilized in this study. Material densities were perturbed locally and globally so as to change the distribution as well as magnitude of the nuclide field within the system.

Interpretation of the Adjoint Functions

Perturbations and responses were matched so that the three components of the perturbation formulism (N^*, P^* and Γ^* effects) could be studied separately. Before presenting detailed calculation results, however, the

general effects of any perturbation to the nuclide field should be completely understood. For the purpose of this study, the effect of a nuclide density variation in the mathematical model of a nuclear system is broken into three distinct components. As noted earlier, the response of interest is a functional of the nuclide field, the flux normalization and the flux distribution in both energy and space. That is,

$$R = \int f[\underline{N}(\vec{r},t),\ \alpha(t),\ \psi(\vec{r},E,t)]\ \delta(t-t_f)\ d\vec{r}\,dE\,dt \quad . \tag{4.1}$$

Therefore, the change in a response due to some design perturbation is reflected through the subsequent variation in the nuclide field, flux normalization and/or flux distribution. These three components fully account for the observed response in the perturbed state.

In the examples to follow a variation in R due to a nuclide change is termed the "direct effect" or "N^* effect," a variation in R due to a flux normalization change is called the "P^* effect" and a change in the response due to a variation in the flux distribution is said to be the "Γ^* effect." It should be noted, however, that the contribution of these separate effects to the overall response is somewhat blurred in multistep problems due to the jump conditions that are applied at the time boundaries. However, for one time-step problems the N^*, P^* and Γ^* effects can be tabulated separately displaying the relative contribution of each effect to the overall perturbed response.

The "N^* effect" is due to a direct nuclide change or one coupled through the burnup chain. For example, if the desired response was the ^{233}U inventory at the end-of-cycle (EOC), then a perturbation in the initial ^{233}U concentration would directly contribute to the perturbed response. Likewise, a variation in the ^{232}Th density at beginning-of-cycle

(BOC) would contribute to the perturbed EOC ^{233}U inventory through the burnup chain,

$$^{232}Th \xrightarrow{(n,\gamma)} {}^{233}Pa \xrightarrow{\lambda} {}^{233}U \quad .$$

However, a perturbation in ^{238}U cannot directly affect the response of interest. Thus, the N^* effect for ^{238}U would be zero. Thus one can interpret the adjoint nuclide density vector, $\underline{N}^*(\vec{r},t)$, as the "direct" importance of a nuclide variation to the desired response.

The "P^* effect" is the contribution to the total perturbed response due to a change in the overall flux normalization. The reference normalization is calculated from the power constraint imposed upon the system,

$$\alpha = \frac{P}{\int_{\substack{\text{all}\\ \text{space}}} \underline{N}^T(\vec{r})\, \underline{\underline{E}}_p\, \underline{\underline{\sigma}}_f(\vec{r})\, \underline{\psi}(\vec{r})\, d\vec{r}} \quad . \tag{4.2}$$

From this one sees that if any nuclide having a nonzero microscopic fission cross section is perturbed, there will be a corresponding variation in α. This normalization factor also appears in the transmutation equation and, therefore, will result in a perturbed nuclide field at future times. Thus the $P^*(t)$ adjoint function represents the importance of a normalization change to the integral response of interest.

It should be noted that the P^* effect is not nearly as well behaved as the N^* effect. Much of the direct contribution to the response can be estimated by an analysis of the burnup chains involved. In many cases, however, it is not even clear what algebraic sign the P^* contribution should have. Considering the same example as above (i.e., ^{233}U response and perturbation), one sees that α would decrease with an increase in

^{233}U. This would result in less ^{232}Th capture which would tend to decrease the ^{233}U EOC inventory. However, the ^{233}Pa and ^{233}U loss rates would also decrease, thereby increasing the ^{233}U inventory. Since these tend to cancel each other, it is not clear what sign the P^* effect should carry in systems containing comparable amounts of ^{232}Th and ^{233}U.

The last and probably most interesting contribution to the total change in the response is due to the "Γ^* effect." The spectral and spatial redistribution of the neutron flux field induced by some material perturbation is accounted for in this term. The $\Gamma^*(\vec{r},E)$ adjoint function, therefore, represents the importance of a variation in the neutron flux field within the system to the desired response.

It is the addition of this term that makes the time-dependent perturbation theory utilized in this study superior to those presented by others.[7-9] In most cases the importance of a change in the flux field to the response of interest was assumed to be minimal and therefore excluded from the perturbation formulisms. Thus, the depletion perturbation theory presented here represents the most general approach to the problem, in that all first-order effects are considered.

The price of this generality is the added complexity associated with the computation of the generalized adjoint flux. However, its benefit is that it allows a complete analysis to be performed and also permits the analysis of perturbations not possible with theories that exclude the flux effect. For example, variations in structural, coolant or fission product densities quite often have no direct effect on the response of interest. Also, since they are nonfissionable nuclides, they cannot contribute to the P^* effect. Thus, their contribution to the perturbed response is due solely to their indirect effect on the neutron

balance of the unperturbed system. Several cases where the Γ^* effect plays a dominant role will be illustrated in the numerical examples to follow.

One-Dimensional Calculations

Several sample problems illustrating the use, accuracy, and benefits of depletion perturbation theory have been formulated. However, a one-dimensional spherical fast reactor model was the real workhorse of this study. It was first utilized as a check on the equations coded into DEPTH and later used to validate the depletion perturbation theory in general.

This simplified 1-D calculational model, shown in Figure 4.1, consists of a three-region core surrounded by two radial blanket regions. The reference nuclide concentrations for this system, listed in Table 4.1, are representative of an "equilibrium cycle" $^{233}U/^{238}U$ denatured LMFBR with a ThO_2 radial blanket. Some of the data employed in the burnup calculations performed using this model are given in Table 4.2. Information concerning the transmutation processes modeled in the calculations may be useful in understanding some of the results to follow. In addition, selected data from reference depletion calculations using both 1-group and 9-group cross sections are tabulated in Table 4.3. The unperturbed responses are presented so that actual perturbed responses can be calculated from the $\Delta R/R$ values given later.

Lastly, given in Table 4.4 are the material perturbations made to the reference system. It should be noted that only one nuclide was varied for each case. This was done so that the interpretation of the results would be a rather straightforward procedure. When several perturbations are

CZ = Core Zone
RB = Radial Blanket

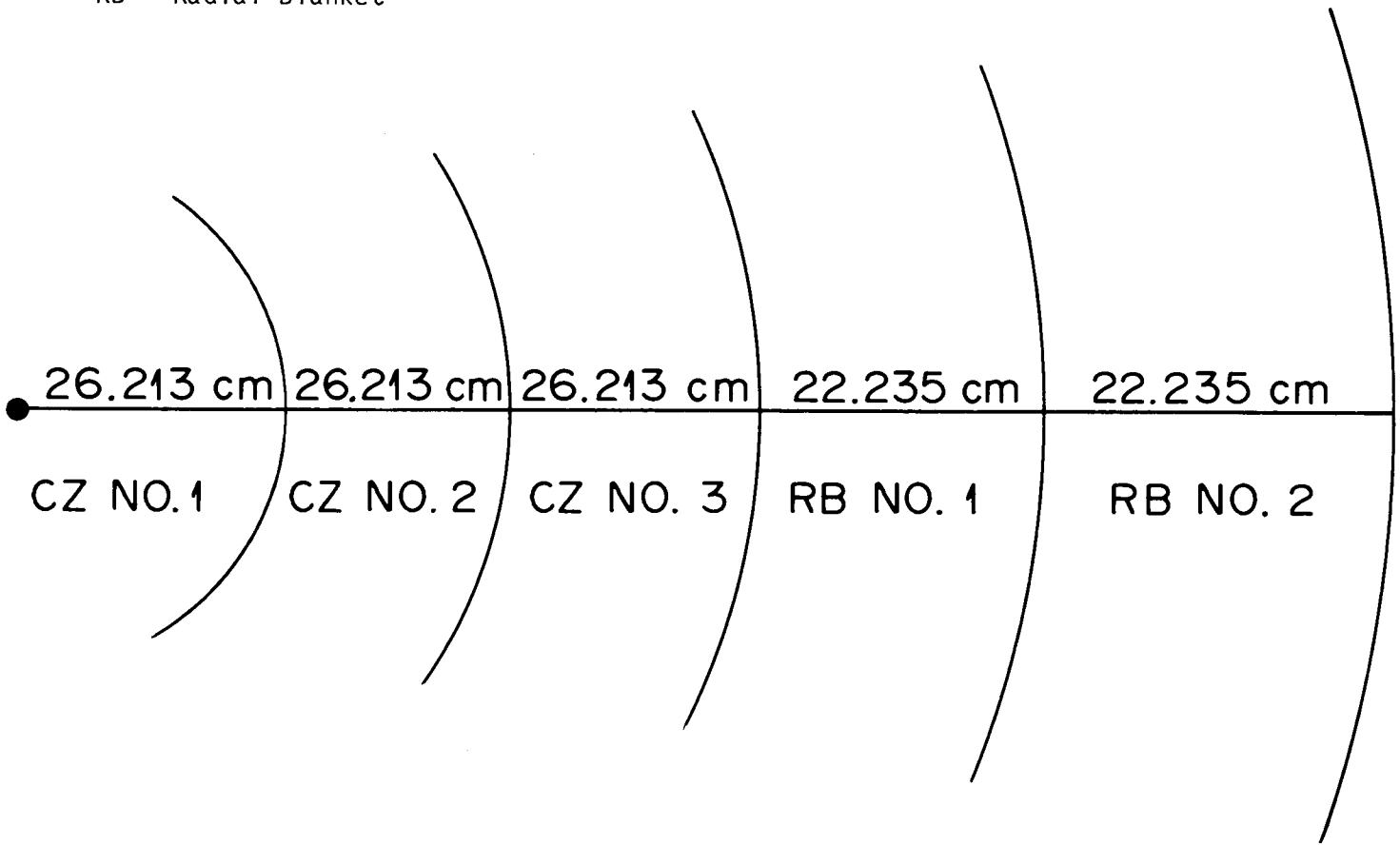

Figure 4.1. 1-Dimensional Spherical Reactor Calculational Model.

TABLE 4.1

REFERENCE BOC NUCLIDE DENSITY VECTORS FOR 1-D MODEL

Nuclide	CZ #1	CZ #2	CZ #3	RB #1	RB #2
TH228	0.0	0.0	0.0	0.0	0.0
TH232	2.7669E-03	2.7669E-03	2.7669E-03	1.4475E-02	1.4475E-02
PA231	0.0	0.0	0.0	0.0	0.0
PA233	0.0	0.0	0.0	0.0	0.0
U 232	0.0	0.0	0.0	0.0	0.0
U 233	8.2324E-04	8.2324E-04	8.2324E-04	1.6422E-04	1.6422E-04
U 234	0.0	0.0	0.0	0.0	0.0
U 235	6.2594E-06	6.2594E-06	6.2594E-06	0.0	0.0
U 236	0.0	0.0	0.0	0.0	0.0
U 238	4.1970E-03	4.1970E-03	4.1970E-03	0.0	0.0
NP237	0.0	0.0	0.0	0.0	0.0
NP239	0.0	0.0	0.0	0.0	0.0
PU238	0.0	0.0	0.0	0.0	0.0
PU239	1.5467E-04	1.5467E-04	1.5467E-04	0.0	0.0
PU240	8.6224E-06	8.6224E-06	8.6224E-06	0.0	0.0
PU241	3.2695E-07	3.2695E-07	3.2695E-07	0.0	0.0
PU242	1.1106E-08	1.1106E-08	1.1106E-08	0.0	0.0
AM241	0.0	0.0	0.0	0.0	0.0
AM243	0.0	0.0	0.0	0.0	0.0
CM244	0.0	0.0	0.0	0.0	0.0
FP RL	0.0	0.0	0.0	0.0	0.0
NA	8.5936E-03	8.5936E-03	8.5936E-03	7.0091E-03	7.0091E-03
SS COR	1.4757E-02	1.4757E-02	1.4757E-02	0.0	0.0
O 16	1.6959E-02	1.6959E-02	1.6959E-02	2.3358E-02	2.3358E-02

TABLE 4.2

DATA SPECIFIED FOR TRANSMUTATION PROCESS

	Transmutations Specified				Decay Data	
	Parent	Daughter	Process		Nuclide	Decay Constants (1/Sec)
1)	TH232	PA233	(N,G)	1)	TH228	1.155999E-08
2)	TH232	PA231	(N,2N)	2)	TH232	1.579999E-18
3)	PA231	U 232	(N,G)	3)	PA231	6.311998E-13
4)	PA233	U 232	(N,2N)	4)	PA233	2.970999E-07
5)	PA233	U 233	DECAY	5)	U 232	2.967999E-10
6)	PA233	U 234	(N,G)	6)	U 233	1.359999E-13
7)	U 232	TH228	DECAY	7)	U 234	8.859997E-14
8)	U 232	U 233	(N,G)	8)	U 235	3.080000E-17
9)	U 233	U 232	(N,2N)	9)	U 236	9.149999E-16
10)	U 233	U 234	(N,G)	10)	U 238	4.870000E-18
11)	U 234	U 235	(N,G)	11)	NP237	9.979996E-15
12)	U 235	U 236	(N,G)	12)	NP239	3.413998E-06
13)	U 236	NP237	(N,G)	13)	PU238	2.539999E-10
14)	U 238	NP237	(N,2N)	14)	PU239	8.999998E-13
15)	U 238	NP239	(N,G)	15)	PU240	3.339998E-12
16)	NP237	PU238	(N,G)	16)	PU241	1.559999E-09
17)	NP239	PU239	DECAY	17)	PU242	5.779996E-14
18)	PU238	PU239	(N,G)	18)	AM241	4.800001E-11
19)	PU239	PU240	(N,G)	19)	AM243	2.749998E-12
20)	PU240	PU241	(N,G)	20)	CM244	1.219999E-09
21)	PU241	PU242	(N,G)			
22)	PU241	AM241	DECAY			
23)	PU242	AM243	(N,G)			
24)	AM243	CM244	(N,G)			

TABLE 4.3

SELECTED DATA FROM REFERENCE 1-D DEPLETION CALCULATIONS

Reactor Power Level 1000 MW(t)						
Selected Data	1-Group Calc Time (Days)			9-Group Calc Time (Days)		
	0.0	91.3	274	0.0	91.3	274
K_{eff}	1.0523	1.0136	0.9686	1.0116	0.9707	0.9245
C8/F9 in cz #1	0.1463	--	--	0.1490	0.1508	--
^{232}U Inventory (KG)	0.0	0.0698	0.2879	0.0	0.0592	0.2404
^{233}U Inventory (KG)	1016.1	980.70	981.98	1016.1	984.33	998.91
^{239}Pu Inventory (KG)	125.07	148.90	192.68	125.07	149.50	194.60

TABLE 4.4

MATERIAL PERTURBATIONS MADE TO REFERENCE SYSTEM

Case #	Nuclide Perturbed at BOC	Location
1	^{232}TH	All core zones
2	^{233}U	All core zones
3	^{233}U	Core zone #3
4	Stainless steel	All core zones
5	Stainless steel	Core zone #1
6	Stainless steel	Core zone #3
7	^{16}O	All core zones

made simultaneously, it often becomes an impossible task to fully understand a particular observed behavior. In many cases cancellation occurs and it is usually not intuitively obvious which effect should dominate. Thus, throughout most of this study, only simple material perturbations were made to the reference system.

Nuclide Inventory Responses (one time step). With the background information now completed, we can finally get to the numerical results. As mentioned earlier, the method used to benchmark the DEPTH module was by comparison of perturbation theory results with direct calculation. Tables 4.5 and 4.6 display the first of several comparisons to be presented. They compare time-dependent linear perturbation theory results with direct calculations for nuclide inventory responses after one depletion timestep (91 full power days). Results using both 1-group and 9-group cross sections are tabulated.

Several points need to be emphasized regarding these results. Let us first concentrate on the last few columns of both tables. Except for a few perturbation/response pairs ($^{233}U/^{232}U$ combinations), the depletion perturbation theory (DPT) results and direct calculations are in excellent agreement. The percent error in the predicted ΔR is generally in the range of only a few percent or less. It should be noted that the perturbation theory in general is only accurate to first order. Thus, these are extremely good results for perturbations on the order of 10% or more.

A second area needing some emphasis is the individual contribution of the three adjoint functions to the total perturbed response. The one depletion-step problems being discussed were designed for exactly this purpose. Perturbation/response pairs were chosen to highlight individual

TABLE 4.5

COMPARISON OF DPT RESULTS WITH DIRECT COMPUTATIONS FOR THE 1-D, 1-GROUP CALCULATIONS

Specified Response (T_f = 91 days)	Case[a] #	Percent Change in Response: Perturbation Results: N^* Effect	P^* Effect	Γ^* Effect	Total	Direct Calculation	% Diff.
^{232}U Inventory	1	1.9667	-0.1259	-0.0132	1.8275	1.8262	0.07
	2	7.1593	-8.7678	-0.0432	-1.6517	-1.4181	16.47
	3	4.0180	-4.7849	-0.0079	-0.7748	-0.7180	7.90
^{233}U Inventory	1	0.1802	0.0035	-0.0083	0.1754	0.1752	0.11
	2	5.8338	0.2420	-0.0256	6.0502	6.0901	-0.66
	3	4.2197	0.1321	0.0591	4.4109	4.4148	-0.09
^{239}Pu Inventory	1	--	-0.0160	0.0019	-0.0141	-0.0141	0.00
	2	--	-1.1119	0.0075	-1.1044	-1.0443	5.76
	3	--	-0.6068	-0.0062	-0.6130	-0.6071	0.97

[a] See Table 4.4.

TABLE 4.6

COMPARISON OF DPT RESULTS WITH DIRECT COMPUTATIONS FOR THE 1-D, 9-GROUP CALCULATIONS

Specified Response (T_f = 91 days)	Case[a]	Percent Change in Response: Perturbation Results: N^* Effect	P^* Effect	Γ^* Effect	Total	Direct Calculation	% Diff.
^{232}U Inventory	1	2.1705	-0.1189	0.0534	2.1050	2.0985	0.31
	2	7.3401	-8.8703	2.5673	1.0370	1.2806	-19.02
	3	4.0213	-4.8351	1.5027	0.6890	0.8531	-19.24
	4	--	--	-2.8108	-2.8108	-2.7300	2.96
^{233}U Inventory	1	0.8134	0.0029	0.0058	0.1805	0.1801	0.22
	2	5.8030	0.2162	-0.0465	5.9726	6.0735	-1.66
	3	4.1991	0.1178	0.0929	4.4099	4.4145	-0.10
	4	--	--	-0.0698	-0.0698	-0.0687	1.60
^{239}Pu Inventory	1	--	-0.0154	-0.0306	-0.0460	-0.0468	-1.70
	2	--	-1.0646	-0.2058	-1.2704	-1.2716	-0.09
	3	--	-0.6253	-0.1330	-0.7583	-0.7425	2.13
	4	--	--	0.1294	0.1294	0.1291	0.23

[a] See Table 4.4.

effects. In particular, the ^{233}U perturbations paired with the ^{233}U response has the "N^* effect" as the dominant term. The change in the ^{239}Pu inventory due to perturbation cases 1-3 are mainly due to the "P^* effect". Finally, as indicated in Table 4.6 the Γ^* effect" is singled out with the stainless steel material variation (case 4). This method of separating the different effects was used to prove that each adjoint function was being properly computed in DEPTH and that they could accurately predict changes in the response due to direct effects, normalization effects and/or flux distributional variations. Careful examination of Tables 4.5 and 4.6 clearly shows that this goal has been accomplished.

With the assurance that everything was being calculated correctly, an attempt was made to explain the isolated discrepancies apparent in Tables 4.5 and 4.6. Further investigation has shown that the observed differences relative to the direct calculations can be directly attributed to nonlinear effects. In fact, if the magnitude of the perturbation is reduced to only a few percent, then the direct and perturbation results become essentially identical.

The degree of nonlinearity varies markedly among the different perturbation/response pairs investigated, with the $^{233}U/^{232}U$ pair being the worst offender. Figures 4.2 through 4.4 show the nonlinear nature of several perturbation/response pairs. The straight lines represent the linear perturbation results while the indicated points are based on direct calculations. Figure 4.2 displays the nonlinearity of the ^{232}U and ^{239}Pu responses in the 1-group calculations due to the increase in the ^{233}U concentration throughout the core. In both these cases the nonlinear behavior can be attributed to the large flux normalization

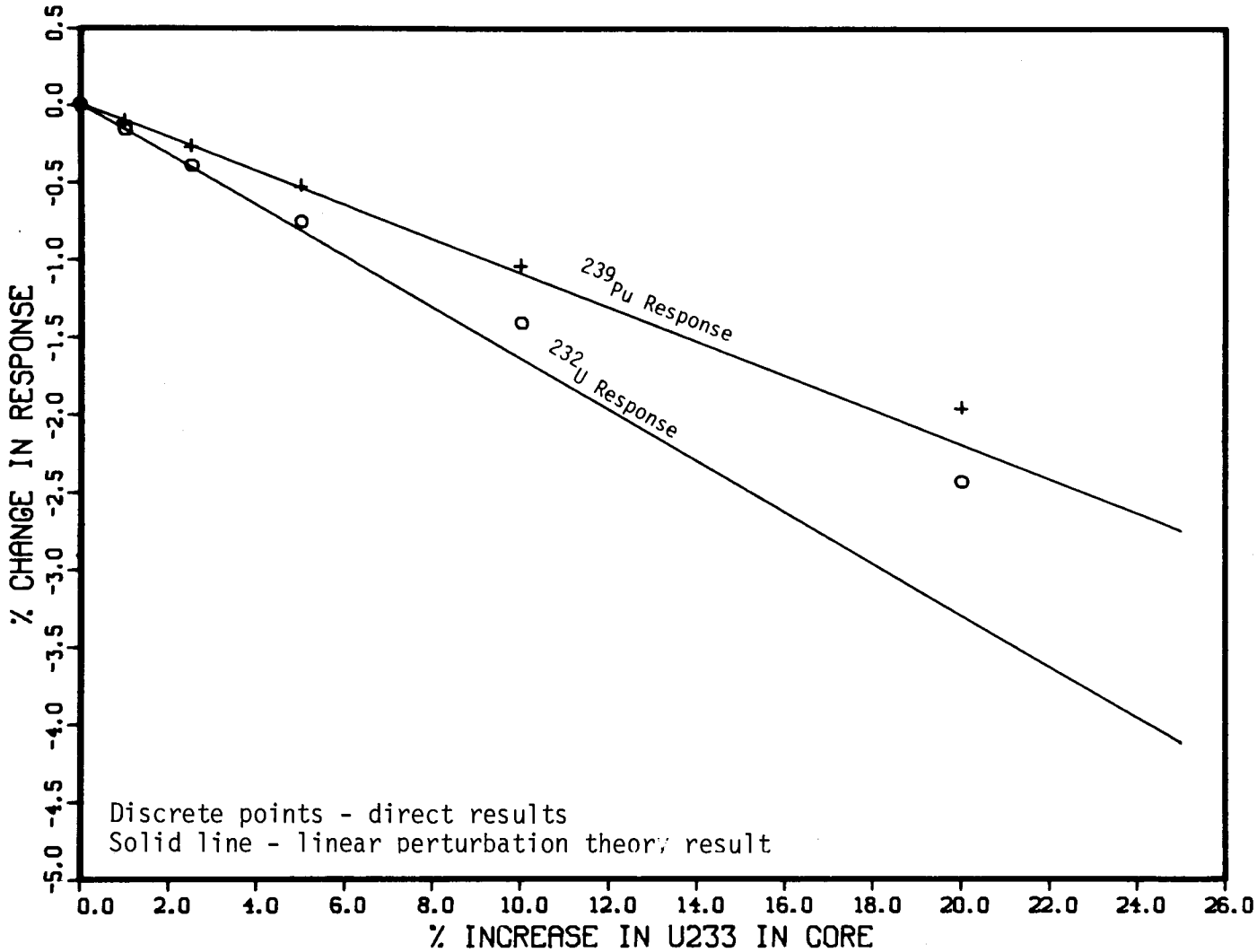

Figure 4.2. Nonlinear Behavior in the 1-D, 1-Group Calculation Due to Large P^* Effects.

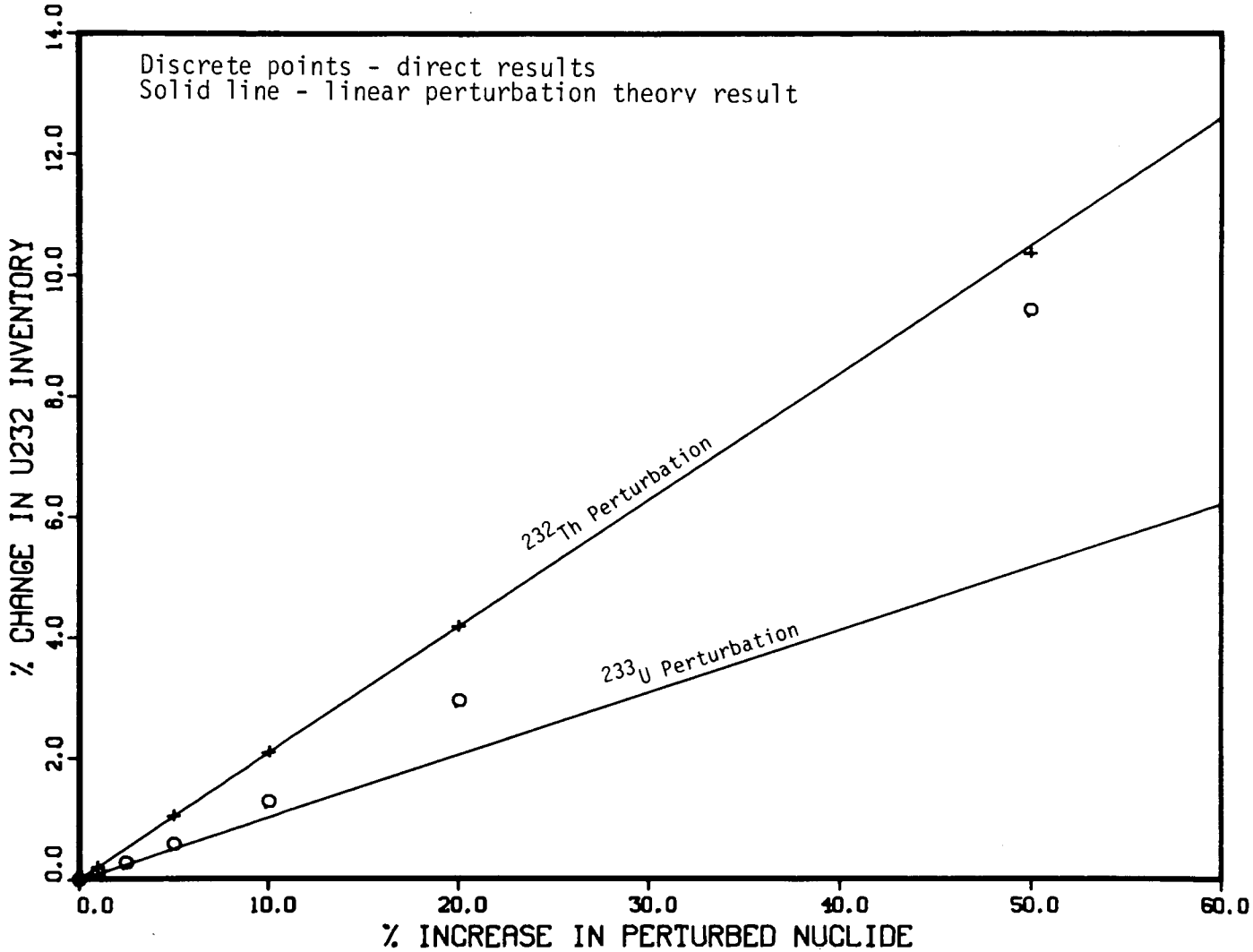

Figure 4.3. Comparison of Nonlinear Behavior Due to Large N* and P* Effects in the 1-D, 9-Group Calculation.

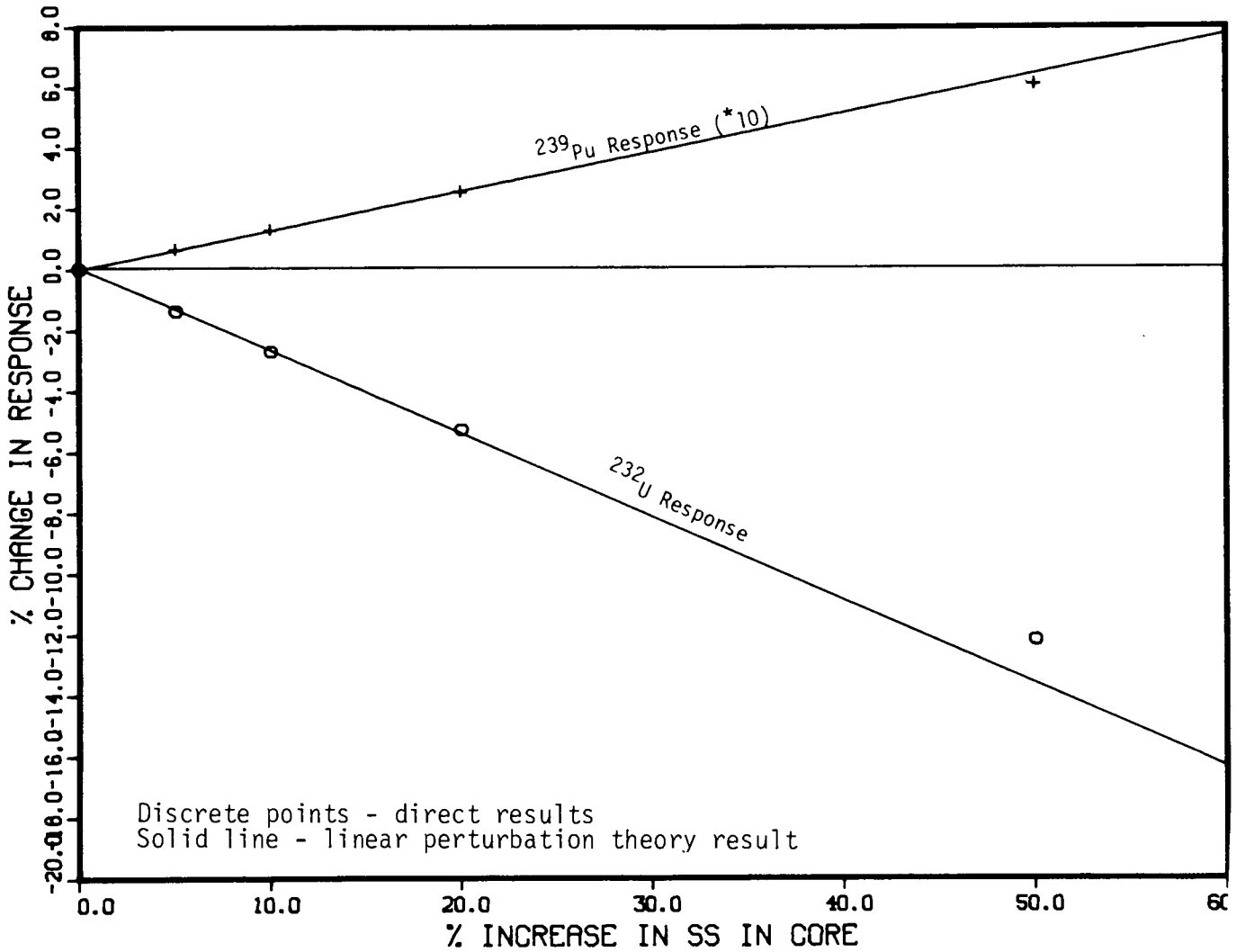

Figure 4.4. Nonlinear Behavior in the 1-D, 9-Group Calculation Due to Large Γ^* Effects.

change associated with the ^{233}U perturbation. For example, a 7% decrease in flux normalization resulted from the 10% increase in ^{233}U concentration. Figure 4.3 emphasizes this observation even further by displaying the effects of different perturbations; one (^{233}U) causing a large normalization change and the other (^{232}Th) affecting the flux magnitude only minimally. Here one see that the results of perturbations of up to 50% in the ^{232}Th density can be accurately predicted. This is due to the N^* effect being the dominant contribution to the perturbed ^{232}U response for a ^{232}Th perturbation. It should be emphasized that in the limit of no flux change (P^* and Γ^* effects are zero), the N^* effect can predict the perturbed response exactly. Therefore, whenever this term dominates, accurate results can be expected for even large material perturbations.

The converse of this statement is also true. If the P^* effect contributes significantly to the overall response, then nonlinear behavior will become apparent with an increase in the perturbation magnitude. This is just the observation made from Figures 4.2 and 4.3. The reason for the extreme nonlinearity of the $^{233}U/^{232}U$ combination relative to the $^{233}U/^{239}Pu$ pair is that the P^* effect is approximately eight times the magnitude of the total ^{232}U response variation.

Another source of nonlinear behavior is from the Γ^* contribution to the overall response. Nonlinearities can be expected when there are large spatial and spectral variations in the flux distribution. This type of nonlinearity can be observed in Figure 4.4 for the ^{232}U and ^{239}Pu responses. The stainless steel density variation in the 9-group problem mainly affected the neutron spectrum rather than

its spatial distribution. Since the production of ^{232}U through (n, 2n) reactions with ^{232}Th and ^{233}U has a high energy threshold, the ^{232}U inventory can be expected to be very sensitive to the first group flux. Figure 4.5 compares the important energy ranges of the reference spectrum at core center to that for the case of the 50% increase in structural material in the core. In this case the first group flux is reduced by about 8% relative to the reference calculation. This large difference is the reason for the nonlinearities observed for the ^{232}U response in Figure 4.4. On the other hand, the ^{239}Pu inventory in the reactor is not nearly as sensitive to spectral changes as the ^{232}U response and, therefore, exhibits a relatively linear and very weak relationship to the stainless steel density in the core.

A final point needs to be made concerning the nonlinear nature of some perturbation/response pairs. Since we are admittedly working with a linear perturbation theory, one cannot expect reliable results for very large perturbations. However, numerical experiments to date have indicated that in many cases very accurate predictions can be made for perturbations as high as 50%. It seems that behavior similar to the $^{233}U/^{232}U$ combination is an exception rather than the rule. Therefore, one should exercise caution when cancelling effects ($N^* = 7.3\%$ and $P^* = -8.9\%$) similar to that for the $^{233}U/^{232}U$ case are observed. In most other cases, experience and intuition should be used as a guide in judging the reliability of perturbation theory results.

By this time the reader should be confident that the DEPTH module is working properly and that the Depletion Perturbation Theory (DPT) utilized in this study can be used to provide reliable estimates of perturbed responses. However, before continuing with examples of more

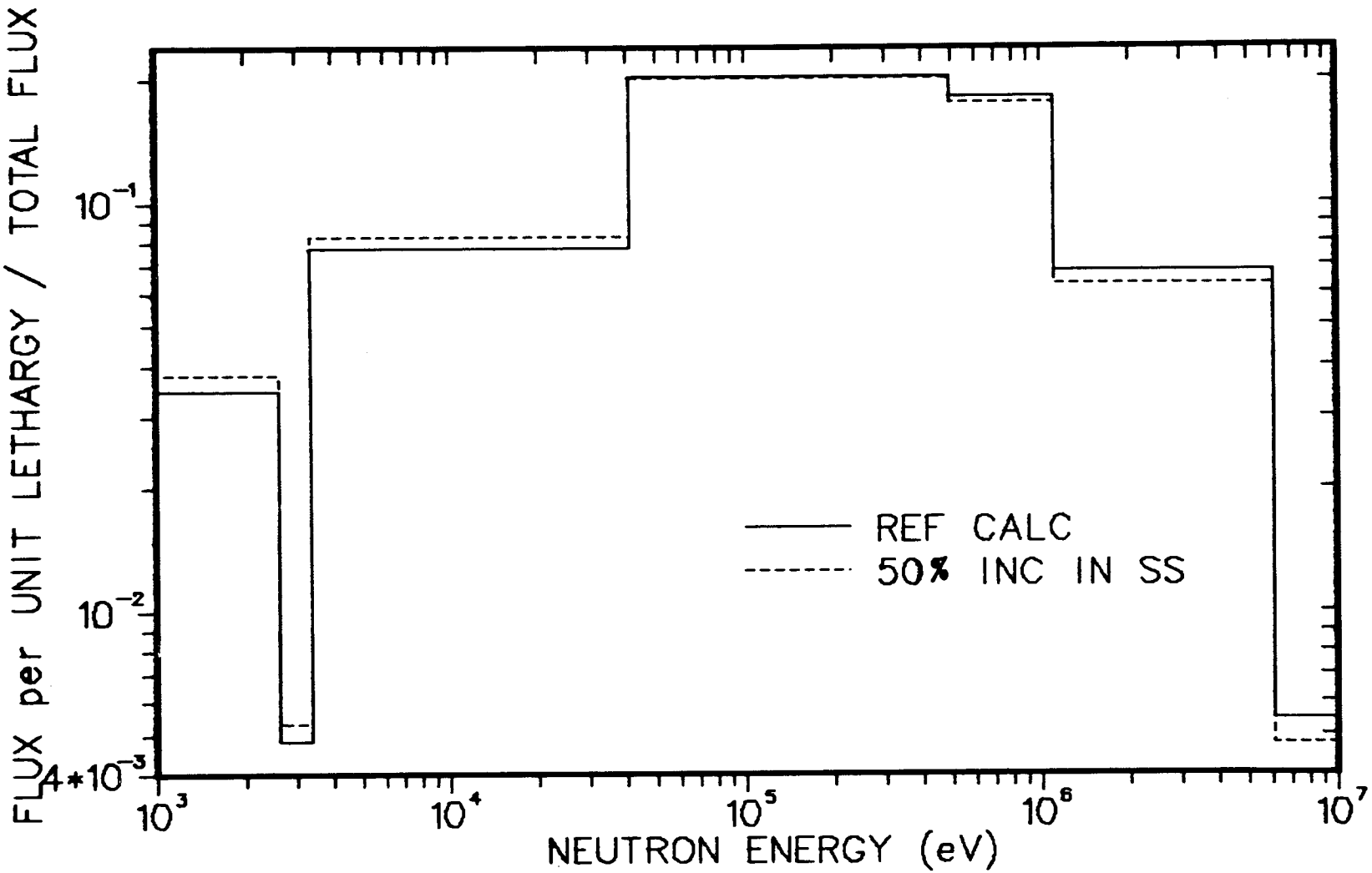

Figure 4.5. Comparison of Flux Spectra at Core Center for a 50% Increase in Stainless Steel Relative to the Reference Case.

realistic depletion problems, one should be aware of some of the details that went into the generation of Tables 4.5 and 4.6.

A Detailed Example. Consider, for example, the ^{232}U response after 91.3 days of reactor operation. The 9-group case (instead of the 1-group calculation) will be considered for the same reasons as mentioned earlier. Although the N^* and P^* effects are very similar, the Γ^* effect is much more interesting for the multigroup calculation. This is due to the strong energy dependence of the ^{232}U response. This energy importance is illustrated in Figure 4.6 where a comparison of 1-group and 9-group ^{232}U responses is made. As apparent, the 1-group response is relatively insensitive to the Γ^* effect caused by the stainless steel perturbation.

The first step in performing a depletion sensitivity analysis is the definition of the desired response functional.† In the present case the response is to be a nuclide inventory at some final time, t_f. Therefore, the response functional can be written as

$$R = \int_{\substack{\text{all}\\ \text{space}}} \underline{h}^T(\vec{r})\ \underline{N}(\vec{r},t_f)\ d\vec{r} \quad , \tag{4.3}$$

where $\underline{h}(\vec{r})$ is a vector that selects the appropriate nuclides for the response of interest. In this instance, it is a constant vector that is only nonzero in the ^{232}U position. The constant converts from atoms to kilograms, since the desired response is kilograms of ^{232}U.

One next needs to determine the three adjoint sources ($\frac{\partial R}{\partial \underline{N}}$, $\frac{\partial R}{\partial \alpha}$ and $\frac{\partial R}{\partial \underline{\Psi}}$ from equations (2.25), (2.30) and (2.32), respectively) that must be

---

†It is assumed that a forward reference depletion calculation has already been performed. See Figure 3.1, page 26.

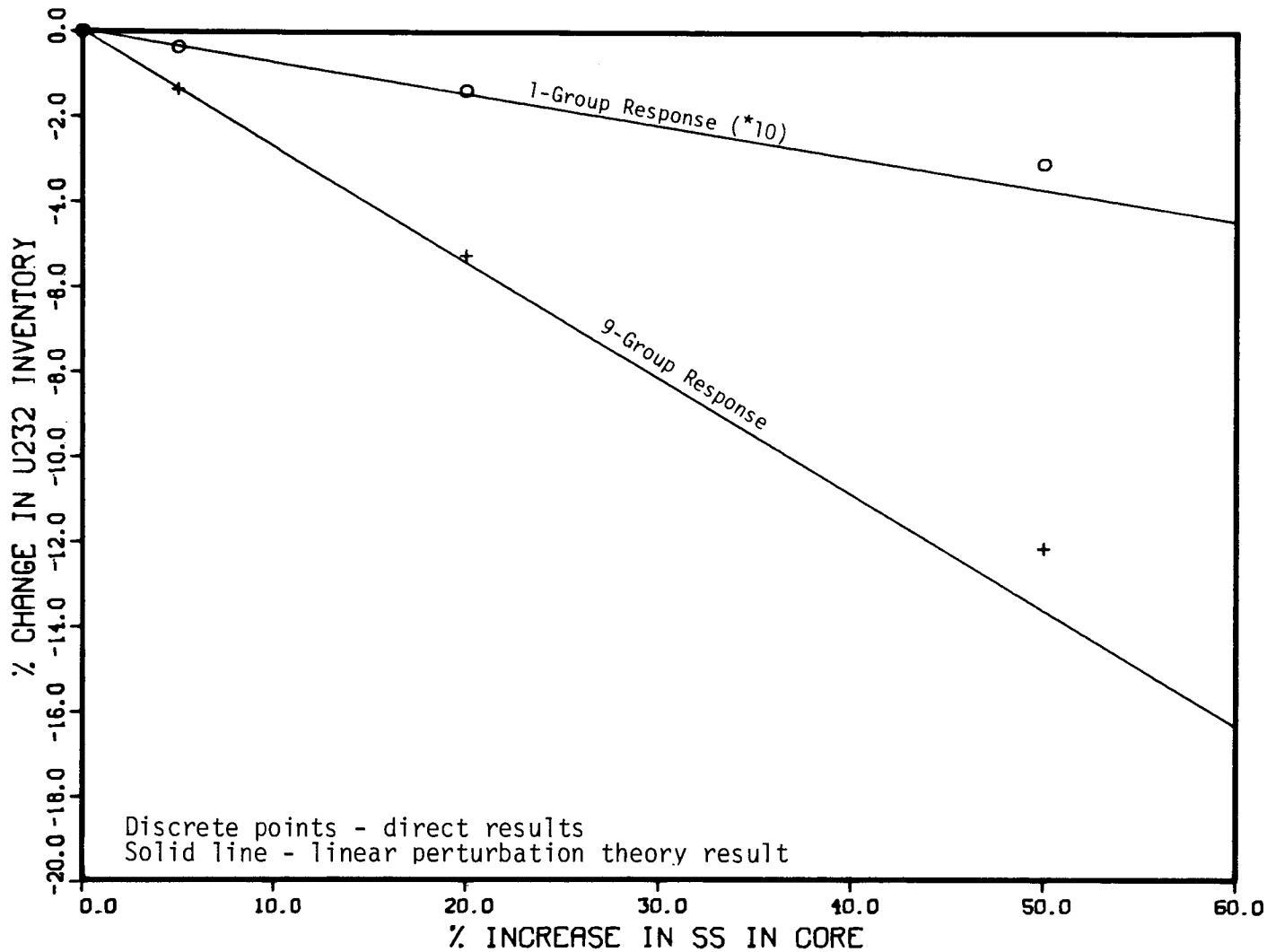

Figure 4.6. Comparison of Γ^* Effects for the 1-Group and 9-Group ^{232}U Inventory Responses.

supplied to DEPTH. For a pure nuclide response $\partial R/\partial\alpha$ and $\partial R/\partial\underline{\psi}$ are zero, and $\partial R/\partial\underline{N}$ is given by,

$$\frac{\partial R}{\partial \underline{N}_z} = \frac{1}{v_z} \int_{v_z} \frac{\partial R}{\partial \underline{N}(\vec{r})}\, d\vec{r}$$

$$= \frac{1}{v_z} \int \underline{h}(\vec{r})\, d\vec{r} = \underline{h}_z \quad . \tag{4.4}$$

The result of the operation in equation (4.4) is $\underline{N}_z^*(t_f)$, as shown in Table 4.7.

The DEPTH module is then given calculational control of the problem. Starting with $\underline{N}_z^*(t_f)$ as the final-time boundary condition, $\underline{N}^*(t_0^+)$ is calculated via equation (2.24). Table 4.8 displays the results of this calculation. As apparent, the only nonzero terms are those that can contribute directly to the ^{232}U response. Examination of Table 4.2, page 45, shows that ^{231}Pa, ^{233}Pa and ^{233}U have a direct parent/daughter relationship to ^{232}U through the burnup chains. Also, ^{232}Th is involved in the production of ^{232}U through its production of ^{231}Pa and ^{233}Pa. In fact, the relative magnitudes of the $\underline{N}^*(t_0^+)$ terms indicate that the main ^{232}U production path begins with ^{232}Th, with the chain, $^{232}Th \xrightarrow{(n,2n)} {}^{231}Pa \xrightarrow{(n,\gamma)} {}^{232}U$.

During the calculation of $\underline{N}^*(t_0^+)$, DEPTH also preserved the data necessary for the P^* and $\underline{S}^*$ integrals given in equations (2.30) and (2.32). A P^* value of 6.899E-11 kg/watt was calculated using equation (2.30). This was then used to evaluate the P^* effect jump condition in equation (2.27), with the resultant P^* effect being given in Table 4.9. Here it can be seen that only the fissionable isotopes have nonzero P^* effects. Also the nuclides with the largest fission cross sections (^{233}U, ^{235}U, ^{239}Pu, and ^{241}Pu) dominate this contribution to the overall response.

TABLE 4.7

FINAL-TIME ADJOINT NUCLIDE DENSITY VECTORS
FOR ^{232}U INVENTORY RESPONSE

Nuclide	CZ #1	CZ #2	CZ #3	RB #1	RB #2
TH228	0.0	0.0	0.0	0.0	0.0
TH232	0.0	0.0	0.0	0.0	0.0
PA231	0.0	0.0	0.0	0.0	0.0
PA233	0.0	0.0	0.0	0.0	0.0
U 232	3.8525E-01	3.8525E-01	3.8525E-01	3.8525E-01	3.8525E-01
U 233	0.0	0.0	0.0	0.0	0.0
U 234	0.0	0.0	0.0	0.0	0.0
U 235	0.0	0.0	0.0	0.0	0.0
U 236	0.0	0.0	0.0	0.0	0.0
U 238	0.0	0.0	0.0	0.0	0.0
NP237	0.0	0.0	0.0	0.0	0.0
NP239	0.0	0.0	0.0	0.0	0.0
PU238	0.0	0.0	0.0	0.0	0.0
PU239	0.0	0.0	0.0	0.0	0.0
PU240	0.0	0.0	0.0	0.0	0.0
PU241	0.0	0.0	0.0	0.0	0.0
PU242	0.0	0.0	0.0	0.0	0.0
AM241	0.0	0.0	0.0	0.0	0.0
AM243	0.0	0.0	0.0	0.0	0.0
CM244	0.0	0.0	0.0	0.0	0.0
FP RL	0.0	0.0	0.0	0.0	0.0
NA	0.0	0.0	0.0	0.0	0.0
SS COR	0.0	0.0	0.0	0.0	0.0
O 16	0.0	0.0	0.0	0.0	0.0

TABLE 4.8

$\underline{N}_z^*(t_0^+)$ FOR ^{232}U INVENTORY RESPONSE
(1-D, 9-GRP. PROB.)

Nuclide	CZ #1	CZ #2	CZ #3	RB #1	RB #2
TH228	0.0	0.0	0.0	0.0	0.0
TH232	7.5411E-06	4.4361E-06	1.2074E-06	5.2982E-08	6.3133E-10
PA231	4.3597E-02	3.4025E-02	1.8826E-02	6.6132E-03	1.0329E-03
PA233	6.0386E-05	4.7032E-05	2.4323E-05	3.2087E-06	2.4978E-07
U 232	3.5585E-01	3.6250E-01	3.7277E-01	3.8048E-01	3.8377E-01
U 233	4.8482E-05	3.8249E-05	2.0167E-05	2.7024E-06	2.1144E-07
U 234	0.0	0.0	0.0	0.0	0.0
U 235	0.0	0.0	0.0	0.0	0.0
U 236	0.0	0.0	0.0	0.0	0.0
U 238	0.0	0.0	0.0	0.0	0.0
NP237	0.0	0.0	0.0	0.0	0.0
NP239	0.0	0.0	0.0	0.0	0.0
PU238	0.0	0.0	0.0	0.0	0.0
PU239	0.0	0.0	0.0	0.0	0.0
PU240	0.0	0.0	0.0	0.0	0.0
PU241	0.0	0.0	0.0	0.0	0.0
PU242	0.0	0.0	0.0	0.0	0.0
AM241	0.0	0.0	0.0	0.0	0.0
AM243	0.0	0.0	0.0	0.0	0.0
CM244	0.0	0.0	0.0	0.0	0.0
FP RL	0.0	0.0	0.0	0.0	0.0
NA	0.0	0.0	0.0	0.0	0.0
SS COR	0.0	0.0	0.0	0.0	0.0
O 16	0.0	0.0	0.0	0.0	0.0

TABLE 4.9

P^* EFFECT FOR ^{232}U INVENTORY RESPONSE
(1-D, 9-GRP. PROB.)

Nuclide	CZ #1	CZ #2	CZ #3	RB #1	RB #2
TH228	0.0	0.0	0.0	0.0	0.0
TH232	-2.5012E-07	-1.8975E-07	-9.4375E-08	-1.2737E-08	-1.0060E-09
PA231	-4.6855E-06	-3.5533E-06	-1.7734E-06	-2.7027E-07	-2.3491E-08
PA233	-4.6855E-06	-3.5533E-06	-1.7734E-06	-2.7027E-07	-2.3491E-08
U 232	-9.0297E-06	-6.8496E-06	-3.4616E-06	-6.5026E-07	-7.1129E-08
U 233	-6.0875E-05	-4.6232E-05	-2.4248E-05	-7.0188E-06	-1.0155E-06
U 234	-7.9284E-06	-6.0124E-06	-3.0149E-06	-4.9894E-07	-4.7278E-08
U 235	-4.2717E-05	-3.2445E-05	-1.7044E-05	-5.0682E-06	-7.4010E-07
U 236	-2.5338E-06	-1.9220E-06	-9.5684E-07	-1.3514E-07	-1.0997E-08
U 238	-1.1446E-06	-8.6830E-07	-4.3192E-07	-5.8868E-08	-4.6704E-09
NP237	-9.2558E-06	-7.0194E-06	-3.5185E-06	-5.8267E-07	-5.5550E-08
NP239	-8.9717E-06	-6.8034E-06	-3.4053E-06	-5.4466E-07	-4.9879E-08
PU238	-2.9019E-05	-2.2026E-05	-1.1359E-05	-2.7227E-06	-3.5821E-07
PU239	-4.2506E-05	-3.2271E-05	-1.6801E-05	-4.5936E-06	-6.4214E-07
PU240	-9.5565E-06	-7.2486E-06	-3.6521E-06	-6.4933E-07	-6.7256E-08
PU241	-5.7762E-05	-4.3872E-05	-2.3036E-05	-6.8720E-06	-1.0040E-06
PU242	-7.6500E-06	-5.8019E-06	-2.9082E-06	-4.7289E-07	-4.4806E-08
AM241	-6.3653E-06	-4.8277E-06	-2.4069E-06	-3.5426E-07	-3.0047E-08
AM243	-5.3146E-06	-4.0308E-06	-2.0099E-06	-2.9347E-07	-2.4860E-08
CM244	-1.5001E-05	-1.1380E-05	-5.7669E-06	-1.1062E-06	-1.2417E-07
FP RL	0.0	0.0	0.0	0.0	0.0
NA	0.0	0.0	0.0	0.0	0.0
SS COR	0.0	0.0	0.0	0.0	0.0
O 16	0.0	0.0	0.0	0.0	0.0

In fact, comparison of Tables 4.8 and 4.9 show that the $^{233}U\ P^*$ effect more than cancels the $^{233}U\ N^*$ effect. This is the same observation made for the specific examples given previously.

DEPTH's next task is to calculate the generalized adjoint source needed for the $\Gamma^*(\vec{r},E)$ calculation to be performed in the VENTURE module. The final source as calculated using equation (2.32) is given in Table 4.10. The most obvious characteristic here is the shape of the source as a function of energy. As mentioned earlier, the ^{232}U inventory is highly sensitive to the first group flux. The generalized adjoint source reflects this high energy importance with a large positive source in group 1 and negative sources elsewhere. An increased flux in group 1 increases the ^{232}U inventory through various (n,2n) production routes while an increased neutron density in the other groups decrease the ^{232}U inventory through neutron capture reactions.

As a check on this adjoint source, the orthogonality condition of equation (2.35) was calculated. The integral of the forward flux and adjoint source over space and energy gave a value of 1.50E-07. This is about as close to zero as can be expected for numerical calculations of this type, considering that the flux shape magnitude is on the order of unity. Thus, this source calculation is considered quite reliable.

Calculational control is now given to the VENTURE module where the $\Gamma^*(\vec{r},E)$ adjoint function and the perturbation integrals of equations (3.9)-(3.11) are calculated. The details of these calculations are beyond the scope of this report. However, it is quite interesting to examine the "uncontaminated" generalized adjoint flux. This is displayed as a 3-D plot in Figure 4.7. As apparent it quite generally displays the same characteristics as the generalized adjoint source. The large

TABLE 4.10

ADJOINT SOURCE VECTORS FOR ^{232}U INVENTORY RESPONSE
(1-D, 9-GRP. PROB.)

Group	CZ #1	CZ #2	CZ #3	RB #1	RB #2
1	1.5885E 01	1.5063E 01	1.3791E 01	6.4016E 00	2.9478E 00
2	-1.1504E-01	-1.1342E-01	-1.1115E-01	-4.2227E-02	-4.3118E-02
3	-5.2105E-02	-5.2158E-02	-5.2553E-02	-6.3252E-03	-8.6478E-03
4	-5.0199E-02	-5.2799E-02	-5.7314E-02	-5.6561E-03	-1.0596E-02
5	-6.6003E-02	-7.3513E-02	-8.6604E-02	-5.3297E-03	-1.7821E-02
6	-1.0744E-01	-1.2329E-01	-1.5107E-01	-5.4242E-03	-3.0464E-02
7	-1.4984E-01	-1.7648E-01	-2.2504E-01	8.6523E-04	-5.2911E-02
8	-1.0061E 00	-1.0392E 00	-1.1172E 00	9.1377E-02	-2.7706E-01
9	-1.2991E 02	-1.2814E 02	-1.2498E 02	-2.3366E 01	-2.4119E 01

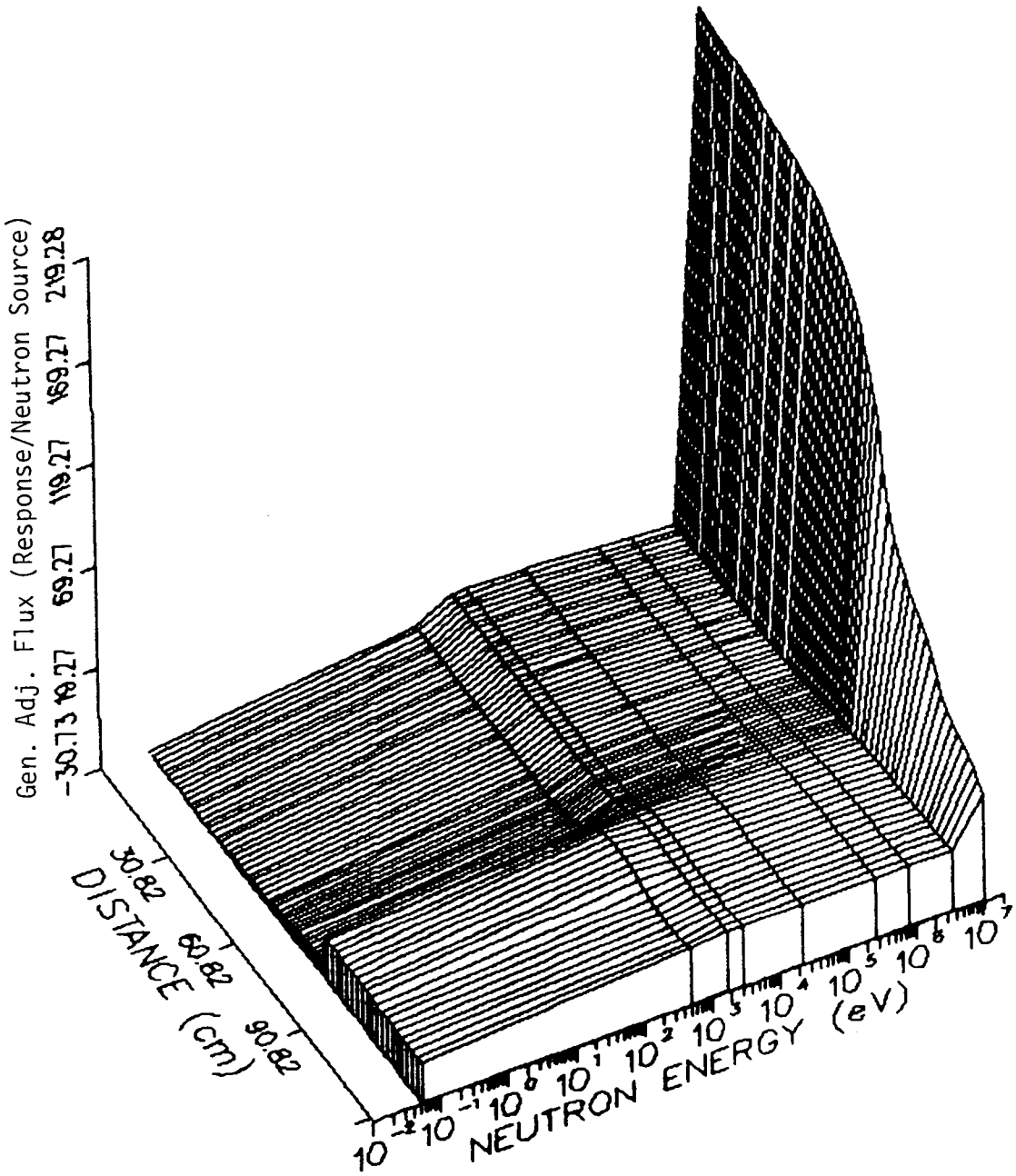

Figure 4.7. ^{232}U "Uncontaminated" Generalized Adjoint Flux.

positive peak at high energies and negativity elsewhere, therefore, characterizes the ^{232}U response. This plot is essentially a map of the importance of a change in the flux shape to the response of interest as a function of space and energy.

To be more precise, $\Gamma^*(r_0,E_0)$ is the importance to the response of a change in the neutron source at the phase space point r_0, E_0. To see this, we insert an arbitrary neutron source, $Q(\vec{r},E)$, into the first term of the K-functional in equation (2.15). The functional now becomes

$$K(\underline{Q}) = R - \sum_k \sum_i \int_{\substack{\text{all}\\ \text{space}}} \underline{\Gamma}^{*T}{}^{ik}(\vec{r})[(\underline{\underline{L}} - \lambda\underline{\underline{F}})\ \underline{\psi}(\vec{r}) - \underline{Q}(\vec{r})]^{ik} \tag{4.5}$$

$$+ \text{ other terms}$$

Also, equation (2.21) would have to be modified to include this additional term,

$$\Delta R = \left[\frac{\partial K}{\partial P}\ \delta P\right] + \left[\frac{\partial K}{\partial \underline{C}}\ \delta\underline{C}\right] + \left[\frac{\partial K}{\partial \underline{Q}}\ \delta\underline{Q}\right] . \tag{4.6}$$

But from equation (4.5) one sees that

$$\left[\frac{\partial K}{\partial \underline{Q}}\ \delta\underline{Q}\right] = \sum_k \sum_i \int_{\substack{\text{all}\\ \text{space}}} (\underline{\Gamma}^{*T}(\vec{r})\ \Delta\underline{Q}(\vec{r}))^{ik}\ d\vec{r} \ . \tag{4.7}$$

Thus, the above interpretation of $\Gamma^*(\vec{r},E)$ as an importance function to a change in the neutron source seems to be correct.

Now returning to our present example, one sees that if the $\Gamma^*(\vec{r},E)$ shown in Figure 4.7 is multiplied by the change in the neutron source caused by the perturbation and integrated over space and energy, then the change in the response due to this effect will result. The estimate of the variation in the neutron source at each point in the reactor,

$\Delta \underline{Q}_N(\vec{r})$, is just the term that makes up the Γ^* effect in equation (2.28). That is,

$$\Delta \underline{Q}_N(\vec{r}) = \frac{\partial}{\partial \underline{N}(\vec{r})} \{(\underline{\underline{L}} - \lambda \underline{\underline{F}}) \underline{\psi}(\vec{r})\} \Delta \underline{N}(\vec{r}) \quad . \tag{4.8}$$

The detailed derivation of how the Γ^* effect is calculated is given in Appendix B. Of importance here is the fact that the total Γ^* effect is comprised of several components, one accounting for each term of the time-independent diffusion equation. The neutron source at a point can be affected in four ways; by leakage, removal, inscatter or fission. The total variation in the neutron source due to a nuclide perturbation can, in general, have all four mechanisms present. For example, a material perturbation in a given region will change the diffusion coefficient and thus the leakage from the region. It will also change the absorption and scattering properties of the region. Therefore, variations in the removal (absorption plus outscatter) and inscatter sources can be expected. Finally, if the material has a nonzero fission cross section, the local fission source will also be altered. The sum of these four components will give the total variation in the neutron source. This source variation when folded with its importance to the response of interest will give the change in the response due to the nuclide perburbation.

Each component of the Γ^* effect for the ^{232}U response for each nuclide in core zone #1 of the 9-group calculation is given in Table 4.11. These numbers when multiplied by the region volume and nuclide perturbation give the change in the ^{232}U inventory due to the indirect flux (neutron source) variation within the reactor. Consider, for example, that a 10% increase in the stainless steel concentration in

TABLE 4.11

Γ^* EFFECT IN CORE ZONE #1 FOR ^{232}U INVENTORY RESPONSE
(1-D, 9-GRP, PROB.)

Nuclide	Leakage	Removal	Inscatter	Fission	Total
TH228	0.0	0.0	0.0	0.0	0.0
TH232	-4.35851E-10	3.36695E-06	-3.00773E-06	-2.48268E-08	3.33950E-07
PA231	-3.25430E-10	1.45304E-05	-3.61645E-06	-5.45853E-07	1.03678E-05
PA233	-4.44316E-10	7.60728E-06	-3.60710E-06	-5.45853E-07	3.45388E-06
U 232	-1.21711E-10	7.20842E-06	-2.17634E-06	-9.84970E-07	4.04699E-06
U 233	1.74297E-11	2.31336E-05	-2.13738E-06	-6.25021E-06	1.47460E-05
U 234	-6.08228E-10	7.75180E-06	-2.80742E-06	-8.13632E-07	4.13014E-06
U 235	-6.36472E-01	1.91671E-05	-2.33262E-06	-4.22218E-06	1.26116E-05
U 236	-2.93729E-10	5.70900E-06	-3.09938E-06	-2.74511E-07	2.33481E-06
U 238	-5.11321E-10	3.20494E-06	-3.06311E-06	-1.27214E-07	1.41003E-08
NP237	9.09712E-11	1.77193E-05	-4.52813E-06	-1.04421E-06	1.21471E-05
NP239	-1.03671E-10	1.47974E-05	-4.12163E-06	-9.43491E-07	9.73222E-06
PU238	2.21999E-10	1.29030E-05	-7.95031E-07	-3.18982E-06	8.91837E-06
PU239	-6.18126E-10	1.80926E-05	-2.14067E-06	-4.86784E-06	1.10834E-05
PU240	-5.47321E-10	7.12664E-06	-2.06264E-06	-1.16798E-06	3.89547E-06
PU241	-1.79443E-10	2.26436E-05	-2.83880E-06	-6.63802E-06	1.30575E-05
PU242	2.22480E-10	6.27908E-06	-1.74163E-06	-9.03317E-07	3.63435E-06
AM241	5.06874E-09	1.82029E-04	-5.07635E-06	-8.45469E-07	1.76112E-04
AM243	-9.63066E-10	1.05614E-05	-4.62072E-06	-6.91799E-07	5.24792E-06
CM244	3.78691E-10	7.78695E-06	-1.14131E-06	-1.99423E-06	4.65180E-06
FP RL	-2.13645E-09	4.01732E-06	-3.96950E-06	0.0	4.56894E-08
NA	-5.74237E-10	1.91993E-06	-2.58897E-06	0.0	-6.69615E-07
SS COR	1.74913E-10	4.37720E-08	-1.16099E-06	0.0	-1.11704E-06
O 16	-8.83474E-10	1.49721E-06	-1.73684E-06	0.0	-2.40520E-07

core zone #1 is made. For a one time-step problem, the only contribution to the perturbed response is due to the Γ^* effect. Thus one sees from the "total" column in Table 4.11 that a decrease in the ^{232}U inventory at 91.3 days can be expected due to this perturbation. In fact, the amount of decrease will be approximately

$$\Delta R/R = [(\Gamma^* \text{ effect})_{ss} \ (\Delta N_{ss}) \ V_1 * 100]/R$$

$$= (-1.1170\text{-}6)(1.4757\text{-}3)(7.5449\text{+}4)(100)/(5.9184\text{-}2)$$

$$= -0.2101\%$$

This agrees very well with the direct calculational result of −0.2058%.

Of this total change, one sees from Table 4.11 that the major contribution was due to a change in the inscatter source for that region. This agrees with our intuition since we already know that stainless steel has a relatively large effect on the neutron spectrum in the system. Thus, it is not surprising to see a change in the ^{232}U response due to a change in the scattering source.

The final step in an adjoint depletion calculation is the determination of $\underline{N}_z^*(t_0^-)$. This importance function is a combination of the N^*, P^*, and Γ^* effects. The jump conditions specified in equation (2.26) and (2.29) are used for this purpose. In the present example, the shuffling/discharge operator, $\underline{\underline{P}}_{SD}$, is the identity matrix. The result of the time-step jump condition is displayed in Table 4.12. It is this sensitivity function that is used in equation (2.23) to determine the change in the final-time response function due to initial-time design variations.

TABLE 4.12

$\underline{N}_z^*(t_0^-)$ FOR ^{232}U INVENTORY RESPONSE
(1-D, 9-GRP. PROB.)

Nuclide	CZ #1	CZ #2	CZ #3	RB #1	RB #2
TH228	0.0	0.0	0.0	0.0	0.0
TH232	7.6250E-06	4.4625E-06	1.0956E-06	4.0796E-08	3.0750E-09
PA231	4.3603E-02	3.4029E-02	1.8827E-02	6.6213E-03	1.0329E-03
PA233	5.9155E-05	4.6136E-05	2.3776E-05	3.0267E-06	2.4394E-07
U 232	3.5584E-01	3.6250E-01	3.7227E-01	3.8048E-01	3.8377E-01
U 233	2.3527E-06	4.4008E-06	3.4561E-06	-3.3746E-06	-7.3049E-07
U 234	-3.7983E-06	-2.8931E-06	-1.6075E-06	-3.8180E-07	-3.4242E-08
U 235	-3.0106E-05	-2.2070E-05	-1.1110E-05	-4.3658E-06	-6.8117E-07
U 236	-1.9901E-07	-1.9827E-07	-2.8503E-07	-8.4480E-08	-1.7782E-09
U 238	-1.1305E-06	-8.8056E-07	-5.2491E-07	-6.8106E-08	-2.3300E-09
NP237	2.8913E-06	2.1978E-06	5.9421E-07	-2.2882E-07	-1.6195E-08
NP239	7.6056E-07	6.8380E-07	3.6452E-08	-2.5818E-07	-1.5330E-08
PU238	-2.0100E-05	-1.4683E-05	-7.1591E-06	-2.2888E-06	-3.2171E-07
PU239	-3.1423E-05	-2.2966E-05	-1.1135E-05	-3.9094E-06	-5.8672E-07
PU240	-5.6610E-06	-4.1753E-06	-2.0846E-06	-5.1215E-07	-4.9169E-08
PU241	-4.4705E-05	-3.2580E-05	-1.5748E-05	-5.9165E-06	-9.2581E-07
PU242	-4.0156E-06	-2.9171E-06	-1.4646E-06	-3.6288E-07	-3.0421E-08
AM241	1.6975E-04	1.2945E-04	5.5959E-05	4.4808E-06	4.4248E-07
AM243	-6.6658E-08	-3.0068E-08	-1.7369E-07	-1.4684E-07	-6.5358E-10
CM244	-1.0349E-05	-7.5546E-06	-3.5670E-06	-8.9840E-07	-1.0335E-07
FP RL	4.5689E-08	2.0569E-08	-1.5031E-07	-2.4579E-08	5.9771E-09
NA	-6.6961E-07	-5.5141E-07	-3.1509E-07	-1.5743E-08	-1.2597E-09
SS COR	-1.1170E-06	-8.4434E-07	-4.1651E-07	0.0	0.0
O 16	-2.4052E-07	-2.3474E-07	-1.7039E-07	-1.1298E-08	-6.6474E-10

It should be noted that the values of $\underline{N}_z^*(t_0^-)$ given in Table 4.12 are not sensitivity coefficients as written. However, they can easily be converted into standard sensitivity coefficients. First, redefine $\underline{N}_z^*$ to be $\underline{N}_z^*$ multiplied by the zone volume, V_z (see Table 4.13),

$$\underline{N}_z^* = \underline{N}_z^* V_z \tag{4.9}$$

Now the perturbation expression becomes,

$$\Delta R = \sum_z \underline{N}_z^{*T} \Delta \underline{N}_z = \sum_z \sum_y N_{yz}^* \Delta N_{yz} \quad , \tag{4.10}$$

where the y index refers to nuclide y. Now define the sensitivity coefficient, $S_{x,y,z,t}$, as the percent change in response x due to a 1% change in nuclide y in zone z at time t. From this definition it can be seen that,

$$S_{x,y,z,t} = \frac{N_{y,z,t}}{R_x} \quad N_{x,y,z,t}^* \quad , \tag{4.11}$$

where $N_{y,z,t}$ and R_x are the reference nuclide density and unperturbed response, respectively. This equation is valid since if one multiplies by $\Delta N/N$, $\Delta R/R$, which is the desired result, is obtained.

The problem with expressing the importance of a nuclide variation to the response in this manner is that if the reference density is zero, then the sensitivity coefficient is also zero. Also, a problem exists in defining the percent change in the nuclide concentration, $\Delta N/N$, for a zero reference concentration. For these reasons, the redefined $\underline{N}_z^*$ as given in equation (4.9) will generally be used as the measure of the importance of a nuclide change to the response of interest.

Hopefully, with the insight gained from the simple example calculation just presented, we can now consider a set of more challenging depletion problems. For the present, we will remain with the 1-D reactor model but extend the depletion perturbation theory analysis to multiple time-step problems and also to more complicated response functionals.

Nuclide Inventory Responses (multiple time steps). Table 4.14 presents a comparison of DPT results with direct calculation for the same perturbation/response pairs discussed earlier. However, the response for this set of calculations was after one year (274 full power days) of reactor operation. The forward and adjoint depletion calculations employed 9-group cross sections, and the total burnup interval was divided into three equal time steps of 91.3 full power days.

As in the single time-step examples, there is excellent agreement with direct calculation except for the ^{233}U perturbation/^{232}U response pair. As noted previously, this is due to the large nonlinear effects observed for the $^{233}U/^{232}U$ combination. Also it should be noted that the percent difference calculated for the multistep problem is comparable to that determined for the one time-step examples. Thus the nonlinear effects are not cumulative with time. This is important since many realistic depletion analysis problems involve the calculation of the reactor operating history over several time steps. If the errors inherent in linear time-dependent perturbation theory were cumulative with time, then the realistic application of the theory would be very restricted.

TABLE 4.13

$\underline{N}_z^*(t_0^-)*V_z$ FOR ^{232}U INVENTORY RESPONSE
(1-D, 9-GRP. PROB.)

Nuclide	CZ #1	CZ #2	CZ #3	RB #1	RB #2
TH228	0.0	0.0	0.0	0.0	0.0
TH232	5.7530E-01	2.3568E 00	1.5706E 00	9.2303E-02	1.0812E-02
PA231	3.2898E 03	1.7972E 04	2.6990E 04	1.4963E 04	3.6318E 03
PA233	4.4632E 00	2.4366E 01	3.4083E 01	6.8481E 00	8.5768E-01
U 232	2.6843E 04	1.9145E 05	5.3438E 05	8.6086E 05	1.3493E 06
U 233	1.7751E-01	2.3242E 00	4.9545E 00	-7.6353E 00	-2.5684E 00
U 234	-2.8658E-01	-1.5280E 00	-2.3044E 00	-8.6384E-01	-1.2040E-01
U 235	-2.2714E 00	-1.1656E 01	-1.5927E 01	-9.8780E 00	-2.3950E 00
U 236	-1.5015E-02	-1.0472E-01	-4.0860E-01	-1.9116E-01	-6.2521E-03
U 238	-8.5293E-02	-4.6406E-01	-7.5248E-01	-1.5409E-01	-8.1921E-03
NP237	2.1814E-01	1.1608E 00	8.5182E-01	-5.1772E-01	-5.6942E-02
NP239	5.7384E-02	3.6115E-01	5.2255E-02	-5.8414E-01	-5.3901E-02
PU238	-1.5165E 00	-7.7545E 01	-1.0263E 01	-5.1786E 00	-1.1311E 00
PU239	-2.3708E 00	-1.2129E 01	-1.5963E 01	-8.8454E 00	-2.0629E 00
PU240	-4.2712E-01	-2.2052E 00	-2.9884E 00	-1.1588E 00	-1.7288E-01
PU241	-3.3729E 00	-1.7207E 01	-2.2575E 01	-1.3386E 01	-3.2552E 00
PU242	-3.0298E-01	-1.5407E 00	-2.0996E 00	-8.2105E-01	-1.0696E-01
AM241	1.2807E 01	6.8367E 01	8.0219E 01	1.0138E 01	1.5557E 00
AM243	-5.0293E-03	-1.5880E-02	-2.4899E-01	-3.3223E-01	-2.2980E-03
CM244	-7.8085E-01	-3.9899E 00	-5.1134E 00	-2.0327E 00	-3.6339E-01
FP RL	3.4472E-03	1.0863E-02	-2.1548E-01	-5.5605E-02	2.1016E-02
NA	-5.0522E-02	-2.9122E-01	-4.5169E-01	-3.5621E-02	-4.4291E-03
SS COR	-8.4280E-02	-4.4593E-01	-5.9708E-01	0.0	0.0
O 16	-1.8147E-02	-1.2398E-01	-2.4426E-01	-2.5564E-02	-2.3372E-03

TABLE 4.14

COMPARISON OF DEPLETION PERTURBATION THEORY METHODS WITH DIRECT METHODS FOR MULTIPLE TIME STEPS (9-GROUP CALCULATION)

Response (t_f = 274 days)	Case[a] #	ΔR/R (DPT) (%)	ΔR/R (Direct) (%)	% Diff.
^{232}U Inventory	1	4.0489	4.0178	0.77
	2	-2.7896	-2.3456	18.93
	3	-1.4545	-1.2645	15.02
	4	-2.6772	-2.6014	2.91
^{233}U Inventory	1	0.6589	0.6559	0.45
	2	4.3256	4.4651	- 3.12
	3	3.6202	3.6391	- 0.52
	4	-0.2535	-0.2496	1.58
^{239}U Inventory	1	-0.2013	-0.2004	0.48
	2	-2.4427	-2.3279	4.93
	3	-1.4336	-1.4039	2.12
	4	0.2703	0.2677	0.96

[a]10% increase in nuclide concentrations at BOC (see Table 4.4, page 47).

Another area of interest in multistep calculations is the relative contribution of the three adjoint functions. As mentioned earlier, the N^*, P^*, and Γ^* effects cannot be easily separated in adjoint calculations involving more than one time step. However, options have been built into DEPTH so that the P^* and Γ^* adjoint calculations can be bypassed. The option to neglect the P^* effect was implemented mainly as an aid in the study of the relative contribution of the various adjoint functions and has no effect on the overall calculation time. The no-Γ^* switch, on the other hand, may be used to eliminate the fixed source adjoint calculation in VENTURE, and thus reduce the computing cost by as much as 90-95%. Therefore, the latter option may be used to some advantage in certain situations where the Γ^* effect is small relative to the N^* and P^* effects. An attempt to single out the N^*, P^*, and Γ^* effects for the same perturbation/response pairs as given in Table 4.14 is displayed in Table 4.15. The first column contains the calculated $\Delta R/R$ values with both the P^* and Γ^* effects set to zero, the second contains just the N^* and P^* effects, and the last tabulates the $\Delta R/R$ values computed from the full depletion perturbation theory.

Similar observations as made for the one time-step problems are apparent. Most notable are the large P^* and Γ^* contributions to the $^{233}U/^{232}U$ pair relative to the direct N^* effect. More important, however, is the fact that for some of the cases shown, the Γ^* effect is small relative to the $N^* + P^*$ effect. In these cases sufficient accuracy can be obtained without the three costly fixed-source adjoint calculations. In many instances a preanalysis of the specific

TABLE 4.15

RELATIVE N^*, P^*, AND Γ^* EFFECTS IN MULTISTEP CALCULATIONS
(1-D, 9-GRP. PROB.)

Response (t_f = 274 days)	Case[a]	Percent Change in Response: N^* Effect (1)	$N^* + P^*$ Effects (2)	$N^* + P^* + \Gamma^*$ Effects (3)	% Diff. $\frac{2 - 3}{3}$
^{232}U Inventory	1	4.514	3.970	4.049	-1.9
	2	4.584	-4.886	-2.790	75.1
	3	2.701	-2.719	-1.455	86.9
	4	--	--	-2.677	-100.0
^{233}U Inventory	1	0.673	0.681	0.659	3.3
	2	4.385	4.330	4.326	0.1
	3	3.337	3.312	3.620	8.5
	4	--	--	-0.254	-100.0
^{239}Pu Inventory	1	0.000	-0.115	-0.201	- 42.8
	2	0.000	-2.048	-2.443	- 16.2
	3	0.000	-1.171	-1.434	- 18.3
	4	--	--	0.270	-100.0

[a]10% increase in nuclide concentration at BOC (see Table 4.4, page 47).

perturbation/response pair to be investigated can determine if the full perturbation theory is cost-effective.

K_{eff} Response. To illustrate the use of depletion perturbation theory (DPT) for the calculation of perturbed responses other than nuclide inventories, consider the straightforward task of determining the reactivity change from some reference state associated with various design options (i.e., fissile enrichments, material volume fractions, or fuel shuffling strategies, etc.). Typically, the variations in both the beginning-of-cycle (BOC) and end-of-cycle (EOC) reactivities are desired. The most direct solution method for this problem is to perform a complete burnup analysis for each design variation to be considered. In this way both the BOC and EOC K_{eff}s can be determined exactly. For realistic calculational models, however, direct solutions such as this quickly become prohibitively expensive, even for only a small number of design variables.

Static perturbation methods have alleviated the problem of determining the effect of BOC design variations on the BOC reactivity. Likewise, the effect of EOC perturbations on the EOC K_{eff} could also be determined using static perturbation theory. However, what is needed in this case is a sensitivity function that relates the EOC state of the reactor to design perturbations at the beginning of the cycle. Depletion perturbation theory can be utilized to bridge this time gap and provide the necessary importance functions.

Table 4.16 illustrates the difference between the sensitivity coefficients just described for the case of our 1-D spherical fast reactor model operating with 20% denatured uranium fuel. The

TABLE 4.16

COMPARISON OF STATIC AND TIME-DEPENDENT SENSITIVITY COEFFICIENTS FOR A ONE TIME-STEP PROBLEM

Nuclide	Location	Case 1 $\frac{(\Delta K/K)\ t_0}{(\Delta N/N)\ t_0}$	Case 2 $\frac{(\Delta K/K)\ t_f}{(\Delta N/N)\ t_f}$	Case 3 $\frac{(\Delta K/K)\ t_f}{(\Delta N/N)\ t_0}$	% Diff. $\frac{\text{Case 3 - Case 2}}{\text{Case 2}}$
^{232}Th	CZ1	-0.0145	-0.0137	-0.0101	-26.0
	CZ2	-0.0570	-0.0560	-0.0460	-17.9
	CZ3	-0.0360	-0.0378	-0.0353	- 6.6
^{233}U	CZ1	0.0544	0.0480	0.0438	- 8.9
	CZ2	0.2235	0.2117	0.2060	- 2.7
	CZ3	0.1810	0.1891	0.2046	8.2
	RB1	0.0061	0.0080	0.0084	5.2
	RB2	0.0003	0.0003	0.0007	111.7
^{238}U	CZ1	-0.0128	-0.0119	-0.0069	-42.1
	CZ2	-0.0480	-0.0469	-0.0315	-32.9
	CZ3	-0.0240	-0.0249	-0.0191	-23.4

Note: t_0 = 0 days and t_f = 91 days.

first two columns represent static perturbation theory results calculated at the beginning-of-cycle (t_0) and after 91 full power days (t_f) of operation. Differences in the nuclide importance to K_{eff} for these two cases can be attributed to a shift in the flux shape toward the outer core regions during the 91-day burn. The last column of sensitivity coefficients, calculated using DPT with $(\Delta K/\Delta N)_{t_f}$ as the initial condition for the adjoint equations, represent the percent change in the EOC K_{eff} due to a 1% perturbation in the BOC nuclide concentration. The difference between case 2 and case 3 sensitivities represent the time-integrated importance of the depletion process to the response of interest. As apparent from the last column in Table 4.16, this contribution can be significant even for short depletion times.

A similar comparison was made for a three time-step calculation which included a full year of reactor operation at 75% capacity factor (274 full power days). Table 4.17, which is constructed similar to Table 4.16, displays the results of this multistep calculation. In this case one sees more pronounced differences between the final-time sensitivities and the time-dependent K_{eff} sensitivity coefficients. This is due to the increased depletion period over which the sensitivities are determined. Thus, as would be expected, the time-integrated importance of the burnup process to the response of interest becomes more significant with increased burnup.

Consider, for example, the sensitivity of K_{eff} to the ^{238}U concentration in core zone #1. From Tables 4.16 and 4.17 one sees that at time zero an increase in the ^{238}U density in CZ #1 would result in an immediate reactivity decrease relative to the reference system. This statement is also valid at any instant throughout the cycle. However,

TABLE 4.17

COMPARISON OF STATIC AND TIME-DEPENDENT SENSITIVITY COEFFICIENTS FOR A MULTIPLE TIME-STEP PROBLEM

Nuclide	Location	Case 1 $\frac{(\Delta K/K)\ t_0}{(\Delta N/N)\ t_0}$	Case 2 $\frac{(\Delta K/K)\ t_f}{(\Delta N/N)\ t_f}$	Case 3 $\frac{(\Delta K/K)\ t_f}{(\Delta N/N)\ t_0}$	% Diff. $\frac{\text{Case 3 - Case 2}}{\text{Case 2}}$
^{232}Th	CZ1	-0.0145	-0.0121	-0.0011	- 90.6
	CZ2	-0.0570	-0.0529	-0.0145	- 72.6
	CZ3	-0.0360	-0.0399	-0.0225	- 43.6
^{233}U	CZ1	0.0544	0.0391	0.0254	- 35.1
	CZ2	0.2235	0.1866	0.1495	- 19.9
	CZ3	0.1810	0.1923	0.2058	7.0
	RB1	0.0061	0.0142	0.0116	- 18.4
	RB2	0.0003	0.0005	0.0013	179.7
^{238}U	CZ1	-0.0128	-0.0105	0.0021	-120.1
	CZ2	-0.0480	-0.0440	0.0008	-101.9
	CZ3	-0.0240	-0.0263	0.0038	- 85.5

Note: t_0 = 0 days and t_f = 274 days

if one considers the effect of a BOC perturbation on the reactivity of the system at future times, an interesting observation can be made. Comparison of the time-dependent sensitivity coefficients for the response at 91 and 274 days show that not only has the magnitude changed but that a sign reversal has also occurred. Thus an increase in the ^{238}U concentration at the BOC actually increases the reactivity at 274 days relative to the reference case.

Effects such as this may be important in certain reactor designs. Large heterogeneous fast breeder reactors, for example, have large amounts of fertile material in high flux regions of the reactor. This results in a small reactivity swing over the cycle (with possible increasing reactivity). The ability to quantify such effects using depletion perturbation theory may prove to be an invaluable design tool.

The sensitivity coefficients for the K_{eff} response generated using the DEPTH module have also been tested against direct computational methods. Table 4.18 displays the results from both the single and multiple time-step problems. As may be observed in Table 4.18, excellent agreement is achieved in all cases except for the stainless steel perturbation in all three core zones for the one time-step problem.

This one exception has the interesting characteristic of a space cancellation effect, giving rise to nonlinear behavior for this particular perturbation/response pair. This nonlinear behavior is displayed in Figure 4.8. However, Figure 4.9 also shows that the percent change in K_{eff} due to a stainless steel perturbation has a linear relationship in each of the separate core zones. The straight lines in these plots represent the linear perturbation results while the indicated points are based on direct calculations. Only with the combined perturbation is the

TABLE 4.18

COMPARISON OF DPT RESULTS WITH DIRECT CALCULATION FOR A K_{eff} RESPONSE

Perturbation[a]		Percent Change in Final-Time K_{eff}					
		t_f = 91 days			t_f = 274 days		
Nuclide	Location	DPT	Direct	% Diff.	DPT	Direct	% Diff.
^{232}Th	CZ1-2-3	-0.915	-0.902	1.44	-0.381	-0.374	1.77
^{233}U	CZ1-2-3	4.544	4.431	2.55	3.806	3.802	0.10
^{233}U	CZ3	2.046	2.038	0.39	2.058	2.052	0.27
SS	CZ1-2-3	-0.078	-0.085	-8.43	-0.148	-0.145	1.72
SS	CZ1	-0.049	-0.048	1.41	--	--	--
SS	CZ2	-0.149	-0.150	-0.77	--	--	--
SS	CZ3	0.120	0.116	2.98	--	--	--
^{16}O	CZ1-2-3	0.211	0.203	3.94	--	--	--

[a] 10% increase in nuclide concentration at BOC

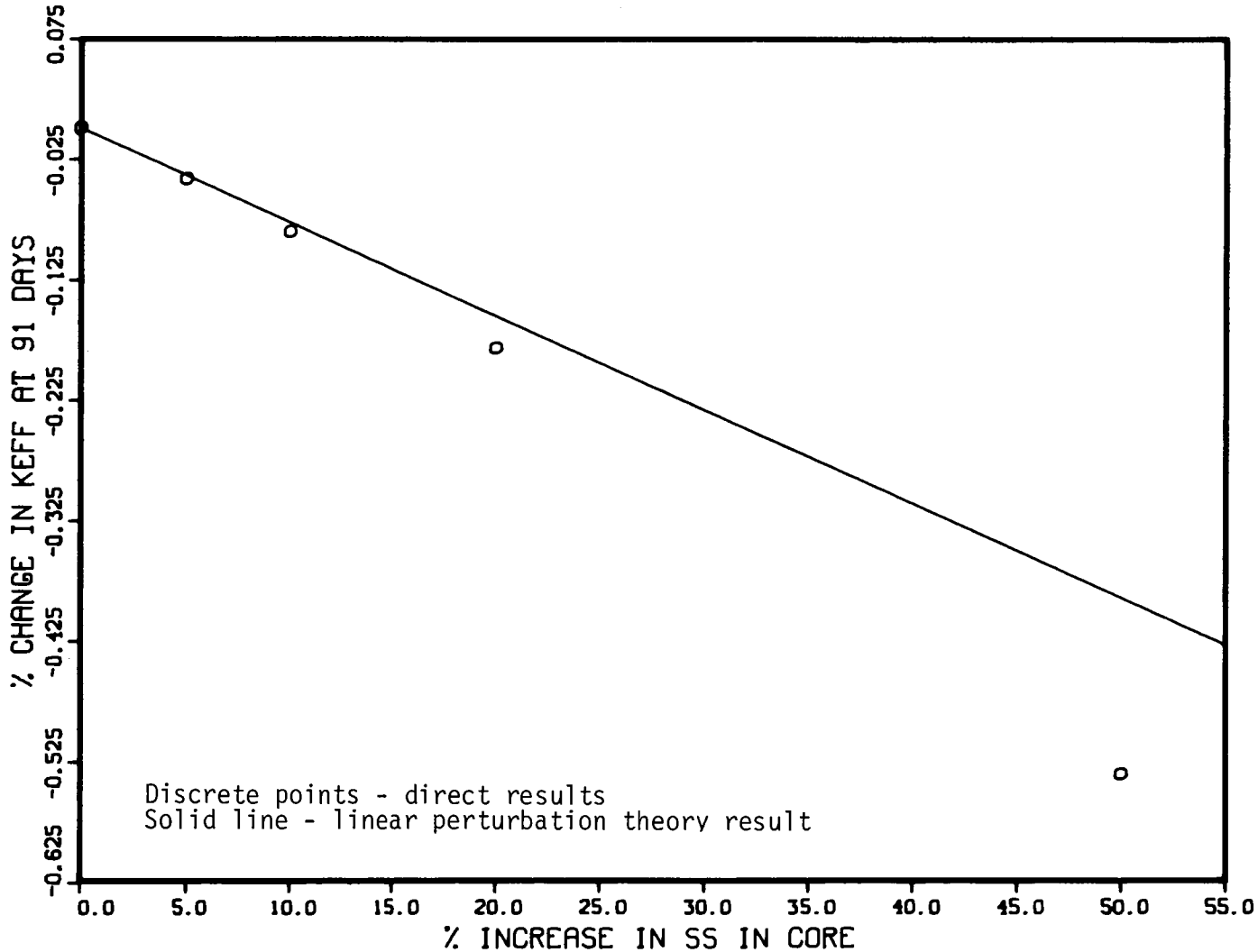

Figure 4.8. Nonlinear Behavior of Uniform Stainless Steel Perturbation on the K_{eff} Response.

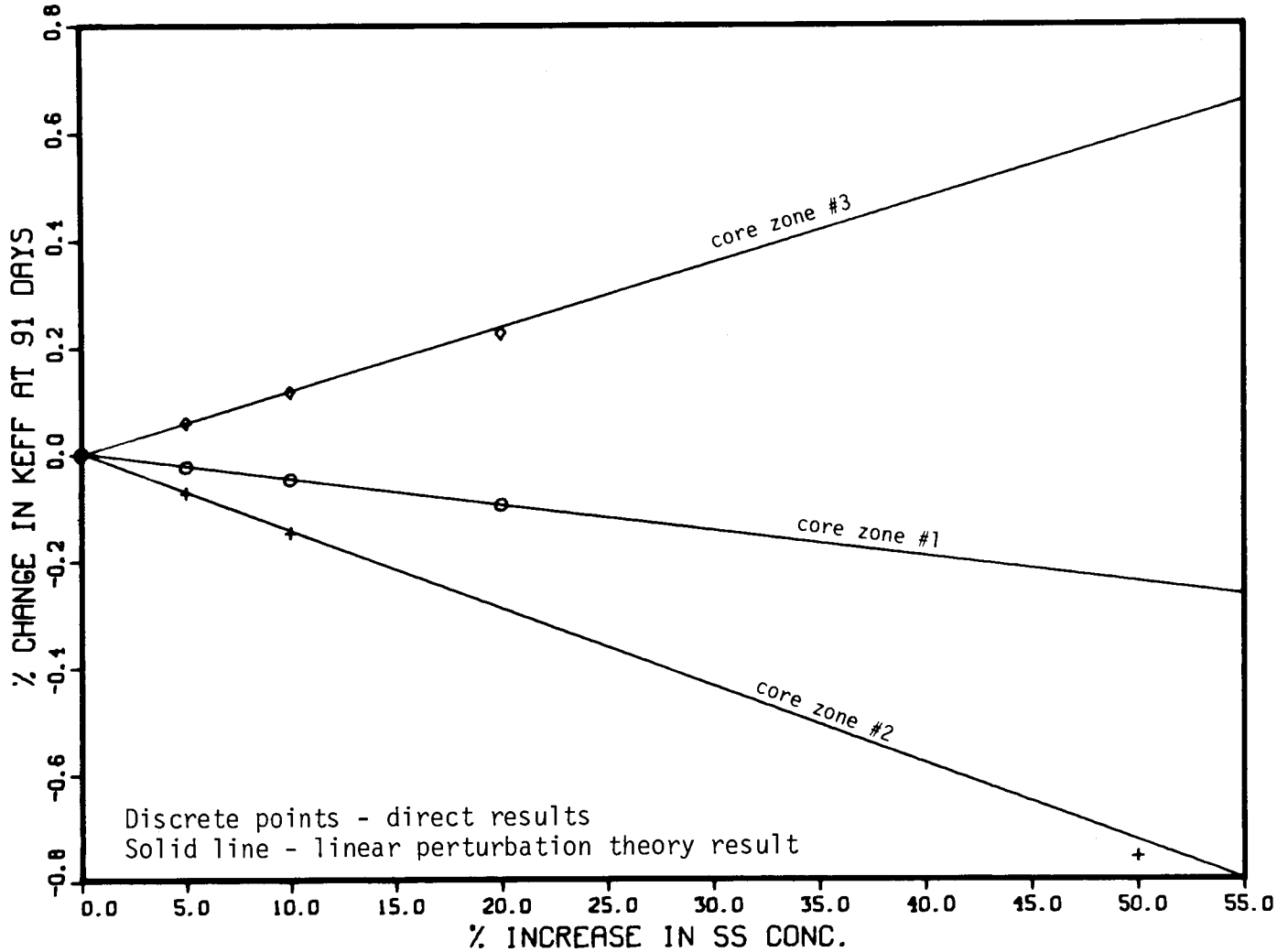

Figure 4.9. Linear Relationship of K_{eff} Response for Separate Stainless Steel Perturbations in Each Core Zone.

positive CZ 3 effect cancelled by the negative CZ 1 and CZ 2 contributions. This same nonlinear behavior is not as apparent in the multiple time-step calculation. In this case, CZ 2 dominates the overall reponse as shown in Table 4.19. Although cancellation is still present, it is considerably reduced for the 274-day burn relative to the 91-day depletion calculation.

The nonlinear behavior occurring here is similar to the effects previously observed for the ^{233}U perturbation/^{232}U response pair. In both cases cancellation of competing effects was the source of the nonlinearity. The $^{233}U/^{232}U$ pair had competing N^* and P^* effects while the uniform stainless steel perturbation for the K_{eff} response had cancellation due to geometry effects. Regardless of the source, cancellation results in nonlinear behavior which cannot be treated with linear perturbation methods. Therefore, caution must be exercised when applying depletion perturbation theory results in these instances.

In addition to the above analyses, the importance of the Γ^* effect to the global K_{eff} response was investigated. Table 4.20 compares the relative contribution of the N^*, P^* and Γ^* effects to the total response for the single time-step problem, while Table 4.21 quantifies the Γ^* effect for the three time-step calculation. From these one can see that in most cases the Γ^* effect is quite small and could be neglected with little error. Here, as in some of the nuclide inventory responses, the costly fixed-source adjoint calculation does not seem to be justified. This is especially important for multistep problems where several $\Gamma^*(\vec{r},E)$ calculations are required.

Even though not of much importance to the overall response for the K_{eff} example, the generalized adjoint flux can usually provide valuable

TABLE 4.19

COMPARISON OF ZONE-WISE CONTRIBUTIONS TO THE TOTAL $\Delta K/K$ FOR THE SINGLE AND MULTIPLE TIME-STEP CALCULATIONS

Perturbation Location	Percent Contribution to Total $\Delta K/K$ for 10% Increase In SS	
	t_f = 91 Days	t_f = 274 Days
CZ #1	62.5	33.2
CZ #2	190.6	121.3
CZ #3	-153.1	- 54.5

TABLE 4.20

RELATIVE CONTRIBUTION OF THE N^*, P^*, AND Γ^* EFFECTS TO THE TOTAL ΔK_{EFF} RESPONSE

Perturbation[a]		Percent Contribution to Total ΔK_{eff} Response at 91 Days			
Nuclide	Location	N^* Effect	P^* Effect	Γ^* Effect	Total $\Delta K/K$ (%)
^{232}Th	CZ1-2-3	99.42	0.44	1.02	-0.915
^{233}U	CZ1-2-3	93.72	6.64	- 0.36	4.544
^{233}U	CZ3	89.71	8.04	2.25	2.046
SS	CZ1-2-3	83.74	--	16.26	-0.078
SS	CZ1	102.56	--	- 2.56	-0.049
SS	CZ2	95.42	--	4.58	-0.149
SS	CZ3	105.93	--	- 5.93	0.120
^{16}O	CZ1-2-3	99.37	--	0.63	0.211

[a]10% increase the nuclide concentration at BOC.

TABLE 4.21

RELATIVE CONTRIBUTION OF THE Γ^* EFFECT TO THE TOTAL $\Delta K/K$ RESPONSE IN THE MULTIPLE TIME-STEP CALCULATION

Perturbation[a]		Percent Change in K_{eff} Response		
Nuclide	Location	$N^* + P^*$ Effects	$N^* + P^* + \Gamma^*$ Effects	% Diff.
^{232}Th	CZ1-2-3	-0.351	-0.381	- 8.03
^{233}U	CZ1-2-3	3.874	3.806	1.78
^{233}U	CZ3	1.987	2.058	- 3.46
SS	CZ1-2-3	-0.133	-0.148	-10.29

[a]10% increase in nuclide concentration at BOC.

information about the neutronic behavior of a particular system. Figures 4.10 through 4.12 display the calculated 9-group K_{eff} generalized adjoint flux at 182.6, 91.3, and 0.0 days, respectively.

Several interesting observations can be made from these plots. At any given time point, one can observe the spatial and spectral distribution of the importance of the addition of a unit neutron source to the EOC K_{eff} response. A low energy source particle near the center of the reactor has a strong negative effect on K_{eff} since the relatively large absorption cross sections of the fissile material at low energies cause an increased burnup of these nuclides. Therefore, a decrease in K_{eff} will result at later times. However, a low energy neutron in the blanket region, where there is a high concentration of fertile material, will tend to breed fissile isotopes and thus cause an increase in K_{eff} at some future time.

At high energies the explanation of the behavior of the K_{eff} generalized adjoint flux is not as straightforward, mainly due to the downscatter process. Also, in this energy region there is not as significant a difference between the fertile and fissile capture rates as in the low energy groups. However, a rough analysis shows that the fertile capture rate in the first three groups is about 2-3 times the fissile burnup rate over the entire core region. Thus an additional source particle in this space-energy region has a greater probability of creating a fissile isotope than destroying one, and therefore, affects the reactivity of the system in a positive manner at future times.

This brief explanation accounts for the observed distribution of the K_{eff} adjoint flux at a single time. However, since there are no drastic changes in the nuclide density field or flux distribution within the

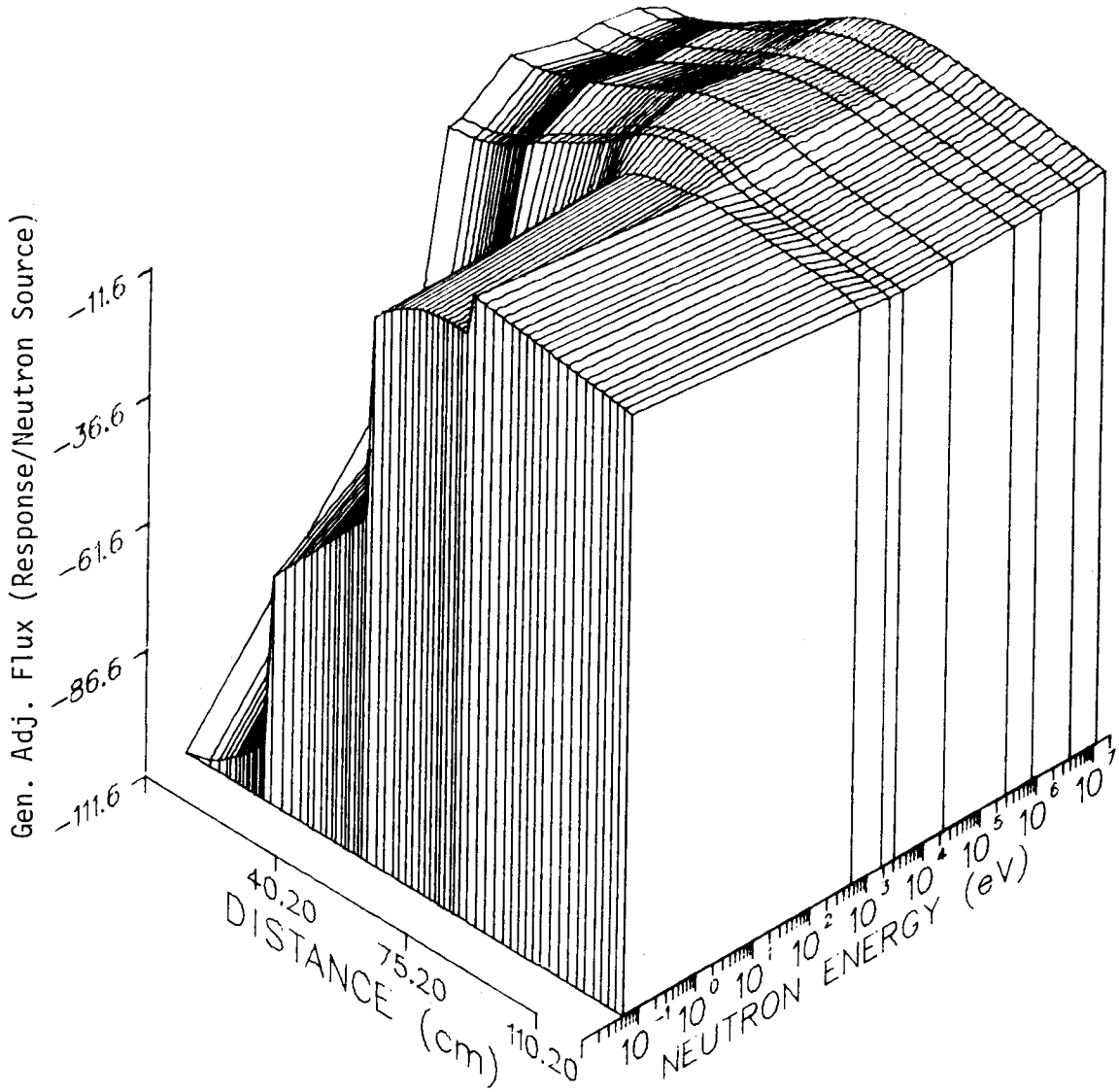

Figure 4.10. EOC K_{eff} Generalized Adjoint Flux at 182.6 Days.

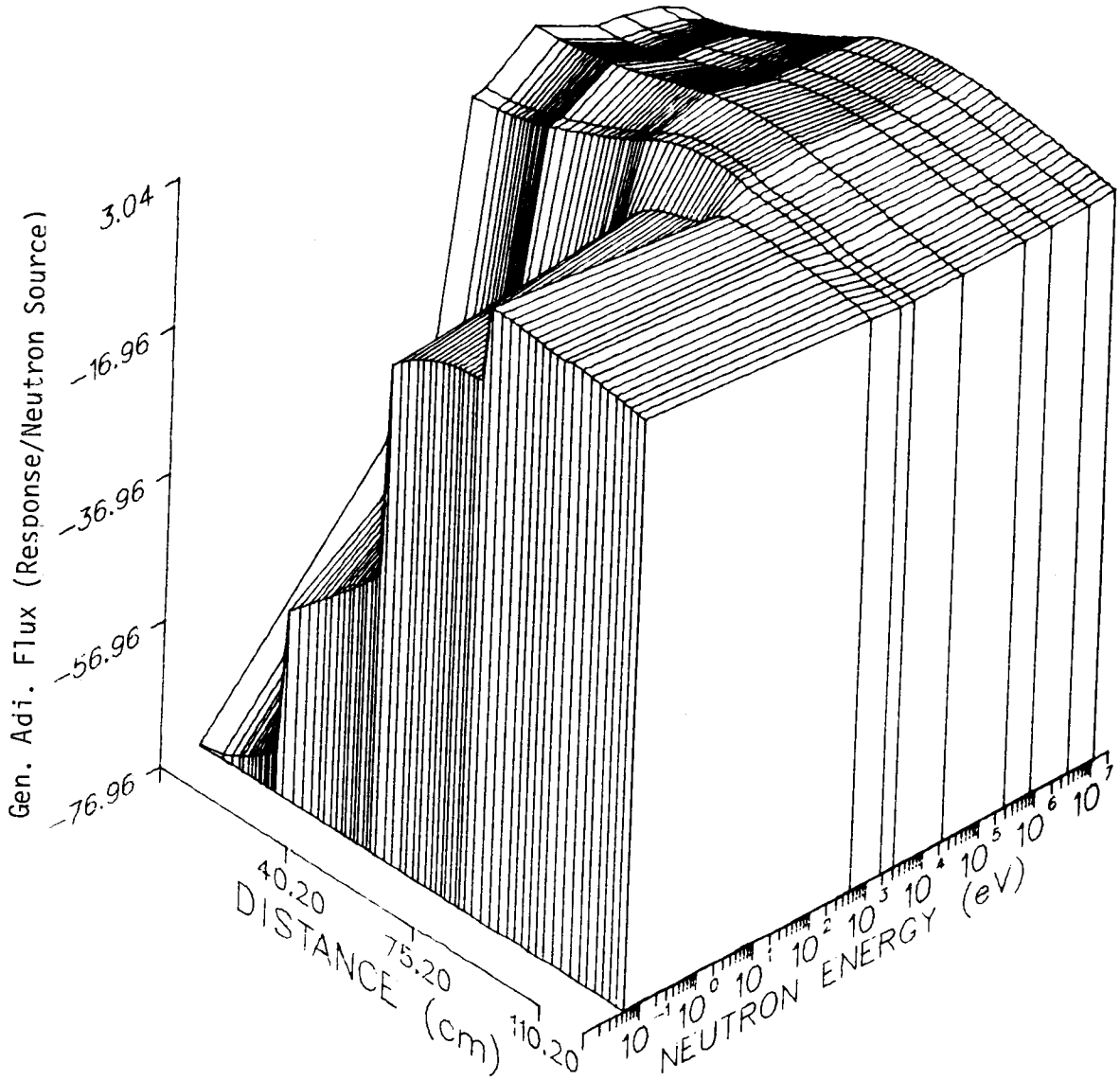

Figure 4.11. EOC K_{eff} Generalized Adjoint Flux at 91.3 Days.

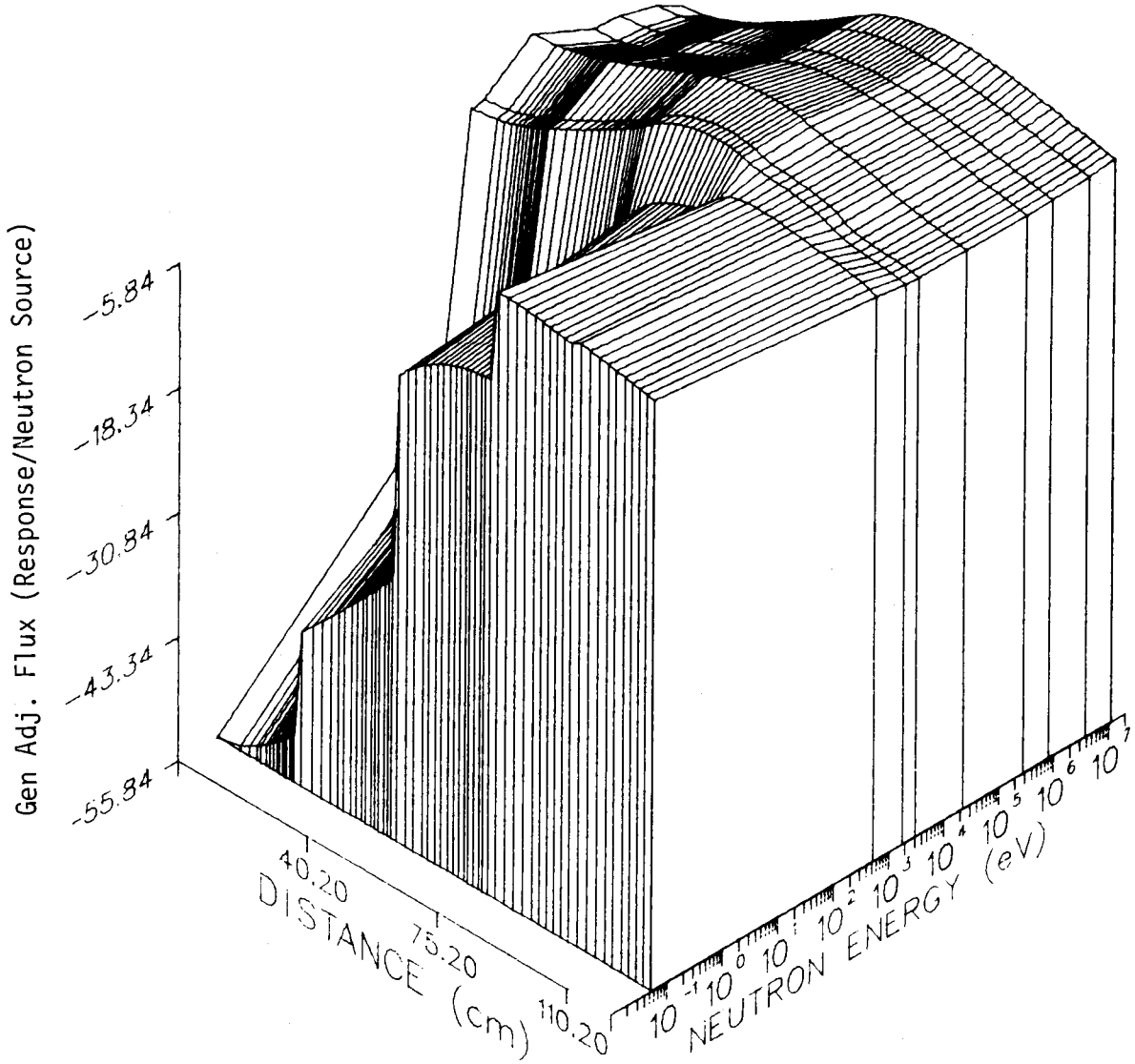

Figure 4.12. EOC K_{eff} Generalized Adjoint Flux at 0.0 Days.

reactor over the 274-day burn, one sees that the K_{eff} adjoint flux distribution remains relatively unchanged over this same period. However, the magnitude of the importance to K_{eff} at 274 days does change with time as shown in Figures 4.10-4.12. This is best seen by concentrating on the lower limit in the adjoint flux plots. The mechanisms responsible for the observed changes with time have not been isolated. If this could be done, one might be able to approximate the K_{eff} adjoint flux at 91.3 and 0.0 days from that calculated at 182.6 days. This approach has been tried with some simple approximations without much success. The whole area of finding some suitable approximation for the generalized adjoint flux needs much further investigation and is beyond the scope of the present study. However, it does represent an interesting area for future research.

Also, although not clearly displayed in the plots, the value of the K_{eff} adjoint flux ranges from +6 to −10 cm^3-sec over most of the space-energy domain of interest. This small variation around zero is the main reason that the Γ^* effect contribution was small for most of the perturbations listed in Table 4.20 and 4.21. In addition, in the calculation of the Γ^* effect, the adjoint flux is weighted with the forward neutron flux and then integrated over energy and spatial regions. This procedure essentially eliminates effects from the observed structure at low energies since the forward flux is relatively low in these groups for the fast reactor model being investigated.

The final point to be made concerning the EOC K_{eff} response is a comparison between the time-dependent generalized adjoint flux distribution and the space-energy distribution of the instantaneous regular adjoint flux. This time-independent importance function is displayed

in Figure 4.13. As can be seen, Figure 4.13 bears no resemblance at all to Figures 4.10-4.12. At any instant in time, a low energy neutron has a higher probability of causing a fission and thus increasing the neutron multiplication factor. Thus, in contrast to the time-dependent case, the instantaneous importance function is relatively high at low energies. Also, the slight increase at very high energies is due to the ^{238}U fission threshold. Lastly, as should be clear, the importance of an additional source neutron to the reactivity cannot be negative. Thus, the regular adjoint flux is always a positive function.

Reaction Rate Ratio Response. The final example to be given utilizing the 1-D spherical reactor model has a microscopic reaction rate ratio as the response of interest. The ^{238}U capture to ^{239}Pu fission ratio (C8/F9) was chosen because of its importance to the breeding ratio calculation in a $PuUO_2$ fast breeder reactor. In addition, the final time for this response was chosen as t_0^+, thus illustrating a static generalized perturbation theory application. This should emphasize the fact that static perturbation theory is just a special case of the more general time-dependent perturbation formulation utilized in this work. In addition, it will point out the usefulness of the DEPTH module for sensitivity studies in areas other than fuel depletion analysis.

First, define the response of interest as the initial C8/F9 ratio in core zone 1, or

$$R = \frac{C8}{F9} = \frac{\int_{cz1} \underline{\sigma}_c^T(\vec{r})\ \underline{\phi}(\vec{r})\ d\vec{r}}{\int_{cz1} \underline{\sigma}_f^T(\vec{r})\ \underline{\phi}(\vec{r})\ d\vec{r}} \tag{4.12}$$

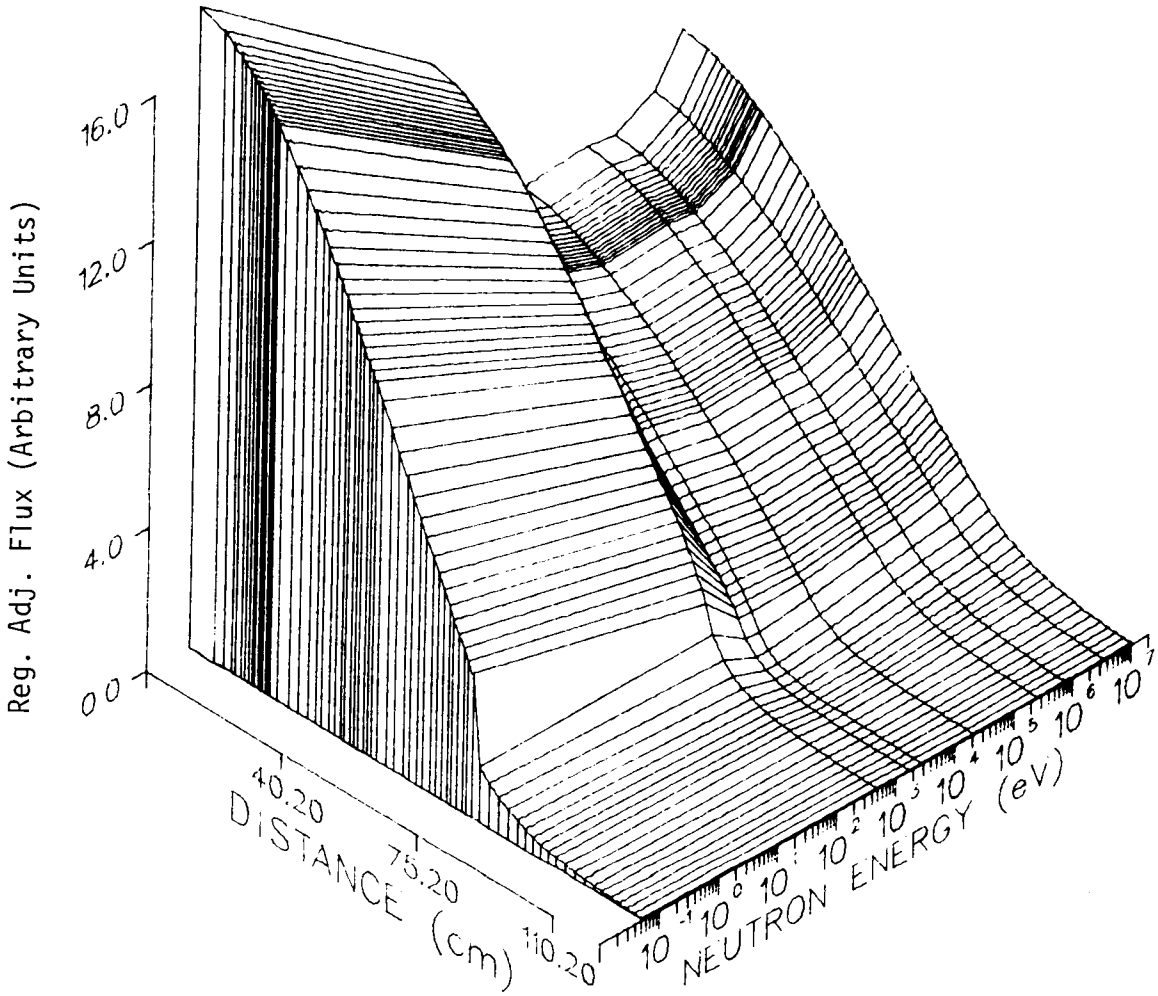

Figure 4.13. 1-D, 9-Group Regular Adjoint Flux.

where

$\underline{\sigma}_c(r)$ = microscopic ^{238}U capture cross-section vector (IGM groups)

$\underline{\sigma}_f(r)$ = microscopic ^{239}Pu fission cross-section vector (IGM).

Then, the three adjoint sources needed as input to DEPTH are given by,

$$\frac{\partial R}{\partial \alpha} = \frac{\partial R}{\partial \underline{N}(\vec{r})} = 0 \quad , \tag{4.13}$$

$$\frac{\partial R}{\partial \underline{\psi}(\vec{r})} = R\alpha \left[\frac{\underline{\sigma}_c(\vec{r})}{C8} - \frac{\underline{\sigma}_f(\vec{r})}{F9} \right] \quad \text{for } \vec{r} \text{ in cz } 1 \quad , \tag{4.14}$$

and

$$\frac{\partial R}{\partial \underline{\psi}(\vec{r})} = 0 \quad \text{for } \vec{r} \text{ not in cz } 1 \quad .$$

Using equations (4.13), (4.14) and (2.32) and the fact that the integrals over time approach zero as the interval of integration becomes zero, one has

$$\underline{S}_z^* = \frac{\partial R}{\partial \underline{\psi}_z} = \begin{cases} R\alpha \left[\dfrac{\underline{\sigma}_{c1}}{C8} - \dfrac{\underline{\sigma}_{f1}}{F9} \right] & \text{for } z = 1 \\ 0 \quad \text{for } z \neq 1 \quad . \end{cases} \tag{4.15}$$

Now, with this adjoint source and the adjoint solution algorithm given in Figure 3.2, page 28, for a one time-step problem (0.001 days), one can perform a static generalized adjoint flux calculation for the C8/F9 response. Thus a static generalized perturbation theory calculation is performed in the same manner as a time-dependent calculation. However, the depletion step in the static case is essentially zero.

A static generalized perturbation theory calculation was performed for the C8/F9 response using the above procedure. In this case, the only contribution to the response is the Γ^* effect. The generalized adjoint source used in this calculation is shown in Table 4.22 and the

TABLE 4.22

ADJOINT SOURCE VECTORS FOR C8/F9 RESPONSE IN CZ 1
(1-D, 9-GRP. PROB.)

Group	CZ #1	CZ #2	CZ #3	RB #1	RB #2
1	-3.0490E 00	0.0	0.0	0.0	0.0
2	-2.1330E 00	0.0	0.0	0.0	0.0
3	-1.2578E 00	0.0	0.0	0.0	0.0
4	-5.0822E-01	0.0	0.0	0.0	0.0
5	2.8576E 00	0.0	0.0	0.0	0.0
6	6.9509E 00	0.0	0.0	0.0	0.0
7	4.3784E 00	0.0	0.0	0.0	0.0
8	-4.6585E 01	0.0	0.0	0.0	0.0
9	-7.7650E 01	0.0	0.0	0.0	0.0

calculated Γ^* effect is displayed in Table 4.23. The Γ^* effects in the latter table are also the $\underline{N}_z^* * V_z$ adjoint nuclide density vectors which are a measure of the importance of a nuclide change to the desired response (see equation (2.23)).

As mentioned earlier, the generalized adjoint flux calculated using an adjoint source similar to the C8/F9 source in Table 4.22 can generally provide useful information about the system being analyzed. However, since the adjoint fixed sources investigated in this study have similar spatial and spectral distributions as the generalized adjoint fluxes, the more easily calculated source functions can be utilized as an aid in understanding the relationship of the neutronic behavior of the system to the response of interest.

The first point to note from Table 4.22 is that the adjoint source is only nonzero in regions where the response is defined. Thus, core zone 1 can be expected to be the most important spatial region. Additionally, since the power normalization factor cancels out of the response, the C8/F9 ratio in CZ 1 is only sensitive to a change in the energy spectrum of the weighting function, $\psi(\vec{r},E)$. Table 4.24, which displays the ^{238}U capture to ^{239}Pu fission cross-section ratio ($^{238}\sigma_c/^{239}\sigma_f$) versus energy, indicates that a shift in the weighting function towards groups 5, 6, and 7 would tend to increase the C8/F9 ratio. In contrast, a further softening of the spectrum would greatly decrease the response of interest. This general trend is the same as observed in Table 4.22. A positive C8/F9 source in groups 5, 6, and 7 and a relatively large negative adjoint source in the lower two energy groups are observed.

TABLE 4.23

$\underline{N}_z^*(t_0^-)*V_z$ FOR C8/F9 RESPONSE IN CZ #1
(1-D, 9-GRP. PROB.)

Nuclide	CZ #1	CZ #2	CZ #3	RB #1	RB #2
TH228	0.0	0.0	0.0	0.0	0.0
TH232	-4.1189E-01	-4.6822E-01	-3.4469E-01	-1.5104E-02	-1.9417E-04
PA231	-6.0111E 00	-4.4125E 00	-1.5724E 00	-1.4724E-01	-3.5445E-03
PA233	-2.3459E 00	-9.6652E-01	-2.0945E-01	-1.6167E-02	-4.5327E-04
U 232	-3.2177E 00	-1.3039E 00	2.9706E-01	3.8240E-02	1.4703E-03
U 233	-2.0369E 01	-6.4181E 00	5.6986E 00	1.0751E 00	4.6022E-02
U 234	-2.3596E 00	-1.0781E 00	1.0091E-01	2.7687E-02	8.9704E-04
U 235	-1.5566E 01	-5.6795E 00	3.3043E 00	7.0372E-01	3.1362E-02
U 236	-1.3123E 00	-8.7134E-01	-3.5502E-01	-1.8476E-02	-3.1770E-04
U 238	-3.9648E-01	-2.2162E-01	-1.2990E-01	7.5615E-03	3.5867E-04
NP237	-7.5302E 00	-5.0640E 00	-1.4367E 00	-1.3872E-01	-3.3149E-03
NP239	-7.4923E 00	-4.4774E 00	-1.0626E 00	-1.0345E-01	-2.4773E-03
PU238	-1.0768E 01	-3.4488E 00	2.4974E 00	4.1105E-01	1.6222E-02
PU239	-1.4844E 01	-4.2736E 00	4.4801E 00	7.8211E-01	3.1935E-02
PU240	-3.4954E 00	-1.2269E 00	6.2716E-01	7.6100E-02	2.2627E-03
PU241	-2.1185E 01	-5.9279E 00	6.4905E 00	1.2210E 00	5.1971E-02
PU242	-3.5550E 00	-1.3708E 00	2.8048E-01	4.4338E-02	1.2950E-03
AM241	-1.4952E 02	-1.1341E 02	-3.6186E 01	-3.5227E 00	-8.2304E-02
AM243	-3.3846E 00	-1.6190E 00	-2.5250E-01	-3.7824E-02	-1.2395E-03
CM244	-5.4279E 00	-1.3347E 00	1.6590E 00	2.0005E-01	6.2940E-03
FP RL	-1.1901E-01	-9.0919E-01	-4.0379E-01	8.0585E-03	5.8889E-04
NA	5.1449E-01	2.1100E-01	5.3264E-02	9.8792E-03	2.5848E-04
SS COR	3.7239E-01	2.4163E-01	4.1550E-02	0.0	0.0
O 16	7.6352E-01	4.2090E-01	5.3476E-02	9.6317E-03	2.2486E-04

TABLE 4.24

^{238}U CAPTURE TO ^{239}Pu FISSION CROSS-SECTION RATIO

Group	$^{238}\sigma_c/^{239}\sigma_f$
1	0.320
2	0.031
3	0.048
4	0.115
5	0.312
6	0.349
7	0.231
8	0.048
9	0.004

The detailed spatial and spectral information contained in the generalized adjoint flux (and source) is lost in the evaluation of the Γ^* effect. However, the overall importance of a nuclide perturbation to the desired C8/F9 response as shown in Table 4.23 is the real quantity of interest. For example, one sees that, in general, an increase in the fission product or heavy metal concentration would decrease the microscopic ^{238}U capture to ^{239}Pu fission ratio in CZ 1. However, an increase in the stainless steel, sodium, or oxygen content tends to increase the microscopic C8/F9 reaction rate ratio.

To test the accuracy of the static perturbation theory calculation, several ^{16}O perturbations of varying magnitude were made to all three core zones. The "sensitivity coefficients" in Table 4.23 indicate that the C8/F9 ratio should increase with an increase in the oxygen concentration. In fact, a uniform 10% increase in the ^{16}O density in the core regions would increase the reference C8/F9 ratio by 1.409%. This agrees very well with the directly calculated value of 1.385%.

Although there is no fundamental difference, only positive nuclide perturbations have been investigated up to this point. For completeness, negative perturbations of the ^{16}O concentration were performed for the ^{16}O perturbation/(C8/F9) response pair. As can be seen from Figure 4.14, good agreement is attained for perturbations as large as 50%. A slight nonlinear behavior is observed for large decreases in the ^{16}O concentration. Figure 4.15 shows that this nonlinearity is due to the rather large change in the zone-averaged flux spectra in CZ 1 for the no-oxygen case relative to the reference calculation. However, even

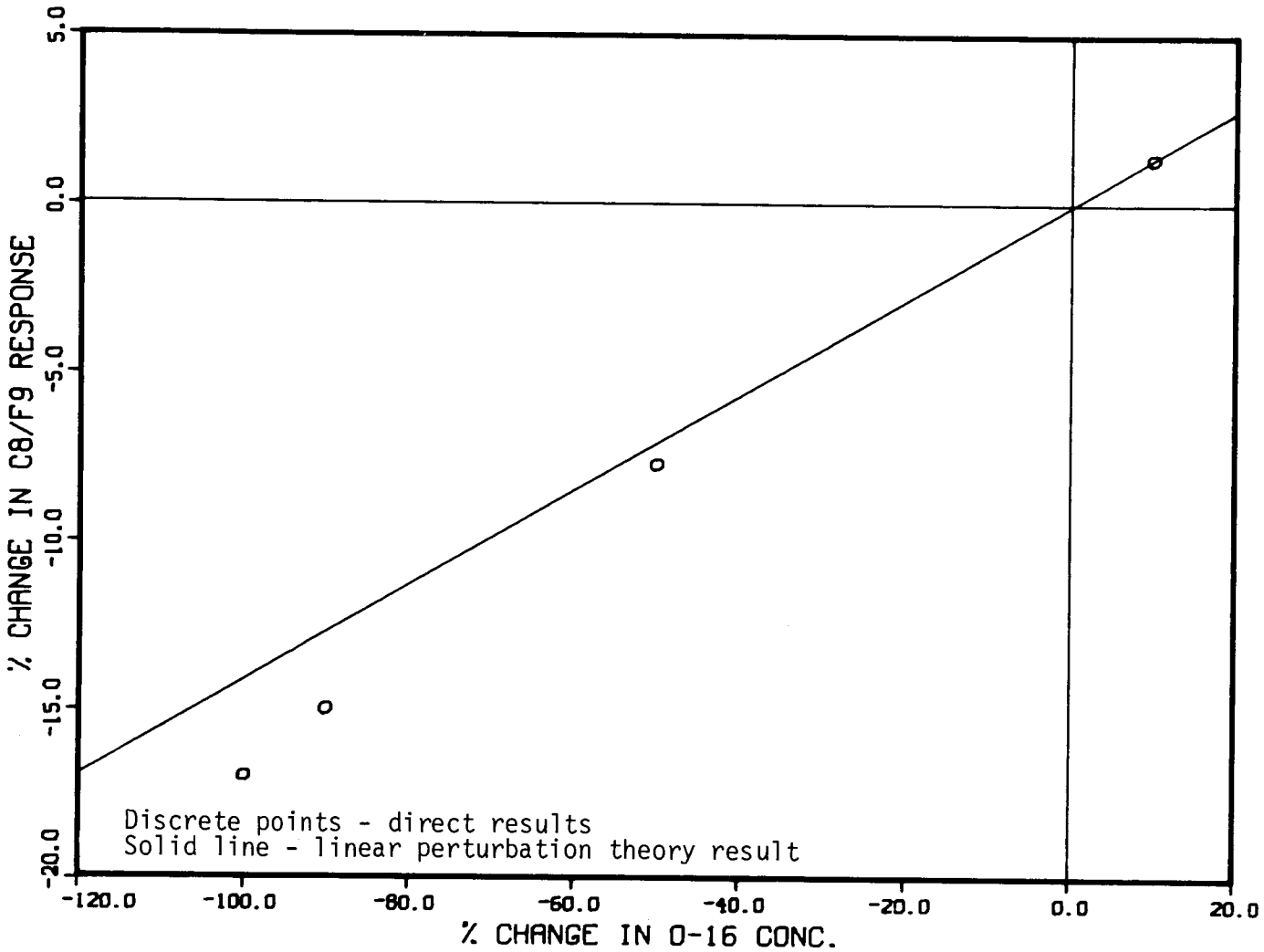

Figure 4.14. Nonlinear Behavior of Microscopic C8/F9 Response in Core Zone 1.

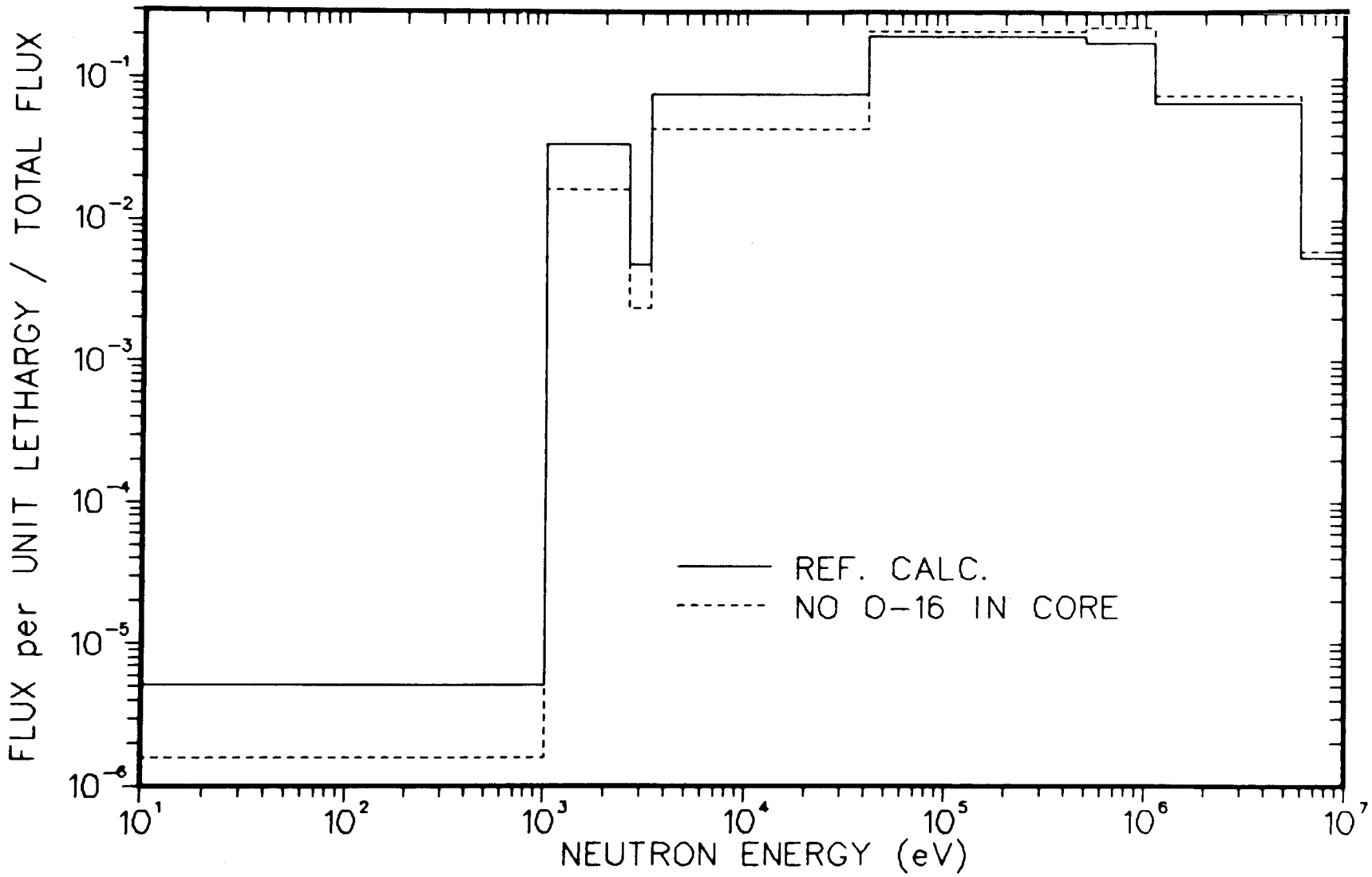

Figure 4.15. Comparison of Flux Spectra in CZ 1 for a 100% Decrease in the O-16 Concentration Relative to the Reference Case.

for a 100% perturbation, the $\Delta R/R$ values calculated with DEPTH and direct methods only differ by about 17%.

The C8/F9 response concludes the analyses performed using the 1-D spherical model shown in Figure 4.1, page 43. The analyses have included a wide range of perturbation/response pairs which illustrated several important characteristics of depletion perturbation theory. In addition, both multigroup and multiple time-step problems were investigated. For all these examples, depletion perturbation theory compared extremely well with the direct re-calculation method. Thus, the DPT methods utilized in this study have proved to be an accurate calculational tool for both static and time-dependent generalized perturbation theory.

Two-Dimensional Calculations

The next step in the evaluation of depletion perturbation theory as an alternate calculational method for burnup analysis, is its application to more realistic two-dimensional reactor analysis problems. The calculational model utilized in this portion of the study is shown in Figure 4.16. The design is based on a General Atomic 1500 MWe $PuUO_2/UO_2$ Gas-Cooled Fast Reactor (GCFR) used as a reference model in the evaluation of some alternate GCFR fuel cycles.[26]

The RZ calculational model contains four homogeneous core zones with corresponding axial blanket regions. A three-row radial blanket configuration is modeled as two separate zones, one containing the first row of assemblies and the second consisting of the outer two radial rows. The whole core is then surrounded by a stainless steel structure and shield region. These eleven separate regions are then further subdivided into subzones. The core and axial blanket zones have three subzones. The

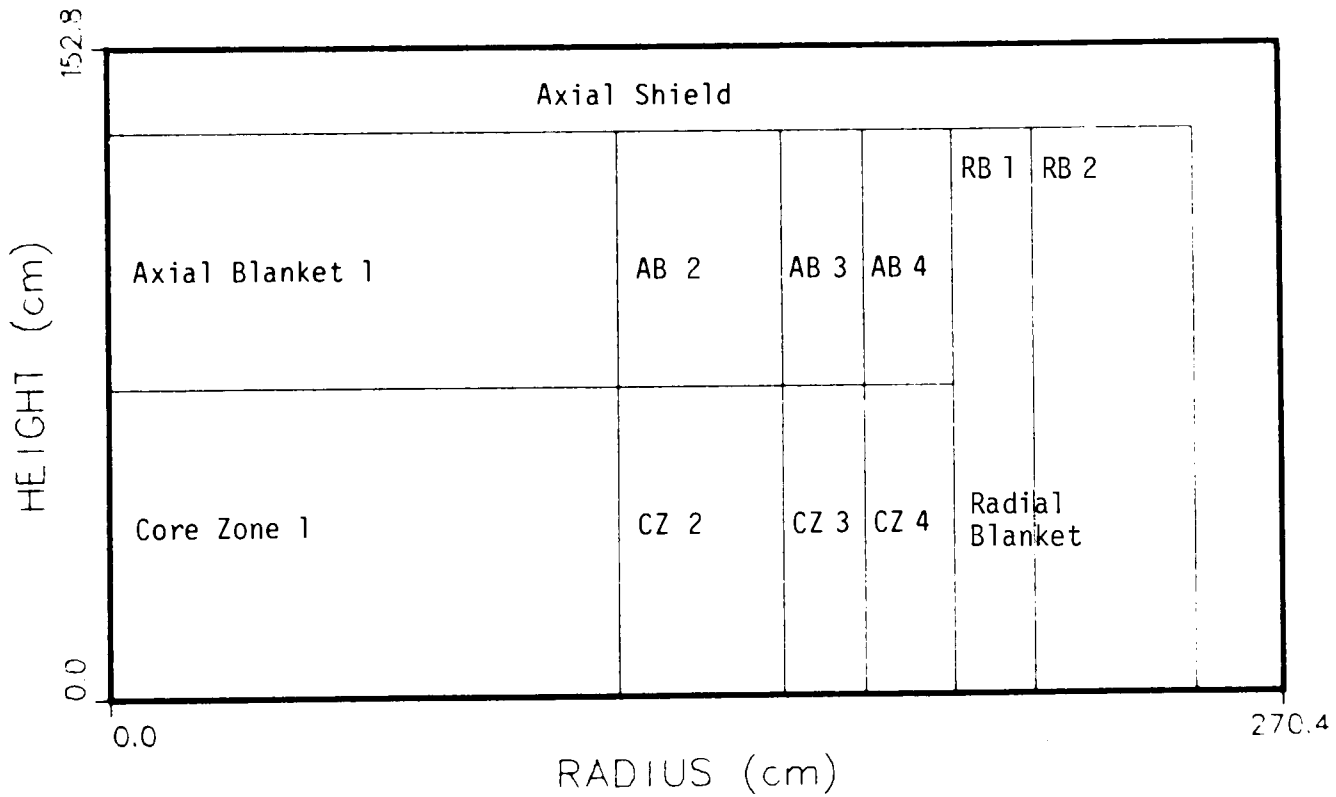

Figure 4.16. Two-Dimensional Model of 1500 MWe GCFR.

two radial blanket zones have six subzones and the shield consists of only one subzone. Each subzone is depleted with the zone-averaged flux and the nuclide concentration within a zone can be written as,

$$\underline{N}_z = \frac{1}{v_z} \sum_s \underline{N}_{sz} \, v_{sz}$$

where

$\underline{N}_z$ = zone-averaged nuclide density vector (NNUC isotopes)

$\underline{N}_{sz}$ = subzone-averaged nuclide density vector (NNUC)

v_z = volume of zone z

v_{sz} = volume of subzone s in zone z.

The purpose of the subzone modeling is to allow for fuel management operations in multicycle calculations. For example, the core and axial blanket regions would be on a three-year refueling schedule since they each have three subzones. One subzone in each zone is discharged and refueled each year. For the present analysis, however, it is only necessary to understand that there is a total of 37 regions (subzones) being depleted with eleven different zone-averaged fluxes. Each region can be perturbed separately and the desired response can be defined in a single region or a combination of regions.

A depletion perturbation analysis, similar to that performed for the 1-D spherical model, has been performed for this two-dimensional GCFR configuration. However, the responses investigated were limited to nuclide responses. This type of response functional was chosen because of its relatively simple expressions for the adjoint sources needed as input to DEPTH. A computer code for the evaluation of the sources for the more complex responses (K_{eff}, C8/F9, etc.) is not

presently available and hand calculations for a 37-region, 9-group model could be extremely tedious. However, with the experience gained from the 1-D calculations, it is felt that the nuclide inventory responses investigated provide a representative set of typical two-dimensional depletion perturbation theory calculations.

Table 4.25 gives a complete description of the perturbation/response pairs utilized in the 2-D analysis. The ^{239}Pu inventory was chosen as the most important nuclide response for a $PuUO_2/UO_2$ GCFR. The plutonium inventory in the entire reactor as well as in the fourth axial blanket zone was chosen as responses of interest. This allows the investigation of the effects of a perturbation on both a global and localized response. As will be shown later, the Γ^* effect plays the dominant role in the prediction of localized responses. Lastly, it should be pointed out that the third perturbation contains a set of nuclide variations. This is more realistic of an actual design variation to be considered in a core design situation since it involves an exchange of materials rather than an increase or decrease in a single nuclide.

Table 4.26 summarizes a comparison of DPT results with direct calculation for the total ^{239}Pu inventory response after one depletion time step. This table, in contrast to those shown previously, gives the actual change in kilograms of the perturbed ^{239}Pu inventory relative to the reference case. Excellent agreement is obtained with the total DPT result and the directly calculated perturbed response. In all cases, the percent difference in the calculated and predicted ΔR is only on the order of a few percent. Thus, two-dimensional problems seem to create no problems for the time-dependent perturbation theory methods within the DEPTH module.

TABLE 4.25

DESCRIPTION OF PERTURBATION/RESPONSE PAIRS
UTILIZED IN THE 2-D ANALYSES

Reference Model:

$PuUO_2/UO_2$ 1500 MWe GCFR

Homogeneous four core-zone model

Nine-group GCFR cross sections

Responses:

1. ^{239}Pu inventory in entire reactor
2. ^{239}Pu inventory in axial blanket #4

Perturbations:

1. Increased fission product concentration in CZ 1 (1.0E-3 atoms/barn-cm)
2. Increased ^{239}Pu concentration by 10% in CZ 1
3. Replaced 10% of ^{238}U with ^{232}Th in radial blankets

TABLE 4.26

DPT VERSUS DIRECT CALCULATION FOR THE TOTAL ^{239}Pu INVENTORY AT 91 DAYS IN THE 2-D GCFR MODEL

	Change in Response[a] (KG)					
	Perturbation Results					
Perturbation	N^* Effect	P^* Effect	Γ^* Effect	Total	Direct[b] Calc.	Diff. (%)
Δ FISSP	--	--	7.93	7.93	8.11	-2.2
Δ ^{239}Pu	102.90	-4.34	-5.80	92.76	92.62	0.2
Δ^{238}U	-16.25	0.39	13.13	-2.73	--	--
Δ^{232}Th	--	-0.08	-15.97	-16.05	--	--
SUM	-16.25	0.31	-2.84	-18.78	-18.45	1.8

[a]Reference ^{239}Pu inventory = 4151.4 kg.

[b]The $^{238}U/^{232}Th$ variations represents a single perturbation to the reactor, therefore, there are no direct results for the individual variations.

Particularly interesting in this set of examples is the relative contribution of the three adjoint functions to the total perturbed response. The Γ^* effect is the only contributor for the fission product perturbation with excellent agreement obtained with direct calculation. Also, as would be expected, the N^* effect dominates the ^{239}Pu perturbations. However, the relative contributions for the last set of perturbations are not as obvious. Here one observes large competing N^* and Γ^* effects for the ^{238}U variation and a large decrease in the response due to the ^{232}Th perturbation's Γ^* effect. Thus, the indication from the total column of Table 4.26 is that the majority of the ^{239}Pu inventory decrease is due to the addition of the ^{232}Th rather than the reduction of the ^{238}U concentration in the radial blankets.

At first glance, this is a rather surprising result. However, further investigation verifies this observed phenomena. Clearly, a negative N^* effect due to a decreased ^{238}U concentration is expected. However, the observed Γ^* effects are not as apparent. Assume for the moment that the radial blanket can be approximated as a nonmultiplying infinite slab. In this case, the one-group flux at some thickness x in the blanket can be written as,[27]

$$\phi(x) = A e^{-x/L} \tag{4.16}$$

where A is a constant proportional to the neutron source strength from the core and L is the neutron diffusion length. The diffusion length can be written as

$$L = \sqrt{D/\Sigma_a} = \sqrt{\frac{1}{3\Sigma_{tr}\Sigma_a}} \tag{4.17}$$

where

$$\Sigma_{tr} = \underline{N}^T \underline{\sigma}_{tr} \text{ and } \Sigma_a = \underline{N}^T \underline{\sigma}_a \quad .$$

Thus, the diffusion length is inversely related to the nuclide density vector, $\underline{N}$. Therefore, a decrease in the ^{238}U concentration will increase the diffusion length and tend to flatten the flux distribution across the slab thickness. This increased average flux in the blanket will increase the ^{238}U capture rate and ^{239}Pu inventory at some later time. Similarly, the addition of thorium to the system reduces the average flux level and subsequent ^{239}Pu inventory. Thus the results indicated in Table 4.26 can be readily explained.

The above observation for the perturbation to the radial blanket zones can be generalized to include any region whose flux distribution and magnitude are determined by the neutron removal characteristics of the region. Included in this category are both axial and radial blankets, control rods, and structural or shielding material regions of the reactor. In all of these regions the average flux level is a strong function of the nuclide density vector $\underline{N}$. Thus perturbations in these types of reactor environments can be expected to have large Γ^* effects relative to the total perturbation effect. This is emphasized in Table 4.27 which gives the spatial distribution of the percent contribution of the Γ^* effect for a unit ^{238}U density perturbation in the respective zones. As can be seen, the contribution of the Γ^* effect is very large in regions away from the main neutron source of the reactor (central core regions). Thus, in general, one can conclude that the $\Gamma^*(\vec{r},E)$ calculation is essential if perturbations are to be made in other than the central core regions of the reactor.

TABLE 4.27

SPATIAL DISTRIBUTION OF THE RELATIVE CONTRIBUTION OF THE $^{238}U\ \Gamma^{*}$ EFFECT TO THE TOTAL ^{239}Pu INVENTORY

Location	$^{238}U\ \Gamma^{*}$ Effect/^{238}U Total Effect (%)
CZ 1	12.8
CZ 2	-5.0
CZ 3	-35.5
CZ 4	-116.7
AB 1	-80.9
AB 2	-99.2
AB 3	-137.9
AB 4	-234.4
RB 1	-475.9
RB 2	-491.3

The above general effect is especially magnified for the present case of the ^{239}Pu response because of the importance of the blanket regions to the overall ^{239}Pu inventory. The spatial distribution of the energy-averaged generalized adjoint flux for the total ^{239}Pu inventory is shown in Figure 4.17. From this one sees that, in general, the addition of a source neutron in either the axial or radial blanket regions will increase the response, while increased source strength in the central core regions will decrease the ^{239}Pu inventory at 91.3 days. This indicates that the conversion ratio is less than unity in the core and greater than unity in the blankets.

It should be noted that Figure 4.17 displays only the higher energy features of the ^{239}Pu adjoint flux. The energy averaging was performed using

$$\Gamma^*(\vec{r}) = \frac{\sum_g \Gamma_g^*(r)\,\Delta E_g\, f_g}{\sum_g \Delta E_g\, f_g} \quad , \tag{4.18}$$

with $f_g = 1.0$ for all g. Therefore, the group-wise adjoint fluxes were averaged using the weighting function shown in the first half of Table 4.28. In contrast, the second half of Table 4.28 gives a weighting function that tends to display the low energy features of the importance function. The total ^{239}Pu inventory adjoint flux averaged over groups 6 through 9 is displayed in Figure 4.18. In general, the same features as displayed for the higher energies are apparent. However, the gradient of the adjoint flux at the core/blanket boundaries is much steeper at lower energies.

An analysis similar to that just presented for the total ^{239}Pu inventory was performed for a ^{239}Pu inventory response in the fourth

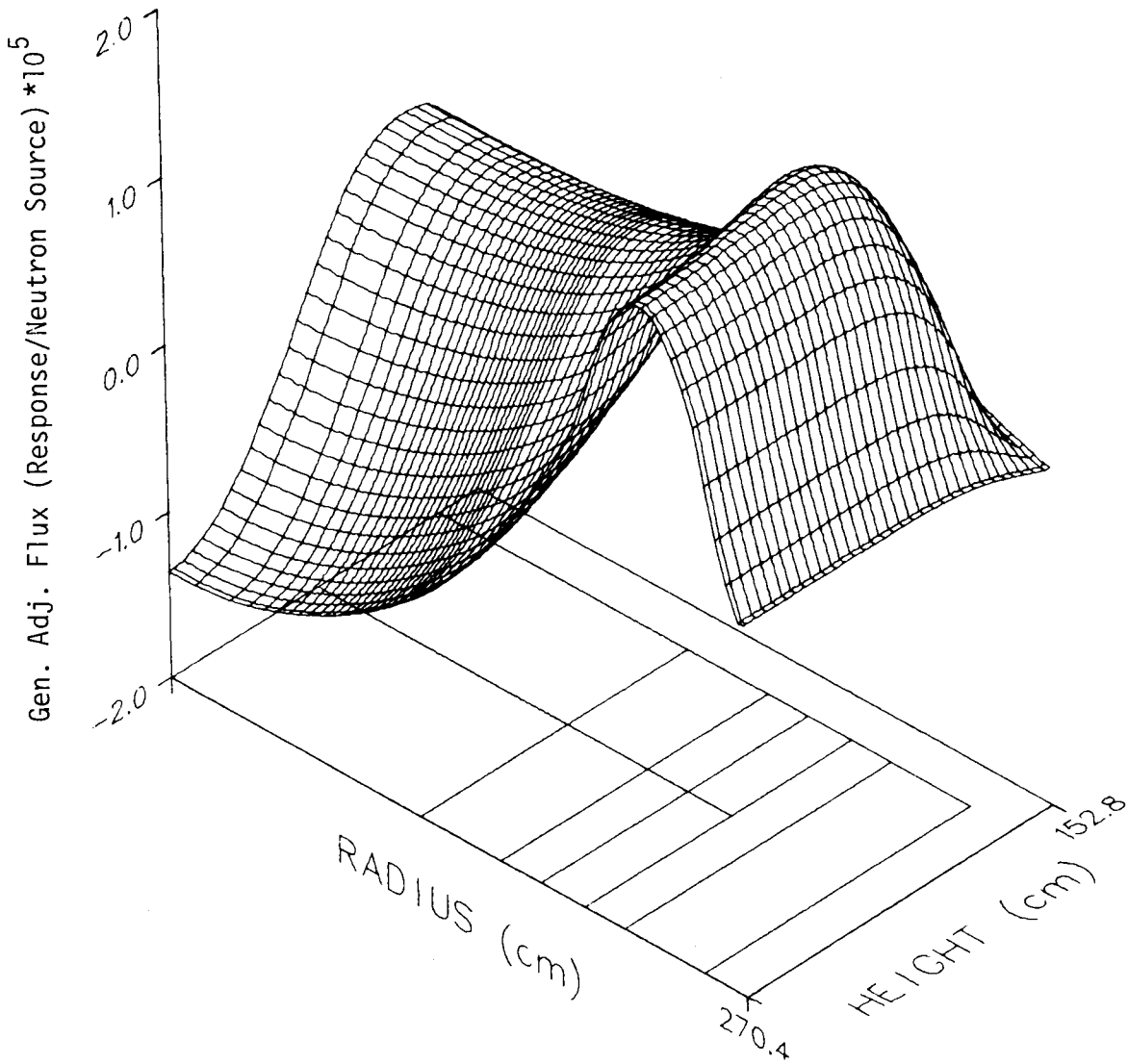

Figure 4.17. Total ^{239}Pu Generalized Adjoint Flux Averaged Over All Energy Groups.

TABLE 4.28

WEIGHTING FUNCTIONS[a] FOR ADJOINT FLUX AVERAGING

Energy Group	Upper Energy Boundary (ev)	Averaging Over Groups 1-9		Averaging Over Groups 6-9	
g		f_g	W_g	f_g	W_g
1	1.492+7	1.0	5.934-1	0.0	0.0
2	6.065+6	1.0	3.323-1	0.0	0.0
3	1.108+6	1.0	4.090-2	0.0	0.0
4	4.979+5	1.0	3.063-2	0.0	0.0
5	4.087+4	1.0	2.515-3	0.0	0.0
6	3.355+3	1.0	4.974-5	1.0	2.212.1
7	2.613+3	1.0	1.072-4	1.0	4.768.1
8	1.013+3	1.0	6.790-5	1.0	3.019-1
9	1.000-1	1.0	6.697-9	1.0	2.978-5

[a] $W_g = \dfrac{f_g \, \Delta E_g}{\sum_g f_g \, \Delta E_g}$

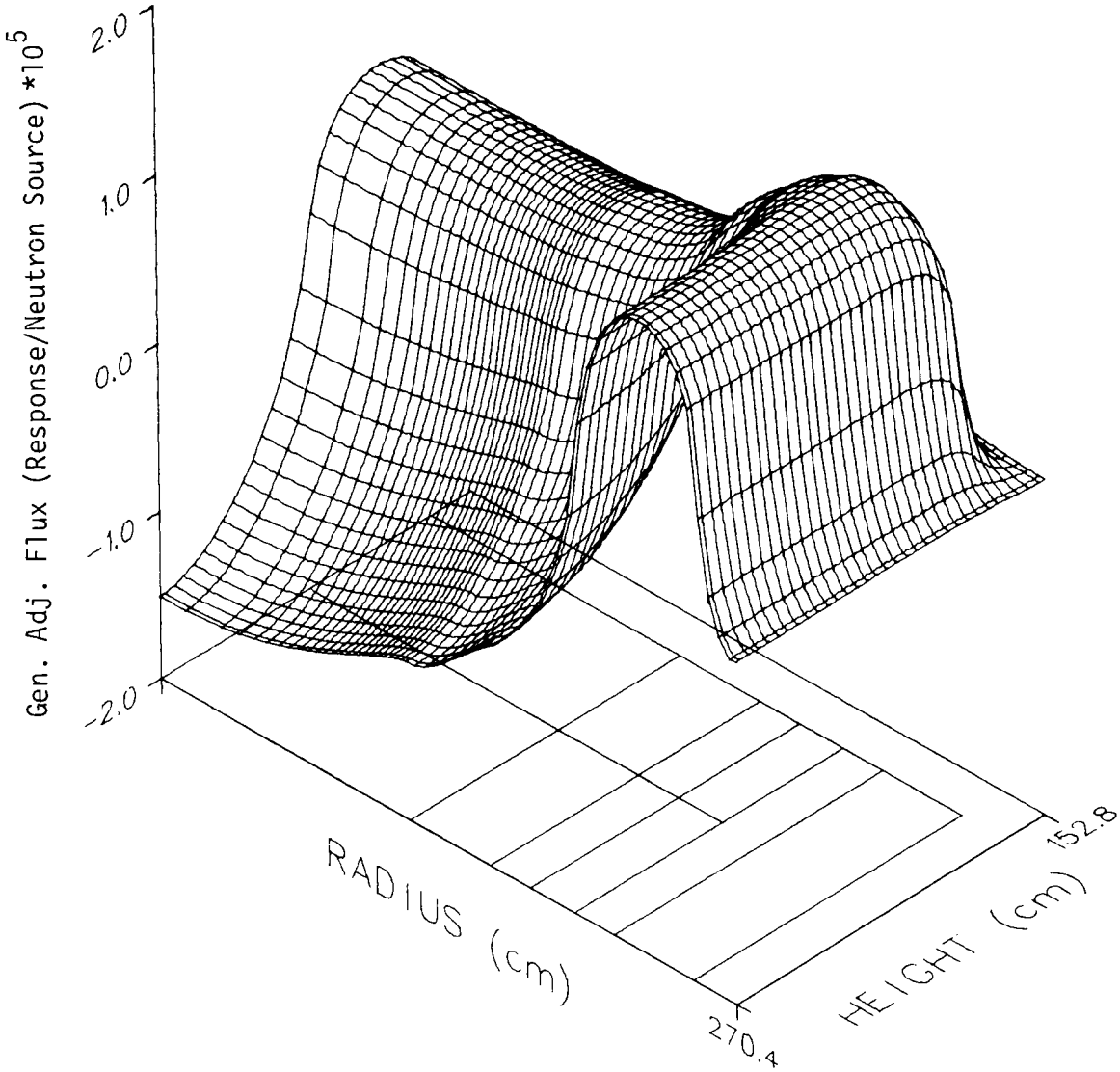

Figure 4.18. Total ^{239}Pu Generalized Adjoint Flux Averaged Over Groups 6-9.

axial blanket zone. This response was chosen to highlight the Γ^* effect for all of the perturbation cases. A comparison of DPT results with direct calculation for this response is given in Table 4.29. The percent change in the desired response is presented since the reference ^{239}Pu inventory in AB#4 is only 7.21 Kg. As in most cases, good agreement between calculated and predicted response variations is obtained. These show that accurate predictions can be made for localized responses. In addition, these examples emphasize that the effects of perturbations in regions far removed from the location of interest can easily be determined.

Table 4.29 shows that the fission product perturbation in CZ 1 caused an 8.5% increase in the ^{239}Pu inventory in the fourth axial blanket region. Similarly, a 10% increase in the BOC ^{239}Pu concentration in CZ 1 produced a 6% decrease in the desired response. Lastly, one sees that the radial blanket perturbation had little overall effect on the axial blanket ^{239}Pu inventory after 91 days of reactor operation. The ability to quantify region to region coupling effects such as these may be quite useful in reactor design analyses.

The AB #4 ^{239}Pu generalized adjoint fluxes shown in Figures 4.19 and 4.20 display the geometric coupling for the present example. Figure 4.19 emphasizes the higher neutron energies while Figure 4.20 displays the low energy importance of a neutron source variation to the ^{239}Pu inventory in AB #4. Obviously, this importance peaks in the region where the response is defined and approaches zero in the unimportant outer shield regions of the reactor. At all energies, an increased neutron source at the center of the core decreases the response. However, the importance of a low energy neutron source in the blankets and outer

TABLE 4.29

DPT VERSUS DIRECT CALCULATION FOR THE ^{239}Pu INVENTORY AT 91 DAYS IN THE FOURTH AXIAL BLANKET ZONE OF THE 2-D GCFR MODEL

	Percent Change in Response[a]					
	Perturbation Results					
Perturbation	N^* Effect	P^* Effect	Γ^* Effect	Total	Direct[b] Calc.	Diff. (%)
Δ FISSP	--	--	8.903	8.903	8.504	4.7
Δ ^{239}Pu	--	-2.321	-3.690	-6.011	-5.958	0.9
Δ ^{238}U	--	0.211	0.958	1.168	--	--
Δ ^{232}Th	--	-0.045	-1.624	-1.669	--	--
SUM	--	0.166	-0.666	-0.500	-0.497	0.8

[a]Reference ^{239}Pu inventory = 7.215 kg.

[b]The $^{238}U/^{232}Th$ variations represent a single perturbation to the reactor; therefore, there are no direct results for the individual variations.

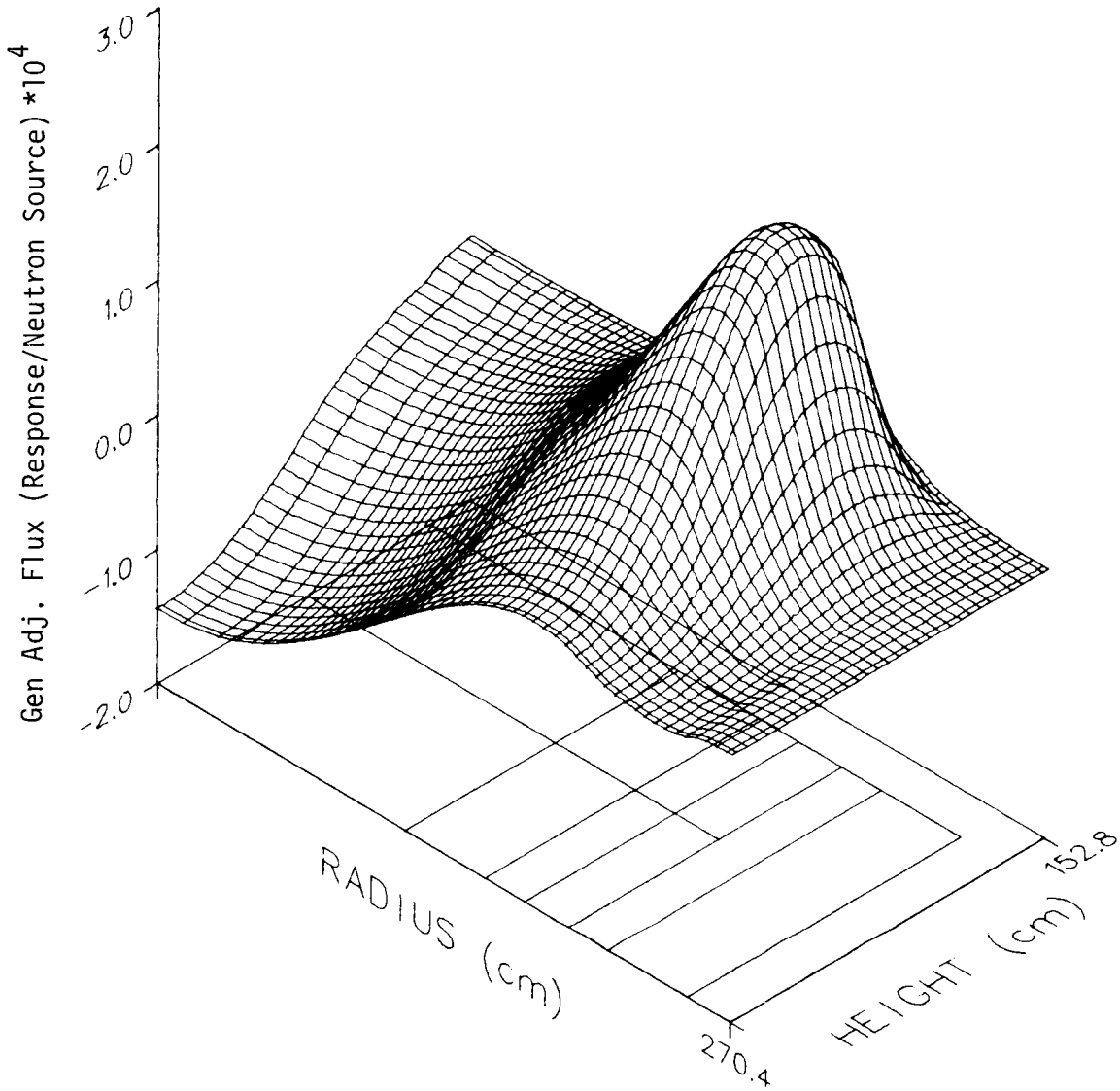

Figure 4.19. Axial Blanket #4 ^{239}Pu Generalized Adjoint Flux Averaged Over All Energy Groups.

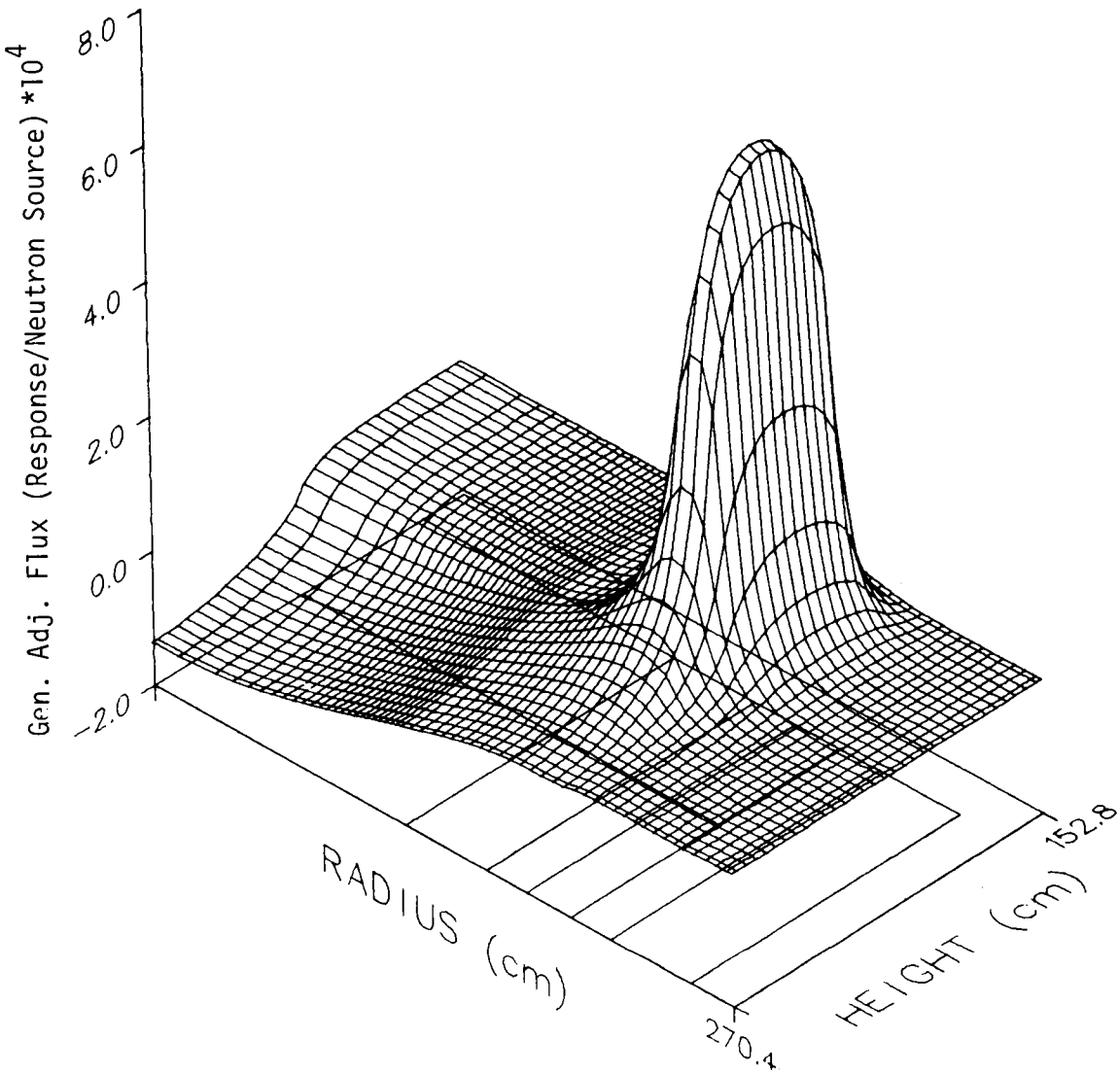

Figure 4.20. Axial Blanket #4 ^{239}Pu Generalized Adjoint Flux Averaged Over Groups 6-9.

core regions is nearly zero except for the large positive spike centered over the fourth axial blanket zone.

The above examples were for a one time-step depletion calculation and were primarily intended to emphasize the Γ^* effects contribution to the overall perturbed response. A comparison with direct calculation was also performed for the total ^{239}Pu inventory response after one year. The main goal here was to confirm the predictive capability of DPT for more realistic burn times when utilizing the more complicated 2-D geometry. Table 4.30 clearly shows that this goal has been achieved. In all cases there is excellent agreement between calculated and predicted perturbed responses, with a maximum difference between the two methods of less than 2%.

Since this latter calculation is representative of a typical depletion calculation, it will also be employed to compare the relative computing requirements of the forward and adjoint computations. Table 4.31 makes this comparison for only the central processing unit (CPU) time and number of input/output operations (IO) since the memory requirements of the forward and adjoint calculations are identical.

As mentioned in Section III, a reference forward calculation differs from a base case in that a regular adjoint and perturbation computation are required at each flux-eigenvalue calculation. Thus a forward calculation to be followed by a set of adjoint solutions requires roughly 2.3 times the CPU time and 2.5 times the IO operations as a base depletion calculation. However, this penalty has to be paid only once, since only one reference calculation is needed for any number of adjoint solutions. However, the penalty incurred in the adjoint calculation (45% greater

TABLE 4.30

DPT VERSUS DIRECT CALCULATION FOR THE EOC TOTAL ^{239}Pu INVENTORY RESPONSE IN THE 2-D GCFR MODEL

Perturbation	Change in Response[a] (KG) DPT Result	Direct[b] Result	Diff. (%)
Δ FISSP	28.22	28.24	-0.1
Δ ^{239}Pu	54.33	54.12	0.4
Δ ^{238}U	-8.79	--	--
Δ ^{232}Th	-47.21	--	--
SUM	-56.00	-55.07	1.7

[a]Reference EOC ^{239}Pu inventory = 4525.8 kg.

[b]The $^{238}U/^{232}Th$ variations represent a single perturbation to the reactor; therefore, there are no direct results for the individual variations.

TABLE 4.31

COMPARISON OF RELATIVE COMPUTING REQUIREMENTS FOR THE FORWARD AND ADJOINT DEPLETION CALCULATIONS[a]

	Relative CPU Time	Relative IO Count
Base Forward Calculation	1.00	1.00
Reference Forward Calculation	2.29	2.46
Adjoint Calculation[b]	1.45	1.35

[a]Four flux-eigenvalue solutions were performed in the forward calculations and only three flux computations were done in the adjoint case.

[b]Very recent improvements in the numerical calculation of the generalized adjoint flux within VENTURE will essentially eliminate the additional cost noted here.[28]

CPU time and 35% more IO operations) relative to the base forward case will be observed for each response to be investigated.

The additional computing requirements of the adjoint calculation can be attributed to the convergence properties of the generalized adjoint flux. In the calculational models investigated in this study, the forward flux was a slowly varying function of space and energy. However, the same cannot be said for the generalized adjoint fluxes. The ^{232}U 1-D adjoint flux, for example, had a large spike in the first energy group and the AB #4 ^{239}Pu 2-D adjoint flux had somewhat of a spatial discontinuity in the response domain at low energies. Because of this erratic distributional behavior and the fact that there is less experience with the numerical methods utilized to solve the generalized adjoint equations, one should not be surprised that the adjoint solutions converge much slower than the forward flux-eigenvalue solution. In fact, many of the adjoint solutions could not be converged below a maximum relative point flux deviation of .01 - .001 compared to .0001 - .00001 for the forward calculation. However, investigation has shown that although point convergence is relatively poor, integral parameters are converged very well. Since only integrals of $\Gamma^*(\vec{r},E)$ are involved in the calculation of the Γ^* effect, the poor point convergence presents no problems when considering the accuracy of the perturbation results.

For the present comparison, the outer iteration limit in the adjoint case was set at 30 whereas the average number of iterations per eigenvalue calculation in the base case was only 16.8. Thus, the main difference between a forward and adjoint calculation is in the number of iterations required for convergence of the point fluxes. Limiting the adjoint iteration count to 20-25 would result in a 15-30% reduction in

computing requirements for the adjoint calculation and put the forward and adjoint flux computation on a more equal base. Such an iteration limit should not seriously compromise the accuracy of the integral parameters needed for the evaluation of the Γ^* effect.

Although the cost per computation is slightly greater for the adjoint depletion calculation, its real cost benefit results from the fact that the effect of any number of perturbations can be analyzed with only one adjoint computation. For example, only one adjoint calculation was required to obtain the DPT results for the three perturbations given in Table 4.30. However, three complete forward depletion calculations were required to obtain the direct results for these same perturbations. Thus, even for this simple example, DPT has a considerable cost advantage over direct methods. Therefore, in more realistic parametric design studies where the effects of many design alternatives are desired, depletion perturbation theory would definitely be the most cost-effective analysis technique.

Lastly, it should be emphasized that Table 4.31 contains only a rough comparison of computing requirements for the forward and adjoint solutions. It is primarily intended as a guide not an absolute comparison of the two methods.

Multicycle Calculations

The final set of examples to be presented in support of depletion perturbation theory will involve multicycle calculations utilizing the 2-D GCFR calculational model described in the last section. These examples will require the application of the adjoint refueling discontinuity equation (equation (2.29)). This operation is necessary because of

the nuclide density discontinuity associated with the forward refueling operation.

The time-step initial condition for the nuclide field within the reactor can be written as,

$$\underline{C}^{ik} = \underline{\underline{P}}_{SD}^{ik} \; \underline{Z}^{ik^-} + \underline{M}^{ik} \tag{4.19}$$

where

$$\underline{C}^{ik} = \begin{bmatrix} \underline{N}_1 \\ \cdot \\ \cdot \\ \cdot \\ \underline{N}_{NREG} \end{bmatrix}^{ik} \qquad \underline{Z}^{ik^-} = \begin{bmatrix} \underline{N}_1 \\ \cdot \\ \cdot \\ \cdot \\ \underline{N}_{NREG} \end{bmatrix}^{ik^-} \qquad \underline{M}^{ik} = \begin{bmatrix} \underline{M}_1 \\ \cdot \\ \cdot \\ \cdot \\ \underline{M}_{NREG} \end{bmatrix}^{ik}$$

with

$\underline{C}^{ik}$ = initial condition vector (NREG) of region-averaged nuclide vectors (NNUC),

$\underline{Z}^{ik^-}$ = vector (NREG) of region-averaged final nuclide density field vectors (NNUC) for the time step prior to the ik time interval,

$\underline{M}^{ik}$ = region vector (NREG) of nuclide vectors (NNUC) specifying makeup feed composition for the ik time interval,

$\underline{\underline{P}}_{SD}^{ik}$ = shuffling/discharge matrix (NREG*NREG) consisting of the identity matrix (NNUC*NNUC) in various locations so as to represent the desired nuclide discontinuity,

NREG = number of regions in problem,

NNUC = number of exposure nuclides.

It is the change in this initial condition, $\Delta\underline{C}^{ik}$, which, when multiplied by the importance function and integrated over space, gives the predicted variation in the response of interest (see equation (2.23)). A change in the initial condition from the reference state can be written as,

$$\Delta \underline{C}^{ik} = \Delta \underline{\underline{P}}_{SD}^{ik} \; \underline{Z}^{ik^-} + \Delta \underline{M}^{ik} \quad . \tag{4.20}$$

Thus, an initial condition perturbation can be caused by a variation in either the shuffling/discharge operator or the makeup feed vector.

The initial condition equation also fully describes the reactor refueling operation. The Z^{ik^-} vector represents the state of the reactor prior to refueling. The P_{SD}^{ik} matrix operates on $\underline{Z}^{ik^-}$, relocating or discharging fuel assemblies as desired. Lastly, the M^{ik} vector represents the addition of makeup fuel to the reactor, thus completing the refueling process. The completely refueled reactor represents the initial condition for the next cycle.

With only slight modification the above sequence could also be used to describe nuclide discontinuities other than the refueling process. Control rod movement or nuclide searches at time-step boundaries can also be easily accommodated. In these cases the M^{ik} vector will have a different meaning but it will be treated mathematically the same as before. Also in many cases of interest, the $\underline{\underline{P}}_{SD}^{ik}$ operator will just be a diagonal matrix with the identity matrix (NNUC*NNUC) in each position along the diagonal. This dictates that no fuel shuffling or discharge is to occur.

An example illustrating the application of equation (4.19) may be helpful. Consider a simple three-region problem. The nuclide density field prior to refueling is

$$\underline{Z}^- = \begin{bmatrix} \underline{N}_1 \\ \underline{N}_2 \\ \underline{N}_3 \end{bmatrix}^- \quad .$$

Assume we wish to discharge zone 3, shuffle zone 1 to zone 3, and add fresh makeup fuel to the now empty zone 1. This can be accomplished by the following,

$$\begin{bmatrix} \underline{N}_1 \\ \underline{N}_2 \\ \underline{N}_3 \end{bmatrix} = \begin{bmatrix} 0 & 0 & 0 \\ 0 & \underline{\underline{I}} & 0 \\ \underline{\underline{I}} & 0 & 0 \end{bmatrix} \begin{bmatrix} \underline{N}_1 \\ \underline{N}_2 \\ \underline{N}_3 \end{bmatrix}^{-} + \begin{bmatrix} \underline{M}_1 \\ 0 \\ 0 \end{bmatrix}$$

or

$$\begin{bmatrix} \underline{N}_1 \\ \underline{N}_2 \\ \underline{N}_3 \end{bmatrix} = \begin{bmatrix} \underline{M}_1 \\ \underline{N}_2^{-} \\ \underline{N}_1^{-} \end{bmatrix} \tag{4.21}$$

with

$$\underline{\underline{P}}_{SD} = \begin{bmatrix} 0 & 0 & 0 \\ 0 & \underline{\underline{I}} & 0 \\ \underline{\underline{I}} & 0 & 0 \end{bmatrix} .$$

Thus, in general, any fuel management scheme can be represented by equation (4.19).

Continuing this illustration to the adjoint mode may also be helpful. Recall the adjoint refueling discontinuity given by equation (2.29),

$$\underline{Z}^{*ijk^{-}} = \underline{\underline{P}}_{SD}^{T_{ijk}} \; \underline{Z}^{*ijk} . \tag{4.22}$$

Additionally, it must be remembered that since the adjoint equations are solved backwards in time, $\underline{Z}^{*ijk}$ is known before $\underline{Z}^{*ijk^{-}}$. Therefore, assume that the adjoint nuclide density vector prior to the application of the refueling discontinuity is given by

$$\underline{Z}^* = \begin{bmatrix} \underline{N}_1^* \\ \underline{N}_2^* \\ \underline{N}_3^* \end{bmatrix}$$

Now application of equation (4.21) gives

$$\underline{Z}^{*-} = \begin{bmatrix} 0 & 0 & \underline{\underline{I}} \\ 0 & \underline{\underline{I}} & 0 \\ 0 & 0 & 0 \end{bmatrix} \begin{bmatrix} \underline{N}_1^* \\ \underline{N}_2^* \\ \underline{N}_3^* \end{bmatrix} = \begin{bmatrix} \underline{N}_3^* \\ \underline{N}_2^* \\ 0 \end{bmatrix} , \tag{4.23}$$

with

$$\underline{\underline{P}}_{SD}^T = \begin{bmatrix} 0 & 0 & \underline{\underline{I}} \\ 0 & \underline{\underline{I}} & 0 \\ 0 & 0 & 0 \end{bmatrix} .$$

The physical interpretation of the transformation observed in equation (4.23) is not very straightforward, even for this simple example. Adjoint importance shuffling, in general, can be somewhat difficult to comprehend. To help with the explanation, we will further assume that the desired response for this example is a nuclide inventory response in zone 3 and that the P^* and Γ^* effects are small compared to the N^* effect.

Table 4.32 qualitatively shows the expected value of the importance function in the three zones at various times. Since zone 3 is the region of interest, it will have some nonzero importance at the final time, t_f. Before the application of the adjoint refueling discontinuity at t_1, zones 1 and 2 will have acquired a small amount of importance to the response through the P^* and Γ^* effects. The direct effect at this point

TABLE 4.32

QUALITATIVE VALUES OF THE IMPORTANCE FUNCTION IN THE THREE-REGION EXAMPLE

	Qualitative Value		
Time[a]	N_1^*	N_2^*	N_3^*
t_f	0	0	Large
t_1	Small	Small	Large
t_1^-	Large	Small	0
t_0	Large	Small	Small

[a] t_f = final, t_1 = refueling time, t_0 = initial time.

is still assumed to be relatively large compared to these effects. The spatial distribution of the importance at the next time, t_1^-, is the result of the adjoint refueling jump condition. Lastly, at t_0, the P^* and Γ^* effects again add a small contribution, making the zone 3 importance some nonzero value. However, the zone 1 importance is still large relative to that in zone 2 and 3.

With the expected value of the importance function at t_0, we can determine the effect of a nuclide perturbation at t_0 on the response at t_f. Remembering that the response of interest is in zone 3, we see that a perturbation in zone 3 has little effect on the response. However, an initial-time perturbation in zone 1 has a large effect on the desired response. Since we are assuming that the direct effects are dominant, this seems to be contradictory. However, zone 3 is discharged after the first cycle and, therefore, cannot directly contribute to a zone 3 nuclide inventory response at the end of the second cycle. On the other hand, zone 1 assemblies become zone 3 assemblies after refueling and thus a perturbation in zone 1 at t_0 contributes directly to the nuclide inventory variation in zone 3 at the end of the second cycle.

Although somewhat lengthy, the above rationalization seems to validate equations (4.22) and (4.23). In addition, it helps one visualize the adjoint importance refueling operation and the relationship to its forward counterpart. Fuel management operations in a multicycle forward depletion calculation have corresponding importance management operations in the multicycle adjoint mode. In general, if zone y is shuffled to zone z in the forward calculation, then in the adjoint mode, the importance associated with zone z would be shuffled to zone y. Additionally, if zone z was

discharged in the reference calculation, then, after shuffling, the zone z importance would be set at zero.

Numerical calculations confirming the validity of the complete multicycle adjoint formulation just described are not possible at present. A general fuel management module, capable of performing fuel shuffling operations, is not available. However, multicycle depletion calculations can be performed within the VENTURE system if only simple charge/discharge operations are allowed. The nuclide density manipulator module, DENMAN,[22] is used for this purpose.

A simple charge/discharge capability during the adjoint mode has been built into DEPTH. This was a relatively easy process since a discharge fuel management operation in a region causes the adjoint density vector to be set to zero in that zone. This was observed for zone 3 in the previous example. Thus a straightforward but stringent test of equation (4.22) is possible.

The 2-D GCFR calculational model described previously was used to test the multicycle charge/discharge adjoint operation. As before, a nuclide inventory response was chosen as the response of interest. The same perturbations as listed in Table 4.25, page 109, were utilized for the comparison of DPT with direct calculation. However, for multicycle calculations, perturbations from the reference case can be applied to any of the reload batches as well as to the initial core loading.

A four-cycle depletion calculation was chosen as a representative multicycle computation. One-third of the core and axial blanket regions were refueled on an annual basis. In addition, one-sixth of the radial blanket zones were replaced per cycle. The ^{239}Pu and ^{241}Pu inventories in the entire reactor at the end of the fourth cycle (EOC4) were chosen as

the desired responses. The fourth cycle for the above fuel management scheme represents a near equilibrium condition for the core and axial blankets. Thus the end of equilibrium cycle fissile inventories are a natural choice as a response of interest.

The following three tables summarize the results of this comparison. Table 4.33 contrasts the calculated and predicted EOC4 ^{239}Pu inventory response for the fission product and ^{239}Pu perturbations in core zone 1. Similarly, Tables 4.34 and 4.35 compare the perturbed EOC4 ^{239}Pu and ^{241}Pu inventories due to the 10% ^{238}U/^{232}Th perturbation in the radial blanket zones. These perturbation/response pairs included both isolated perturbations as in the case of the ^{239}Pu increase in CZ 1 and multiple nuclide variations over the four cycles as in the fission product and ^{238}U/^{232}Th perturbations. In all these cases, multicycle depletion perturbation theory agrees extremely well with direct calculation.

It should be noted that initial loading perturbations in the core region are not even physically present in the reactor during the fourth cycle. However, the effects of these perturbations are predicted with remarkable accuracy. For example, the isolated initial core ^{239}Pu perturbation's effect on the EOC4 ^{239}Pu inventory was predicted to with an accuracy of 1.7%! Thus the reactor has a memory and DPT can account for this memory effect with excellent precision.

This memory effect is just the combination of the P^* and Γ^* effects made more visible because of the nuclide discontinuity at cycle boundaries. Obviously, a fuel assembly that is no longer in the reactor at the desired response time cannot have any direct effect on the response of interest.

TABLE 4.33

DPT VERSUS DIRECT CALCULATION FOR EOC4 ^{239}Pu INVENTORY RESPONSE FOR FISSION PRODUCT AND PLUTONIUM PERTURBATIONS IN CORE ZONE #1

		Change in Response (KG)		
Design Variation	Time of Perturbation	DPT Result	Direct[a] Result	Diff. (%)
Δ FISSP	initial core	56.23		
	1st reload	30.61		
	2nd reload	21.46		
	3rd reload	10.97		
	SUM	119.27	115.98	2.8
$\Delta^{239}Pu$	initial core	-27.68	-27.21	1.7
$\Delta^{239}Pu$	1st reload	-2.35	-2.43	-3.3

[a]The response of interest here is the EOC4 ^{239}Pu inventory; therefore, there are no direct results prior to the end of of the fourth cycle.

TABLE 4.34

DPT VERSUS DIRECT CALCULATION FOR EOC4 ^{239}Pu INVENTORY RESPONSE FOR THE 10% $^{238}U/^{232}Th$ PERTURBATION TO THE RADIAL BLANKET ZONES

Design Variation	Time of Perturbation	Change in Response (KG) DPT Result	Direct[a] Result	Diff. (%)
Δ ^{238}U	initial core	-16.01		
Δ ^{232}Th		-88.13		
Δ ^{238}U	1st reload	-8.60		
Δ ^{232}Th		-17.94		
Δ ^{238}U	2nd reload	-5.05		
Δ ^{232}Th		-13.68		
Δ ^{238}U	3rd reload	-2.15		
Δ ^{232}Th		-7.74		
	SUM	-159.30	-157.10	1.4

[a]The response of interest here is the EOC4 ^{239}Pu inventory; therefore, there are no direct results prior to the end of the fourth cycle.

TABLE 4.35

DPT VERSUS DIRECT CALCULATION FOR EOC4 ^{241}Pu INVENTORY RESPONSE FOR THE 10% $^{238}U/^{232}Th$ PERTURBATION TO THE RADIAL BLANKET ZONES

Design Variation	Time of Perturbation	Change in Response (KG) DPT Result	Direct[a] Result	Diff. (%)
Δ ^{238}U	initial core	.0463		
Δ ^{232}Th		-.1264		
Δ ^{238}U	1st reload	.0134		
Δ ^{232}Th		-.0361		
Δ ^{238}U	2nd reload	.0308		
Δ ^{232}Th		-.0604		
Δ ^{238}U	3rd reload	.0290		
Δ ^{232}Th		-.0572		
	SUM	-.1606	-.1590	1.0

[a]The response of interest here is the EOC4 ^{241}Pu inventory; therefore, there are no direct results prior to the end of the fourth cycle.

However, it still can have affected the response through a flux magnitude or distributional variation prior to its removal from the system.

Consider the increase in the ^{239}Pu initial loading to CZ 1. This perturbation increased the ^{239}Pu inventory in the reactor during the first three cycles. However, the last of the assemblies with increased ^{239}Pu concentration are discharged during the third cycle refueling operation. Thus, there can be no direct contribution to the desired response. The initial perturbation, however, reduced the overall magnitude of the flux and shifted the spatial distribution of the neutron flux toward core center. Both effects, P^* and Γ^*, respectively, resulted in a decreased average flux in the blanket region over the first three cycles. Thus, the decreased ^{239}Pu production rate in the blanket regions is the major cause of the observed 27 kg deficit in the EOC4 ^{239}Pu inventory relative to the reference depletion calculation.

The other perturbation/response pairs shown in Tables 4.33-4.35 have characteristics similar to those discussed previously. Since the main point to be made is the good comparison of DPT with direct calculations, the fine details of the calculations will be ignored. However, in view of the main objective of the study, the excellent predictive capability of the time-dependent perturbation theory under investigation will be reemphasized one final time. This can be done quite nicely by concentrating on the multiple perturbation cases shown in Tables 4.33-4.35.

The three multiple perturbation examples illustrate the predictive power of multicycle perturbation theory. The four distinct fission product perturbations, when summed to give the total perturbed response, only differ from direct calculations by 2.8%. Similarly, the

eight separate nuclide variations in the radial blanket, when combined to produce the total ΔR, predict the change in the EOC4 ^{239}Pu and ^{241}Pu inventories to an accuracy of 1.4% and 1.0%, respectively. These kinds of results are remarkable when considering the complexity of the problem being solved. Apparently the space, energy and time dependence of the adjoint importance functions of multicycle depletion perturbation theory are taken into account in a consistent and accurate manner.

V. SUMMARY

The goals of the present investigation have been to develop a multicycle depletion perturbation theory formulation, to implement this theory into an existing calculational system, and lastly to verify the accuracy and usefulness of this time-dependent perturbation theory. Although these goals have been realized, there is still a considerable amount of research to be performed in the relatively new field of time-dependent perturbation theory. Therefore, this final section will not only summarize the conclusions of the present study but also recommend several areas needing further research.

Conclusions

The adjoint quasi-static depletion perturbation theory formulation summarized in Table 2.1, page 11, and implemented in the DEPTH module has been shown to fully account for variations in the neutron and nuclide fields arising from variations in the time-step initial conditions. A wide variety of numerical calculations have been performed to verify the accuracy of the coding within the DEPTH module as well as the adequacy and generality of the multicycle depletion perturbation theory. The examples utilized covered the range from 1-group, 1-dimensional reactor models to more complex multigroup, 2-dimensional calculational representations. In addition, several multicycle calculations were performed as a test of the adjoint refueling jump condition. Remarkably good agreement was achieved with direct computation for most of the cases investigated.

The few cases whose accuracy was considered marginal were dominated by nonlinear behavior due to cancellation of competing effects. This nonlinear behavior seems to be the exception rather than the rule.

However, careful examination of the time-dependent importance functions can isolate perturbation/response pairs that have large competing effects. In these cases, experience should be used as a guide in judging the reliability of perturbation theory results.

Also, it has been determined that the full perturbation theory including the N^*, P^*, and Γ^* effects, is generally needed to accurately describe the effect of a particular perturbation. However, certain situations may allow the Γ^* effect to be neglected and thus considerably reduce the cost of the adjoint calculation. Although definite guidelines are not available, perturbation/response pairs dominated by the N^* effect fall into this category. Some preanalysis may be required but one can usually determine with relative ease whether or not the N^* effect should dominate. Additionally, it should be noted that the previous statements are restricted to perturbations near the central core regions of the reactor since it has been determined that the Γ^* effect is quite important in blanket, control rod, or structural regions of the reactor.

Since the full perturbation theory formulation is needed for general application, the computational cost of a complete adjoint calculation relative to a base depletion calculation becomes important. It was shown in the previous chapter that a reference forward calculation had about 2.0-2.5 times the computing requirements as a base case. However, this penalty occurs only once for any number of adjoint computations. Additionally, the cost of the adjoint calculation for each response of interest can be expected to be about 25-50% higher than a base forward calculation.[†]

[†]Very recent improvements in the numerical calculation of the generalized adjoint flux within VENTURE will essentially eliminate this additional expense.[28]

Thus, there seems to be a trade-off in the cost and the type of information desired from a specific depletion analysis. If one only wishes to determine the effects of a few specific perturbations, then the direct calculation method would be less costly. However, if the investigation of the effects of a large number of design variations on a few specific responses is the desired goal, then depletion perturbation theory is the most cost-effective method. Depletion perturbation theory would also be utilized if a generalized static or time-dependent sensitivity or uncertainity analysis were to be performed.

Lastly, it should be noted that static and time-dependent perturbations theory share the same trade-offs. In general, direct calculation is utilized for analysis of problems containing few perturbations and several responses, whereas perturbation theory is employed when the effects of several design variations on a few responses are to be investigated.

In summary, one can conclude that the multicycle depletion perturbation theory capability described in the present document represents an attractive alternate computational method for certain types of burnup analyses. The method has been shown to predict perturbed responses under a variety of circumstances with remarkable accuracy. This technique also allows a considerable savings in time and cost when several design variations or a general sensitivity analysis are to be performed. These benefits could be especially useful for repetitive-type scoping calculations such as those being performed in current alternate fuel cycle studies.

In addition to time and cost advantages, perturbation theory methods permit a better understanding of the mechanisms responsible for the

observed behavior of a given response. In depletion perturbation theory, both space and time-dependent sensitivity coefficients are generated. Analysis of these importance indicators for a variety of important responses can provide a more detailed understanding of the neutronic processes underlying the observed behavior. Thus, multicycle depletion perturbation theory may also lead to improvements in core design and optimization techniques since the indirect effects of design changes on final-time responses such as K_{eff}, fissile inventory, net fissile gain, breeding ratio, power variance, fluence, etc., can be easily quantified.

Recommendations

This report cannot be properly concluded without emphasizing the fact that there is still a considerable amount of research to be performed in the relatively new field of time-dependent perturbation theory. The present investigation has only verified the generality and accuracy of the theory. Many areas need further investigation before depletion perturbation theory becomes a widely used analytical tool. Only three of these general areas will be briefly mentioned here. These include the generalized adjoint flux, multicycle effects, and future applications of DPT.

The determination of the generalized adjoint flux accounts for most of the computing requirements of a complete adjoint depletion calculation. Thus it seems only rational that some effort be made to either improve the numerical calculation of the adjoint flux and/or find some suitable approximation so that at least some of the adjoint flux calculations in a multiple time-step problem can be eliminated. This latter suggestion may not be as impossible as it seems. It should be remembered that only

integrals of the adjoint flux over spatial regions are utilized in the Γ^* effect calculation. Furthermore, the generalized adjoint source is a good indicator of the integral spatial behavior of the pointwise flux. Since the adjoint source is relatively easy and inexpensive to calculate, some reasonable compromise between accuracy and expense may be achievable.

The multicycle capability of the generalized depletion perturbation theory utilized in this study has only been verified for a simple charge/discharge set of fuel management operations. Although its application when using complex fuel shuffling patterns should create no difficulty, the effects of importance shuffling in the adjoint mode should be studied in more detail. In addition, the verification of the predictive capability of the multicycle formulation for a perturbation in the shuffling/discharge operator, as suggested by equation (4.20), should be performed. These tasks would involve the implementation of importance shuffling capability within the DEPTH module.

A second area related to multicycle perturbation theory is the effect of fuel recycle. In the present investigation, the makeup feed vector, $\underline{M}^{ik}$, was assumed to be independent of the operating history of the reactor. However, if self-generated recycle is present, the available feed will be a function of the nuclide densities discharged during previous cycles. This added complication should only affect the adjoint refueling jump condition. Further development of this concept would enhance the capability of the present DPT to include fuel recycle effects.

The last and probably most important area needing further work to be mentioned is the area of realistic application of DPT. The present study has demonstrated the predictive capability DPT. However, at present, the sensitivity coefficients generated in the DEPTH module can

only be manipulated by hand calculation. Therefore, a module to calculate perturbed responses utilizing user-defined design variations would be particularly useful. Similarly, a module to generate the adjoint sources needed as input to DEPTH is required so that a variety of response functionals can be employed. With the development of these modules, depletion perturbation theory could be utilized as an effective tool for time-dependent perturbation analyses.

A somewhat more futuristic application and ultimate goal of static and time-dependent perturbation theory is its use in computer-automated core design studies. The design of a nuclear reactor from neutronic, thermal-hydraulic, structural, and economic viewpoints obviously require that compromises in the material configuration of the reactor be made. Now that time-dependent effects can be treated, perturbation theory methods can generate sensitivity coefficients that reflect the importance of these material compromises on various neutronic, thermal-hydraulic, structural, and economic performance indicators. A library of nuclide sensitivity coefficients for the importance indicators along with a set of user-defined system constraints could be utilized in an optimization package to provide a best estimate design in a single computer calculation. The possibilities of such a system as outlined here are enormous.

The first realistic application of design optimization on this scale may be in determining the optimum fuel shuffling pattern for an operating light water reactor. In this case the design variations may be limited to reload enrichment and fuel location. Since perturbation theory can predict the changes in the desired responses due to an interchange of assemblies (nuclide perturbation), in principle at least, the optimum location of each assembly based on certain system constraints can be

determined. Thus, an automated optimization package based on static and time-dependent perturbation theory, as indicated here, could prove to be an invaluable aid for core design and fuel management analyses.

Finally, it should be emphasized that the above recommendation list of items requiring further study is by no means exhaustive. Its primary goal is to indicate that time-dependent perturbation theory is a relatively new field requiring much further development and that it is a research area that has an enormous potential for useful applications.

LIST OF REFERENCES

1. T. J. Burns and J. R. White, "Preliminary Evaluations of Alternative LMFBR Fuel Cycle Options," Oak Ridge National Laboratory, ORNL-5389 (1978).

2. L. S. Abbott, D. E. Bartine, and T. J. Burns, "Interim Assessment of the Denatured ^{233}U Fuel Cycle: Feasibility and Nonproliferation Characteristics," Oak Ridge National Laboratory, ORNL-5388 (1978).

3. J. R. White and T. J. Burns, "Alternative Heterogeneous GCFR Fuel Cycles," *Trans. Am. Nucl. Soc.*, *32*, 403 (1979).

4. A. Gandini, "Perturbation Methods in Nuclear Reactors from the Importance Conservation Principle," *Nucl. Sci. Eng.*, *35*, 141 (1969).

5. A. Gandini, "A Method of Correlation of Burnup Measurements for Physics Prediction of Fast Power-Reactor Life," *Nuc. Sci. Eng.*, *38*, 1 (1969).

6. M. Komata, "New Interpretations for the Usachev-Gandini Perturbation Theory," *Nucl. Sci. Eng.*, *47*, 489 (1972).

7. A. Gandini, M. Salvatores, and L. Tondinelli, "New Developments in Generalized Perturbation Methods in the Nuclide Field," *Nucl. Sci. Eng.*, *62*, 339 (1977).

8. L. Tondinelli, "Sensitivity of Actinide Concentration During Burn-up With Respect to Nuclear Data," CNEN RT/FI(76)1, CNEN, Rome (1976).

9. M. Williams, C. Weisbin, "Sensitivity and Uncertainty Analysis for Functionals of the Time-Dependent Nuclide Density Field," Oak Ridge National Laboratory, ORNL-5393 (1978).

10. G. Pomraning, "Variation Principle for Eigenvalue Equations," *J. Math. Phys.* *8*, 149 (1967).

11. M. J. Bell, "ORIGEN-The ORNL Isotope Generation and Depletion Code," Oak Ridge National Laboratory, ORNL-4628 (1973).

12. J. M. Kallfelz, et al., "Burnup Calculations with Time-Dependent Generalized Perturbation Theory," *Nucl. Sci. Eng.*, *62*, 304 (1977).

13. M. L. Williams, "Development of Depletion Perturbation Theory for Coupled Neutron/Nuclide Fields," *Nucl. Sci. Eng.*, *70*, 20 (1979).

14. M. L. Williams, J. R. White, J. H. Marable, and E. M. Oblow, "Sensitivity Theory for Depletion Analysis," Proceedings of a Seminar-Workshop on the Theory and Application of Sensitivity and Uncertainty Analysis, ORNL/RSIC-42 (1979).

15. M. L. Williams, J. R. White, and T. J. Burns, "A Technique for Sensitivity Analysis of Space-and-Energy-Dependent Burnup Calculations," *Trans. Am. Nucl. Soc.*, *32*, 766 (1979).

16. T. B. Fowler, D. R. Vondy, and G. W. Cunningham, "Nuclear Reactor Core Analysis Code: CITATION," Oak Ridge National Laboratory, ORNL-TM-2496, Rev. 2 (1971).

17. D. R. Vondy, T. B. Fowler, G. W. Cunningham, and L. M. Petrie, "A Computation System for Nuclear Reactor Core Analysis," Oak Ridge National Laboratory, ORNL-5158 (1977).

18. D. R. Vondy, T. B. Fowler, and G. W. Cunningham, "VENTURE: A Code Block for Solving Multigroup Neutronics Problems Applying the Finite-Difference Diffusion-Theory Approximation to Neutron Transport, Version II," Oak Ridge National Laboratory, ORNL-5062/R1 (1977).

19. D. R. Vondy and G. W. Cunningham, "Exposure Calculation Code Module for Reactor Core Analysis: BURNER," Oak Ridge National Laboratory, ORNL-5180 (1979).

20. D. R. Vondy and T. B. Fowler, "The Code PERTUBAT for Processing Neutron Diffusion Theory Neutronic Results for Perturbation Analysis," Oak Ridge National Laboratory, ORNL-5376 (1978).

21. D. R. Vondy and T. B. Fowler, "RODMOD - A Code for Control Rod Positioning," Oak Ridge National Laboratory, ORNL-5466 (1978).

22. D. R. Vondy, T. B. Fowler, and G. W. Cunningham, "Input Data Requirements for Special Processors in the Computation System Containing the VENTURE Neutronics Code," Oak Ridge National Laboratory, ORNL-5229 (1976).

23. R. D. O'Dell, "Standard Interface Files and Procedures for Reactor Physics Codes, Version IV," Los Alamos Scientific Laboratory, LA-6941-MS (1977).

24. G. E. Bosler, R. D. O'Dell, W. M. Resnik, "LASIP-III, A Generalized Processor for Standard Interface Files," Los Alamos Scientific Laboratory, LA-6280-MS (1976).

25. G. E. Forsythe, M. A. Malcolm, and C. B. Moler, *Computer Methods for Mathematical Computations*, Prentice-Hall, N.J., 1977, pp. 89-90.

26. Letter to Dr. James Horak from Chris J. Hamilton, General Atomic Company, "GCFR Fuel Cycle Information for the ORNL Non-Proliferation Study," Oct. 13, 1977.

27. J. R. Lamarsh, *Introduction to Nuclear Reactor Theory*, Addison-Wesley, Mass., 1972, pp. 138-140.

28. T. B. Fowler, private communication, 1979.

29. M. L. Williams, "Perturbation and Sensitivity Theory for Reactor Burnup Analysis," Oak Ridge National Laboratory, ORNL/TM-7097 (1979).

APPENDIX A

The purpose of this Appendix is to derive the equations programmed into the DEPTH module. An approach similar to that utilized in Refs. 13 and 29 will be taken. The main difference, other than slight variations in notation and the use of discrete variables where possible, is the treatment of nuclide discontinuties at the time-step and cycle boundaries. This additional feature in the present work allows for nuclide searches and multicycle refueling operations during the forward depletion calculation. Such operations are necessary for realistic multicycle depletion analyses.

The notation for the complete set of forward quasi-static depletion equations utilized in this study is given as follows:

1. <u>Nuclide Density Equation</u>:

$$\frac{d}{dt}\,\underline{N}^{ijk}(\vec{r},t) = (\underline{\underline{T}}^{ijk}(\vec{r}) + \underline{\underline{D}})\,\underline{N}^{ijk}(\vec{r},t) \tag{A.1}$$

where $\underline{N}^{ijk}(\vec{r},t)$ = Space-dependent nuclide density vector (NNUC isotopes) at time t within substep j, time step i, and cycle k.

$\underline{\underline{D}}$ = Matrix (NNUC*NNUC) of nuclide decay constants.

and $\underline{\underline{T}}^{ijk}(\vec{r}) = \alpha^{ijk}\,\underline{\underline{X}}^{ik}(\vec{r})\,\underline{\psi}^{ik}(\vec{r})$ (A.2)

with $\underline{\underline{T}}^{ijk}(\vec{r})$ = Space-dependent transmutation matrix (NNUC*NNUC) for ijk interval. Diagonal terms represent loss mechanisms and off-diagonal terms represent production routes.

α^{ijk} = Flux normalization constant, held fixed during ijk interval.

$\underline{\psi}^{ik}(\vec{r})$ = Space-dependent flux shape group vector (IGM) held constant during ik interval.

$\underline{\underline{X}}^{ik}(\vec{r})$ = Space-dependent burnup operator. Consists of a matrix (NNUC*NNUC) of microscopic cross-section vectors (IGM) held constant during the ik interval.

2. Initial Condition on $\underline{N}(\vec{r},t)$:

$$\underline{N}(\vec{r},t)\big|_{t_{ik}} = \underline{C}^{ik}(\vec{r}) \tag{A.3}$$

where $\underline{N}(\vec{r},t_{ik})$ = Initial nuclide density vector (NNUC) for the ik time interval.

and $\underline{C}^{ik}(\vec{r}) = \underline{\underline{P}}^{ik}_{SD}(\vec{r})\ \underline{N}^{ik-}(\vec{r}) + \underline{M}^{ik}(\vec{r})$ (A.4)

with $\underline{N}^{ik-}(\vec{r})$ = Final nuclide density field vector (NNUC) for time step prior to the ik time interval.

$\underline{\underline{P}}^{ik}_{SD}(\vec{r})$ = Shuffling/discharge operator for ik time interval.

$\underline{M}^{ik}(\vec{r})$ = Space-dependent nuclide vector (NNUC) specifying feed composition for the ik time interval.

3. Power Normalization Equation: (Defining equation for α^{ijk})

$$P^{ijk} = \alpha^{ijk} \int_{\substack{all\\space}} \underline{N}^{T\,ijk}(\vec{r})\ \underline{\underline{E}}_p\ \underline{\underline{\sigma}}_f^{ik}(\vec{r})\ \underline{\psi}^{ik}(\vec{r})\ d\vec{r} \tag{A.5}$$

where P^{ijk} = Specified reactor power for ijk time interval.

$\underline{\underline{E}}_p$ = Diagonal matrix (NNUC*NNUC) of nuclide-dependent energy per fission conversion factors.

$\underline{\underline{\sigma}}_f^{ik}(\vec{r})$ = Space-dependent microscopic fission cross-section matrix (NNUC*IGM) held constant during ik interval.

4. Flux Shape Equation: (Time-independent diffusion equation)

$$(\underline{\underline{L}} - \lambda \underline{\underline{F}})^{ik} \; \underline{\psi}^{ik}(\vec{r}) = 0 \tag{A.6}$$

where $\underline{\underline{L}}$ = Leakage, removal and inscatter operator.

$\underline{\underline{F}}$ = Fission source operator.

$\lambda = \dfrac{1}{K_{eff}}$.

5. Flux Shape Normalization:

$$\int_{\substack{\text{all}\\ \text{space}}} (\underline{\psi}^{ik^T}(\vec{r}) \cdot \underline{1}) \, d\vec{r} = 1 \tag{A.7}$$

where the inner product of $\underline{\psi}^{ik}(\vec{r})$ and $\underline{1}$ represent an integration over the discrete energy variable.

Now using equations (A.1)-(A.7) as constraints on the desired response as described in Section II, one can define the following K-functional,

$$\begin{aligned} K(\underline{N},\alpha,\underline{\psi},\lambda,\beta,P,\underline{C}) = {} & R(\underline{N},\alpha,\underline{\psi}) \\ & - \sum_k \sum_i \int_{\substack{\text{all}\\ \text{space}}} d\vec{r} \left[\underline{\Gamma}^{*T}(\vec{r})(\underline{\underline{L}} - \lambda \underline{\underline{F}}) \; \underline{\psi}(\vec{r})\right]^{ik} \\ & + \sum_k \sum_i \sum_j P^{*ijk} \left[P^{ijk} - \alpha^{ijk} \int_{\substack{\text{all}\\ \text{space}}} d\vec{r} \; \underline{N}^{T\,ijk}(\vec{r}) \, \underline{\underline{E}}_p \, \underline{\underline{\sigma}}_f^{ik}(\vec{r}) \, \underline{\psi}^{ik}(\vec{r})\right] \\ & - \sum_k \sum_i \sum_j \int_{\substack{\text{all}\\ \text{space}}} d\vec{r} \int_{\substack{\text{substep}\\ j}} dt \; \underline{N}^{*T\,ijk}(\vec{r},t) \left[\frac{d}{dt} \underline{N}^{ijk}(\vec{r},t) - \right. \\ & \qquad \left. (\underline{\underline{T}}^{ijk}(\vec{r}) + \underline{\underline{D}}) \, \underline{N}^{ijk}(\vec{r},t)\right] \\ & - \sum_k \sum_i \int_{\substack{\text{all}\\ \text{space}}} d\vec{r} \int_{\substack{\text{timestep}\\ i}} dt \; \underline{N}^{*T\,ik}(\vec{r},t) \left[\underline{N}^{ik}(\vec{r},t) - \underline{C}^{ik}(\vec{r},t)\right] \delta(t - t_{ik}) \end{aligned} \tag{A.8}$$

$$- \sum_k \sum_i A^{*ik} \left[\int_{\substack{\text{all}\\ \text{space}}} d\vec{r} \, (\underline{\psi}^{ik}(\vec{r}) \cdot \underline{1}) - 1 \right] ,$$

where $\underline{\Gamma}^{*ik}(\vec{r})$, P^{*ijk}, $\underline{N}^{ijk}(\vec{r},t)$, and A^{*ik} are Lagrange multipliers. The desired adjoint depletion equations defining these Lagrange multipliers are derived by forcing the functional derivative of the K-functional with respect to $\underline{\psi}^{ik}(\vec{r})$, α^{ijk}, $\underline{N}^{ijk}(\vec{r},t)$, and λ^{ik} to vanish. Taking one term at a time, one has,

1. <u>Setting $\partial K/\partial \underline{\psi}^{ik}(\vec{r})$ to Zero:</u>

$$(\underline{\underline{L}} - \lambda \underline{\underline{F}})^{T_{ik}} \underline{\Gamma}^{*ik}(\vec{r}) = \underline{S}^{*ik}(\vec{r}) \tag{A.9}$$

$$\begin{aligned} \text{with } \underline{S}^{*ik}(\vec{r}) = & \frac{\partial R}{\partial \underline{\psi}^{ik}(\vec{r})} - (A^{*ik} * \underline{1}) \\ & + \sum_j \int_{\substack{\text{substep}\\ j}} dt \; \underline{N}^{*T_{ijk}}(\vec{r},t) \frac{\partial}{\partial \underline{\psi}^{ik}(\vec{r})} \left\{ \underline{\underline{T}}^{ijk}(\vec{r}) \, \underline{N}^{ijk}(\vec{r},t) \right\} \\ & - \sum_j P^{*ijk} \, \alpha^{ijk} \, \underline{N}^{T_{ijk}}(\vec{r}) \, \underline{\underline{E}}_p \, \underline{\underline{\sigma}}_f^{ik}(\vec{r}) \quad . \end{aligned} \tag{A.10}$$

2. <u>Setting $\partial K/\partial \alpha^{ijk}$ to Zero:</u>

$$\begin{aligned} P^{*ijk} = & \frac{1}{P^{ijk}} \left[\left(\alpha \frac{\partial R}{\partial \alpha} \right)^{ijk} + \right. \\ & \left. \alpha^{ijk} \int_{\substack{\text{all}\\ \text{space}}} d\vec{r} \int_{\substack{\text{substep}\\ j}} dt \; \underline{N}^{*T_{ijk}}(\vec{r},t) \, \underline{\underline{X}}^{ik}(\vec{r}) \, \underline{\psi}^{ik}(\vec{r}) \, \underline{N}^{ijk}(r,t) \right] . \end{aligned} \tag{A.11}$$

3. <u>Taking Variation with Respect to $\underline{N}^{ijk}(\vec{r},t)$:</u>

Before taking the variation with respect to $\underline{N}^{ijk}(\vec{r},t)$, one needs to rewrite the fourth term on the right-hand side of equation (A.8). Integration in the forward time direction yields,

$$4^{th} \text{ term of (A.8)} = -\sum_k \sum_i \sum_j \int_{\substack{\text{all}\\ \text{space}}} d\vec{r} \left[\underline{N}^{*T}(\vec{r},t)\ \underline{N}(\vec{r},t)\Big|_{t_{ijk+1}^{-}} \right.$$

$$- \underline{N}^{*T}(\vec{r},t)\ \underline{N}(\vec{r},t)\Big|_{t_{ijk}^{+}} \tag{A.12}$$

$$\left. + \int_{t_{ijk+1}^{-}}^{t_{ijk}^{+}} dt\ \underline{N}^{T\,ijk}(\vec{r},t) \left\{ \frac{d}{dt}\ \underline{N}^{*ijk}(\vec{r},t) + (\underline{\underline{T}}^{ijk}(\vec{r}) + \underline{\underline{D}})^T \underline{N}^{*ijk}(\vec{r},t) \right\} \right] .$$

Now substituting (A.12) into (A.8) and taking the variation with respect to $\underline{N}^{ijk}(\vec{r},t)$ gives,

$$\int d\vec{r} \int dt\ \frac{\partial K}{\partial \underline{N}(\vec{r},t)}\ \delta\underline{N}(\vec{r},t) = 0 = \int d\vec{r} \int dt\ \frac{\partial R}{\partial \underline{N}(\vec{r},t)}\ \delta\underline{N}(\vec{r},t)$$

$$- \sum_k \sum_i \int d\vec{r} \left[\underline{\Gamma}^{*T}(\vec{r})\ \frac{\partial}{\partial \underline{N}(\vec{r})}\ \{(\underline{\underline{L}} - \lambda \underline{\underline{F}})\ \underline{\psi}(\vec{r})\}\ \delta\underline{N}(\vec{r}) \right]^{ik+}$$

$$- \sum_k \sum_i \sum_j \int d\vec{r}\ P^{*ijk+}\ \alpha^{ijk+}\ \underline{\underline{E}}_p\ \underline{\underline{\sigma}}_f^{ik+}(\vec{r})\ \underline{\psi}^{ik+}(\vec{r})\ \delta\underline{N}^{ijk+}(\vec{r})$$

$$- \sum_k \sum_i \sum_j \int d\vec{r} \left[\underline{N}^{*T}(\vec{r})\ \delta\underline{N}(\vec{r}) \right]^{(ijk+1)^-} \tag{A.13}$$

$$+ \sum_k \sum_i \sum_j \int d\vec{r} \left[\underline{N}^{*T}(\vec{r})\ \delta\underline{N}(\vec{r}) \right]^{ijk+}$$

$$- \sum_k \sum_i \sum_j \int d\vec{r} \int_{t_{ijk+1}^{-}}^{t_{ijk}^{+}} dt \left[\frac{d}{dt}\ \underline{N}^{*ijk}(\vec{r},t) + \right.$$

$$\left. (\underline{\underline{T}}^{ijk}(\vec{r}) + \underline{\underline{D}})^T \underline{N}^{*ijk}(\vec{r},t) \right] \delta\underline{N}^{ijk}(\vec{r},t)$$

$$- \sum_k \sum_i \int d\vec{r} \left[(\underline{N}^{*T\,ik}(\vec{r})\ \delta\underline{N}^{ik}(\vec{r})) - (\underline{N}^{*T\,ik}(\vec{r})\ \underline{\underline{P}}_{SD}^{ik}(\vec{r})\ \delta\underline{N}^{ik-}(\vec{r})) \right]$$

Equating similar integrands, noting that

$$\delta \underline{N}^{ik+}(\vec{r}) = \delta \underline{N}^{ik}(\vec{r}) = \underline{\underline{P}}_{SD}(\vec{r})\ \delta \underline{N}^{ik-}(\vec{r}) \quad , \tag{A.14}$$

and defining (restricted to final time responses)

$$\frac{\partial R}{\partial \underline{N}(\vec{r},t)} = \underline{N}^{*}(\vec{r},t_f) \quad , \tag{A.15}$$

one obtains the following adjoint equations,

$$\frac{d}{dt}\ \underline{N}^{*ijk}(\vec{r},t) + (\underline{\underline{T}}^{ijk}(\vec{r}) + \underline{\underline{D}})^T\ \underline{N}^{*ijk}(\vec{r},t) = 0 \tag{A.16}$$

and

$$\underline{N}^{*ijk}(\vec{r}) = \underline{N}^{*ijk+}(\vec{r}) + \underline{\Gamma}^{*ijk}(\vec{r})_{effect} + \underline{P}^{*ijk}(\vec{r})_{effect} \tag{A.17}$$

where

$$\underline{\Gamma}^{*ijk}(\vec{r})_{effect} = -\ \underline{\Gamma}^{*T\,ik}(\vec{r})\ \frac{\partial}{\partial \underline{N}^{ik}(\vec{r})}\ \{(\underline{\underline{L}} - \lambda \underline{\underline{F}})\ \underline{\psi}^{ik}(\vec{r})\}\ \text{for}\ \ j = 1$$

$$\underline{\Gamma}^{*ijk}(\vec{r})_{effect} = 0 \quad \text{for}\ j \neq 1 \tag{A.18}$$

$$\underline{P}^{*ijk}(\vec{r})_{effect} = -\ P^{*ijk}\ \alpha^{ijk}\ \underline{\underline{E}}_P\ \underline{\underline{\sigma}}_f^{ik}(\vec{r})\ \underline{\psi}^{ik}(\vec{r}) \tag{A.19}$$

and

$$\underline{N}^{*ijk-}(\vec{r}) = \underline{\underline{P}}_{SD}^{*ijk}(\vec{r})\ \underline{N}^{*ijk}(\vec{r}) \tag{A.20}$$

where $\underline{\underline{P}}_{SD}^{*ik}(\vec{r})$ is the adjoint operator to $\underline{\underline{P}}_{SD}^{ik}(\vec{r})$ (See Section IV for more detailed description of $\underline{\underline{P}}_{SD}^{ik}(\vec{r})$).

4. <u>Setting $\partial K/\partial \lambda^{ik}$ to Zero</u>:

$$\int_{\substack{all\\space}} \underline{\Gamma}^{*T\,ik}(\vec{r})\ \underline{\underline{F}}\ \underline{\psi}^{ik}(\vec{r})\ d\vec{r} = 0 \tag{A.21}$$

5. Additional Relationships:

From equation (A.9) one has

$$\int_{\substack{\text{all}\\\text{space}}} d\vec{r} \quad \underline{\psi}^{T\,ik}(\vec{r})\ \underline{S}^{*ik}(\vec{r}) = 0 \quad . \tag{A.22}$$

Using this result and equation (A.9) multiplied by $\underline{\psi}^{ik}(\vec{r})$ and integrated over all space along with equation (A.10) gives the following definition for A^{*ik},

$$A^{*ik} = \int_{\substack{\text{all}\\\text{space}}} d\vec{r} \quad \underline{\psi}^{ik}(\vec{r})\ \frac{\partial R}{\partial \underline{\psi}^{ik}(\vec{r})} - \sum_{j} \left(\alpha \frac{\partial R}{\partial \alpha}\right)^{ijk} \quad . \tag{A.23}$$

Equations (A.9)-(A.10) and (A.15)-(A.23), define a consistent set of space-continuous burnup equations adjoint to the forward quasi-static depletion formulation described in equations (A.1)-(A.7). The meaning and use of these adjoint equations are fully detailed in the main text of this report.

The above derivation was performed with the dependent variables as continuous functions of space. In realistic depletion problems, zone- or subzone-averaged quantities are almost always used. The zone-averaged flux is calculated and used in the transmutation matrix to produce zone/subzone-averaged nuclide density fields. In problems with subzones it is assumed that the following relationships are true.

$$\underline{N}_z(t) = \frac{1}{V_z} \sum_{s} \underline{N}_{sz}(t)\ V_{sz} \tag{A.24}$$

where

$$V_z = \sum_{s} V_{sz} \tag{A.25}$$

and

$$\underline{\psi}_z = \frac{1}{V_z} \int_{V_z} \underline{\psi}(\vec{r})\, d\vec{r} = \underline{\psi}_{sz} \tag{A.26}$$

where $N_z(t)$ = zone-averaged nuclide vector (NNUC)

$\underline{N}_{sz}(t)$ = subzone-averaged nuclide vector (NNUC)

$\underline{\psi}_z = \underline{\psi}_{sz}$ = zone-averaged flux vector (IGM)

V_z = volume of zone z

V_{sz} = volume of subzone s in zone z.

Using these definitions, a straightforward averaging of the space-continuous adjoint depletion equations can be performed with the following results.

1. <u>Space-Averaged Nuclide Adjoint Equations</u>:

Nuclide adjoint equation:

$$\frac{d}{dt}\, \underline{N}_{sz}^{*ijk}(t) + (\underline{\underline{T}}_{sz}^{ijk} + \underline{\underline{D}})^T\, \underline{N}_{sz}^{*ijk}(t) = 0 \tag{A.27}$$

where

$$\underline{\underline{T}}_{sz}^{ijk} = \alpha^{ijk}\, \underline{\underline{X}}_{sz}^{ik}\, \underline{\psi}_z^{ik} \tag{A.28}$$

and final condition

$$\underline{N}_{sz}^{*}(t_f) = \left.\frac{\partial R}{\partial \underline{N}_{sz}(t)}\right|_{t_f} = \frac{1}{V_{sz}} \int_{V_{sz}} \left.\frac{\partial R}{\partial \underline{N}(\vec{r},t)}\right|_{t_f} d\vec{r} \tag{A.29}$$

and jump condition

$$\underline{N}_{sz}^{*ijk} = \underline{N}_{sz}^{*ijk+} + \underline{\Gamma}_{sz}^{*ijk+} \text{ effect} + \underline{P}_{sz}^{*ijk+} \text{ effect} \tag{A.30}$$

with

$$\underline{\Gamma}^{*ijk+}_{sz} \text{ effect} = -\frac{1}{V_z} \int_{V_z} d\vec{r}\, \underline{\Gamma}^{*T}{}^{ik}(\vec{r}) \frac{\partial}{\partial \underline{N}^{ik}_{sz}} \left\{ (\underline{\underline{L}} - \lambda \underline{\underline{F}})^{ik} \underline{\psi}^{ik}(\vec{r}) \right\} \text{ for } j = 1$$

$$\underline{\Gamma}^{*ijk+}_{sz} \text{ effect} = 0 \quad \text{for } j \neq 1. \tag{A.31}$$

(See Appendix B for details of equation (A.31).)

$$\underline{P}^{*ijk+}_{sz} \text{ effect} = -P^{*ijk}\, \alpha^{ijk}\, \underline{\underline{E}}_p\, \sigma^{ik}_{fsz}\, \underline{\psi}^{ik}_z \tag{A.32}$$

and adjoint refueling discontinuity condition

$$\underline{Z}^{*ijk-} = \underline{\underline{P}}^{T}_{SD}{}^{ijk}\, \underline{Z}^{*ijk} \tag{A.33}$$

with

$$Z^{*ijk} = \begin{bmatrix} \underline{N}^*_1 \\ \vdots \\ \underline{N}^*_{sz} \\ \vdots \\ \underline{N}^*_{NREG} \end{bmatrix}$$ = Vector (NREG) of region-averaged adjoint nuclide vectors (NNUC).

$\underline{\underline{P}}^{ijk}_{SD}$ = Shuffling/discharge matrix (NREG*NREG) consisting of the identity matrix (NNUC*NNUC) in various locations so as to represent the desired nuclide discontinuity. (See Section IV for more details.)

Note when $j \neq 1$

$$\underline{\underline{P}}^{ijk}_{SD} = \begin{bmatrix} \underline{\underline{I}} & & & \\ & \cdot & & \\ & & \cdot & \\ & & & \cdot \\ & & & & \underline{\underline{I}} \end{bmatrix}_{(NREG*NREG)} \qquad \text{with } \underline{\underline{I}} = \begin{bmatrix} 1 & & & \\ & \cdot & & \\ & & \cdot & \\ & & & \cdot \\ & & & & 1 \end{bmatrix}_{(NNUC*NNUC)}$$

2. <u>Space-Averaged Power Normalization Adjoint Equation</u>:

$$P^{*ijk} = \frac{1}{P^{ijk}} \left[\left(\alpha \frac{\partial R}{\partial \alpha}\right)^{ijk} + \alpha^{ijk} \sum_z \sum_s V_{sz} \int_{\text{substep } j} dt\, \underline{N}^{*T}_{sz}{}^{ijk}(t)\, \underline{\underline{X}}^{ik}_{sz}\, \underline{\psi}^{ik}_z\, \underline{N}^{ijk}_{sz}(t) \right]. \tag{A.34}$$

3. Space-Averaged Generalized Adjoint Shape Equation:

$$(\underline{\underline{L}} - \lambda \underline{\underline{F}})^{T_{ik}} \underline{\Gamma}^{*ik}(\vec{r}) = \underline{S}_z^{*ik} \tag{A.35}$$

where

$$\underline{S}_z^{*ik} = \frac{\partial R}{\partial \underline{\psi}_z^{ik}} - (A^{*ik} * \underline{1})$$

$$+ \sum_j \frac{\alpha^{ijk}}{v_z} \sum_s v_{sz} \int_{\text{substep } j} dt \; \underline{N}^{*T_{ijk}}(t) \; \underline{\underline{X}}_{sz}^{ik} \; \underline{N}_{sz}^{ijk}(t) \tag{A.36}$$

$$- \sum_j \frac{1}{v_z} \sum_s v_{sz} \; P^{*ijk} \; \alpha^{ijk} \; \underline{N}_{sz}^{T_{ijk}} \; \underline{\underline{E}}_p \; \underline{\underline{\sigma}}_{fsz}^{ik} \quad .$$

4. Space-Averaged Auxiliary Equations:

$$\int_{\substack{\text{all}\\ \text{space}}} (\underline{\Gamma}^{*T}(\vec{r}) \; \underline{\underline{F}} \; \underline{\psi}(\vec{r}))^{ik} \, d\vec{r} = 0 \tag{A.37}$$

$$\sum_z v_z \; (\underline{\psi}_z^T \; \underline{S}_z^*)^{ik} = 0 \tag{A.38}$$

$$A^{*ijk} = \int_{\substack{\text{all}\\ \text{space}}} d\vec{r} \; \psi^{ik}(\vec{r}) \; \frac{\partial R}{\partial \underline{\psi}^{ik}(\vec{r})} - \sum_j (\alpha \frac{\partial R}{\partial \alpha})^{ijk} \quad . \tag{A.39}$$

Equations (A.36)-(A.39) represent the depletion perturbation formulation programmed into the DEPTH module. Although the detailed notation has been somewhat cumbersome, these adjoint burnup equations look quite similar to the FORTRAN equations in DEPTH and thus allow a fairly easy understanding of the coding within the new module.

APPENDIX B

The purpose of this Appendix is to evaluate the nuclide adjoint jump condition term involving the generalized adjoint shape function, $\underline{\Gamma}^{*}(\vec{r})$. In addition, it will be shown that the resultant volume integrals are equivalent to the perturbation integrals calculated within the VENTURE modular system and stored in the PERTUB interface file.

The first goal is to evaluate the following integral expression,

$$\underline{I}_{sz} = \int_{V_z} d\vec{r} \left[\underline{\Gamma}^{*T}(\vec{r}) \frac{\partial}{\partial \underline{N}_{sz}} \{(\underline{\underline{L}} - \lambda \underline{\underline{F}}) \underline{\psi}(\vec{r})\} \right] \tag{B.1}$$

where the term in the { } is just the time-independent multigroup diffusion equation written using operator notation. The form of the diffusion equation solved by VENTURE is,

$$\begin{aligned} &- D_{r,g} \nabla^2 \psi_{r,g} + [\Sigma_{a,r,g} + \sum_n \Sigma_{s,r,g\to n} + D_{r,g} B_g^2] \psi_{r,g} \\ &= \sum_n [\Sigma_{s,r,n\to g} + \frac{1}{K_{eff}} \chi_{r,g} (\nu\Sigma)_{f,r,n}] \psi_{r,n} \end{aligned} \tag{B.2}$$

where r refers to the space variable, g and n refer to the energy variable and D, Σ_a, Σ_s, $(\nu\Sigma_f)$ and χ are the diffusion coefficient, macroscopic absorption, scattering, and neutron production cross sections, and distribution function for fission neutrons, respectively.

Rewriting equation (B.2) in matrix form and assuming that the cross sections are constant within subzone s in zone z, one has

$$\begin{aligned} &- \underline{\underline{D}}_{sz} \nabla^2 \underline{\psi}(\vec{r}) + [\underline{\underline{\Sigma}}_a + \underline{\underline{\Sigma}}_s^0 + \underline{\underline{DB}}^2]_{sz} \underline{\psi}(\vec{r}) \\ &- [\underline{\underline{\Sigma}}_s^I + \frac{1}{K_{eff}} \underline{\underline{\chi}}\, \underline{\underline{\nu\Sigma}}_f]_{sz} \underline{\psi}(\vec{r}) = 0 \end{aligned} \tag{B.3}$$

where $\underline{\underline{\Sigma}}_s^0$ and $\underline{\underline{\Sigma}}_s^I$ are the outscatter and inscatter terms, respectively. Now taking the derivative of (B.3) with respect to $\underline{N}_{sz}$, one has (neglecting the $\underline{\underline{DB}}^2$ term),

$$\left[\underline{\underline{\sigma}}_{tr}\,\nabla^2 + \underline{\underline{\sigma}}_R - \underline{\underline{\sigma}}_S - \frac{1}{K_{eff}}\,\underline{\underline{\chi}}\,\underline{\underline{\nu\sigma}}_f\right]_{sz}\underline{\psi}(\vec{r}) = 0 \qquad \text{(B.4)}$$

where

$$\underline{\underline{\sigma}}_{tr} = -\frac{d}{d\underline{N}}\,\underline{\underline{D}} = \begin{bmatrix} 3D^2\underline{\sigma}_{tr_1} & & & 0 \\ & \cdot & & \\ & & \cdot & \\ 0 & & & 3D^2\underline{\sigma}_{tr_{IGM}} \end{bmatrix}_{IGM*IGM}$$

$$\underline{\underline{\sigma}}_R = \frac{d}{d\underline{N}}\left(\underline{\underline{\Sigma}}_a + \underline{\underline{\Sigma}}_s^0\right) = \begin{bmatrix} \underline{\sigma}_{a1} + \sum\limits_{\substack{n \\ n\neq 1}} \underline{\sigma}_{s,1\to n} & & & 0 \\ & \cdot & & \\ & & \cdot & \\ 0 & & & \underline{\sigma}_{a_{IGM}} + \sum\limits_{\substack{n \\ n\neq IGM}} \underline{\sigma}_{s,IGM\to n} \end{bmatrix}_{IGM*IGM}$$

$$\underline{\underline{\sigma}}_s = \frac{d}{d\underline{N}}\,\underline{\underline{\Sigma}}_s^I = \begin{bmatrix} 0 & \underline{\sigma}_s^{2\to 1} & \underline{\sigma}_s^{3\to 1} & \cdot & \cdot & \cdot & \underline{\sigma}_s^{IGM\to 1} \\ \underline{\sigma}_s^{1\to 2} & 0 & & & & & \\ \cdot & & \cdot & & & & \\ \cdot & & & \cdot & & & \\ \cdot & & & & \cdot & & \\ \underline{\sigma}_s^{1\to IGM} & & \cdot & \cdot & \cdot & & 0 \end{bmatrix}_{IGM*IGM}$$

$$\underline{\underline{\nu\sigma}}_f = \frac{d}{d\underline{N}}\,\underline{\underline{\nu\Sigma}}_f = \begin{bmatrix} \underline{\nu\sigma}_{f1} & \underline{\nu\sigma}_{f2} & \cdot & \cdot & \cdot & \\ \underline{\nu\sigma}_{f1} & \underline{\nu\sigma}_{f2} & \cdot & & & \\ & & \cdot & & & \\ \underline{\nu\sigma}_{f1} & \underline{\nu\sigma}_{f2} & \cdot & & & \underline{\nu\sigma}_{fIGM} \end{bmatrix}_{IGM*IGM}$$

and

$$\underline{\underline{\chi}} = \begin{bmatrix} \chi_1 & & & & 0 \\ & \chi_2 & & & \\ & & \cdot & & \\ & & & \cdot & \\ & & & & \cdot \\ 0 & & & & \chi_{IGM} \end{bmatrix}_{IGM*IGM}$$

with the microscopic cross-section vectors (NNUC) within the matrices now representing the nuclide dependence of the cross sections.

Now substituting equation (B.4) into (B.1), one obtains the following relations,

$$\underline{I}_{sz} = [\underline{I}_1 + \underline{I}_2 + \underline{I}_3 + \underline{I}_4]_{sz} \tag{B.5}$$

with

$$\underline{I}_1 = \int_{V_z} d\vec{r}\ \underline{\Gamma}^{*T}(\vec{r})\ \underline{\underline{\sigma}}_{tr}\ \nabla^2\ \underline{\psi}(\vec{r}) \tag{B.6}$$

$$\underline{I}_2 = \int_{V_z} d\vec{r}\ \underline{\Gamma}^{*T}(\vec{r})\ \underline{\underline{\sigma}}_{R}\ \underline{\psi}(\vec{r}) \tag{B.7}$$

$$\underline{I}_3 = -\int_{V_z} d\vec{r}\ \underline{\Gamma}^{*T}(\vec{r})\ \underline{\underline{\sigma}}_{s}\ \underline{\psi}(\vec{r}) \tag{B.8}$$

$$\underline{I}_4 = -\frac{1}{K_{eff}} \int_{V_z} d\vec{r}\ \underline{\Gamma}^{*T}(\vec{r})\ \underline{\underline{\chi}}\ \underline{\underline{\nu\sigma}}_{f}\ \underline{\psi}(\vec{r})\ . \tag{B.9}$$

Equations (B.6)-(B.9) can also be written using summation notation as follows,

$$\underline{I}_{1sz} = \sum_g (3D_g^2\ \underline{\sigma}_{trg})_{sz} \int_{V_z} \Gamma_g^*(\vec{r})\ \nabla^2\ \psi_g(\vec{r})\ d\vec{r}\ , \tag{B.10}$$

$$\underline{I}_{2sz} = \sum_g (\underline{\sigma}_{ag} + \sum_{\substack{n \\ n\neq g}} \underline{\sigma}_{sg\to n})_{sz} \int_{V_z} \Gamma_g^*(\vec{r})\ \psi_g(\vec{r})\ d\vec{r}\ , \tag{B.11}$$

$$\underline{I}_{3sz} = -\sum_{g} \sum_{\substack{n \\ n \neq g}} (\underline{\sigma}_{sn \to g})_{sz} \int_{V_z} \Gamma_g^*(\vec{r})\ \psi_n(\vec{r})\ d\vec{r} \quad , \tag{B.12}$$

$$\underline{I}_{4sz} = -\frac{1}{K_{eff}} \sum_{g} (\underline{\nu\sigma}_{f_g})_{sz} \int_{V_z} \left(\sum_{n} \chi_n\ \Gamma_n^*(\vec{r})\right) \psi_g(\vec{r})\ d\vec{r} \quad . \tag{B.13}$$

Using this last set of equations, a numerical result can be obtained for $\underline{I}_{sz}$ and the $\underline{\Gamma}^*_{sz}$ effect jump condition. The volume integrals in the above equations are stored in the PERTUB interface file as the following quantities,

(2D RECORD)

$$T_{z,g} = \frac{1}{K_{eff}} \sum_{i \varepsilon z} v_i\ \psi_{i,g} \sum_{n} \chi_n\ \Gamma^*_{i,n} \tag{B.14}$$

(3D RECORD)

$$S_{z,n,g} = \sum_{i \varepsilon z} v_i\ \Gamma^*_{i,g}\ \psi_{i,n} \tag{B.15}$$

(4D RECORD)

$$W_{z,g} = \sum_{i \varepsilon z} v_i\ \Gamma^*_{i,g}\ \nabla^2\ \psi_{i,g} \tag{B.16}$$

Finally, using (B.10)-(B.16), the expression in equation (B.1) can be written as,

$$\underline{I}_{sz} = \sum_{g} (3D_g^2\ \underline{\sigma}_{trg})_{sz}\ W_{z,g} \tag{B.17}$$

$$+ \sum_{g} (\sigma_{ag} + \sum_{\substack{n \\ n \neq g}} \underline{\sigma}_{sg \to n})_{sz}\ S_{z,g,g}$$

$$- \sum_{g} \sum_{\substack{n \\ n \neq g}} (\underline{\sigma}_{sn \to g})_{sz} \, S_{z,n,g}$$

$$- \sum_{g} (\underline{\nu\sigma}_{fg})_{sz} \, T_{z,g} \quad .$$

It is equation (B.17) that is evaluated within the DEPTH module.

ORNL/TM-7305
Category Distribution UC-77

Internal Distribution

1-2. L. S. Abbott
3. J. Barhen
4. D. E. Bartine
5. S. M. Bowman
6. M. A. Bjerke
7-11. T. J. Burns
12. D. G. Cacuci
13. H. P. Carter/A. A. Brooks/ CSD X-10 Library
14. R. L. Childs
15. J. C. Cleveland
16. G. W. Cunningham
17. H. L. Dodds
18. W. W. Engle, Jr.
19. G. F. Flanagan
20. T. B. Fowler
21. P. M. Haas
22. O. W. Herman
23. D. T. Ingersoll
24. H. E. Knee
25. R. A. Lillie
26. J. L. Lucius
27-31. F. C. Maienschein
32. J. H. Marable
33. P. J. Maudlin
34. J. W. McAdoo
35. C. V. Parks
36. J. A. Renier
37. W. A. Rhoades
38. D. L. Selby
39. C. O. Slater
40. J. S. Tang
41. E. T. Tomlinson
42. D. F. Vondy
43. M. W. Waddell
44. J. J. Wagschal
45. C. F. Weber
46. C. R. Weisbin
47-51. J. R. White
52-56. G. E. Whitesides
57. L. R. Williams
58. M. L. Williams
59. B. A. Worley
60. RSIC
61. Herbert Goldstein (consultant)
62. Paul Greebler (consultant)
63. W. B. Loewenstein (consultant)
64. Richard Wilson (consultant)
65-66. Central Research Library
67. Y-12 Document Ref. Section
68-70. Laboratory Records Dept.
71. Laboratory Records-RC
72. ORNL Patent Section

External Distribution

73. J. M. Kallfelz, School of Nuclear Engineering, Georgia Institute of Technolgy, Atlanta, Georgia 30332.
74. L. F. Miller, School of Nuclear Engineering, University of Tennessee, Knoxville, Tennessee 37919.
75. P. F. Pasqua, School of Nuclear Engineering, University of Tennessee, Knoxville, Tennessee 37919.
76. P. N. Stevens, School of Nuclear Engineering, University of Tennessee, Knoxville, Tennessee 37919.
77. J. N. Rogers, Division 8324, Sandia Laboratories, Livermore, California 94550.
78. Chief, Mathematics and Geoscience Branch, Department of Energy, Washington, DC 20545.
79. Office of Assistant Manager for Energy Research and Development, Department of Energy, ORO, Oak Ridge, Tennessee 37830.
80-172. Given AY - Reactor Computer Codes distribution.
173-338. Given distribution as shown in TID-4500 under UC-77 - Gas-Cooled Reactor Technology.

☆U.S. GOVERNMENT PRINTING OFFICE: 1980-640-245/201